# NUMERICAL SIMULATION OF STRONG GROUND MOTION USING SHEAR DISLOCATION SOURCES

## A DISSERTATION

*submitted in partial fulfilment of the*
*requirements for the award of the degree*
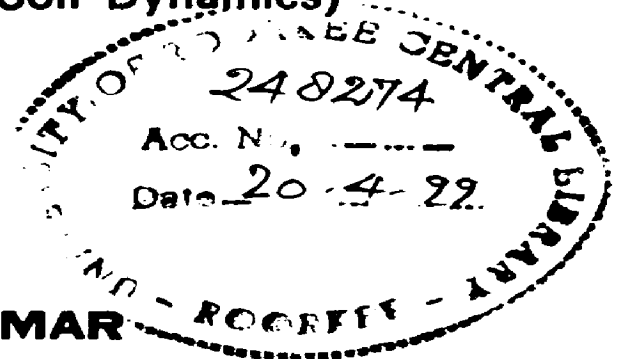*of*

### MASTER OF ENGINEERING

*in*

### EARTHQUAKE ENGINEERING
(With specialization in Soil Dynamics)

*By*

## ARVIND KUMAR

### DEPARTMENT OF EARTHQUAKE ENGINEERING
### UNIVERSITY OF ROORKEE
### ROORKEE-247 667 (INDIA)

## JANUARY, 1999

# CANDIDATE'S DECLARATION

I hereby certify that the work presented in this dissertation titled "NUMERICAL SIMULATION OF STRONG GROUND MOTION USING SHEAR DISLOCATION SOURCES", in partial fulfilment of the requirement for the award of the degree of MASTER OF ENGINEERING in Earthquake Engineering with specialization in SOIL DYNAMICS, submitted to the Department of Earthquake Engineering, University of Roorkee, Roorkee, is an authentic record of my own work carried out for a period of six months from July, 1998 to January, 1999 under the Supervision of Dr. J.P. NARAYAN, Lecturer, Earthquake Engineering Department, University of Roorkee, Roorkee.

The matter embodied in this dissertation has not been submitted for the award of any other degree.

Place : Roorkee

Date : 30 Jan., 1999

(ARVIND KUMAR)

This is to certify that the above statement made by the candidate is correct to the best of my knowledge.

30.1.1999

(Dr. J.P. NARAYAN)
Lecturer
Dept. of Earthquake Engg.
University of Roorkee
Roorkee - 247 667 (U.P.)

# ACKNOWLEDGEMENT

I take this opportunity to express my indebtedness towards my thesis supervisor Dr. J.P. Narayan without whose encouragement and help this work might not have been in its present form.

I also wish to acknowledge the help and encouragement given by all members of the faculty and staff of the Department of Earthquake Engineering.

I am highly obliged and wish to thank all my parents, brothers, sisters, friends and other relatives for their co-operation.

(ARVIND KUMAR)

# ABSTRACT

The very purpose of this dissertation is to present the implementation of shear dislocation sources in 2D parsimonious staggered finite difference grid for the strong ground motion (SGM) simulation and to study the local site effects on its characteristics. The shear dislocation sources have been generated using partial stress drop in the form of Ricker wavelet, to simulate natural tectonic earthquakes realistically. Since the conventional staggered grid method requires large computational memory, hence parsimonious staggered grid method has been used here with an added advantage of reduced requirement of computational time and memory. The local site effects have been studied since they play important roles in the spatial variation of amplitude amplification, changes in signal duration, frequency content, mode conversion and finally the pattern of structural damages. Study of source scaling results corroborates with the relations developed in the past, such as the manner in which variation in stress drop changes the seismic moment. It has also been found that for a given stress drop, change in time step would not give rise to an increase in effective seismic moment. The basin simulation results depict that for the steeply incident waves, the impedance decreases, resonance effects associated with deeper basin structures and mode conversion controls the amplitude amplification and increase in signal duration. Futher, the multiple reflections in the near surface unconsolidated sediments increases the signal duration, depending on the trapping capacity.

# CONTENTS

# LIST OF FIGURES

## 1.1 GENERAL

"Necessity is the mother of invention", because necessity only can activate human brains. These mighty activated human brains are responsible for the emanation of latest Sciences and Technologies. Since there is a good lot of necessity to know about the unsolved conundrum of earthquakes, hence we come across so many latest developments in earthquake technology. Though earthquake predictions have not been made possible till now, yet a lot have been done to know the causes and after effects of earthquakes.

Here, in this dissertation, we are going to deal with the latest advancements in the field of the study of local sites effects on the characteristics of strong ground motion (SGM).

Earthquake resistant design by earthquake engineers is critically dependent upon the ground motions. Hence, there is a great need of help from seismologists to know the realistic ground responses that are sites specific. Since the sample seismic ground motions available from field recordings are still relatively small, hence the main difficulty lies due to unavailability of recorded data of earthquakes of different magnitudes. Indeed in no country have substantial records been obtained in the near field of an earthquake of very strong ground motion, i.e., of magnitude greater than 8.

Earthquake sources are also of various types and depths, and occur in various geological structures, so much interpolation and extrapolation between recorded

ground motion is needed which may be dangerous. For this reason, seismology has already assisted to compute ground responses for specified seismic source types and geological conditions. Very latest advancements are also taking place in the field of Seismology to find out ground responses for specific types of source with certain geological conditions. Here, we have used very latest developments to get ground responses with specified source types and geological conditions.

## 1.2 OUTLINE OF THE THESIS

Though earthquakes of all magnitude ranges give valuable pieces of information and they add to the already existing statistical data which in turn are useful for earthquake predictions, for seismogram analysis and hence for latest scientific developments; yet earthquake engineers are concerned with only those earthquakes whose intensities are widely felt. Since strong ground motions (SGM) always cause vigorous shaking of earth's surface, hence it is of great concern for earthquake engineers. In this thesis, a thorough study of SGM and changes in its characteristics from one location to another location has been made.

With the many factors to influence the natural tectonic earthquakes, the single ultimate cause of all these earthquakes is slip along the fault line. These slips may occur either along the already existing faults, which are known as shear dislocation sources; or they may occur along the newly generated faults, which are called crack generation sources. These two types of sources have been discussed ahead in this thesis. Sudden drop in stress causes slip on the fault surface and then the system attains dynamic state. This sudden drop in stress in known as dynamic stress drop. This has been discussed in later chapter.

After the occurrence of slip, propagation of seismic wave energy takes place in all possible directions. While developing the wave equations, theory of elasticity is adopted. The theory of elasticity is concerned with the strain experienced by the deformable materials subjected to the application of a system of forces. The study of wave propagation and its amplification, attenuation, dispersion etc. is possible with the solution of wave equations.

The solution of the wave equations is found either using the analytical approach or by using the numerical modelling approach. Since numerical modelling approach has certain advantages over the analytical approach (as discussed later in this thesis), hence numerical modeling approach has been used here. There are three different approaches of numerical modelling namely, finite difference method, finite element method and, spectral method.

Since the finite difference (FD) method has certain plus points over other two methods, in its favour, hence finite difference approach has been used in this thesis. Source scaling relations have been used to show the effect of variation in the slip along fault, effects of source frequency and partial stress drop on the characteristics of the ground responses.

Most of the cities are located on or near alluvial valleys. In past, many large cities have suffered great damages which were situated in basins. Hence, the effects of basin and its geometry on ground motion characteristics have been studied elaborately in this dissertation report.

3

## 1.3 OBJECTIVE OF THE THESIS

Strong motion simulation is of prime importance in earthquake engineering due to lack of recorded ground motions in India. Study of source scaling and simulated results depict that the ground motion can be simulated successfully at desired site, taking into account the existing faults, seismicity of the area, stress orientation, seismic section and the local site conditions. So, we have not to wait for the large earthquakes to occur for ground motion records and ultimately for the engineering design and the retrofitting of the existing structures.

• • •

## 2.1  GENERAL

The ground motion which causes considerable damages to the people and their environment is termed as strong ground motion. The ground accelaration greater than 0.05g is generally used to classify strong motion records. Strong ground motion is generally associated with earthquakes having magnitude ≥5. Since only strong ground motions cause damages to structures, hence earthquake engineers are primarily concerned with strong ground motion (SGM). The characteristics of strong ground motion are :

      i) Amplitude

      ii) Frequency content, and

      iii) Duration and motion

## 2.2  AMPLITUDE

The most common way of describing a ground motion is the variation of amplitude (acceleration, velocity or displacement) with time. Only one of these quantities is measured directly and the rest two are computed by integration and/or differentiation. In general, acceleration is measured directly, whereas velocity and displacement are obtained by integration of acceleration record.

### 2.2.1  Peak Acceleration

The most commonly used measure of the amplitude of a particular ground motion is the peak horizontal acceleration. This has natural relationship with the inertial

5

force. Indeed, the largest dynamic force induced in certain type of structures (very stiff structures) are closely related with the peak horizontal acceleration. Vertical acceleration has received less attention than horizontal acceleration in the field of earthquake engineering, because margin of safety taken against the gravity induced static vertical force provide adequate resistance against dynamic force induced by vertical acceleration during earthquakes. In engineering applications, the peak vertical acceleration is assumed to be equal to two-thirds of the peak horizontal acceleration (New mark and Hall, 1982).

## 2.2.2 Peak Velocity

Peak horizontal velocity is another parameter to characterize the amplitude of strong ground motion. Velocity is less sensitive to higher frequency contents of ground motion. Peak horizontal velocity has given accurate indication of earthquake potential for damages and is also related to the earthquake intensity (e.g., Trifunac and Brandy, 1975; Krinitzsky and Chang, 1987).

## 2.2.3 Peak Displacement

Peak displacement is generally associated with the lower frequency contents of an earthquake motion. It is very difficult to measure the peak displacement accurately. That is why, to find out the ground motion, peak acceleration or peak velocity is used.

Following soil parameters and geological conditions have significant effect on the amplification of ground motion at a site:

      i) Depth of soil layer over bed rock.

      ii) Variation of soil type and engineering property with depth.

      iii) Lateral irregularity and surface topography at the site.

## 2.3 FREQUENCY CONTENT

Buildings, bridges, slopes or soil deposits are very sensitive to the frequency at which they are loaded. If the frequency of structure coincides with the frequency of ground motion, resonance will occur which ultimately leads to failure of the structure. The frequency contents of strong ground motion are described by using different types of spectra. Fourier spectra and power spectra directly illustrate the frequency contents of ground motion. Response spectra reflect the influence of the ground motion on structures of varying natural periods. A variety of spectral parameters are available to describe the frequency contents of strong ground motions.

## 2.4 DURATION

Duration of strong ground motion is the most important parameter influencing earthquake damages. If ground motion is for short duration, it may not produce enough load reversals to build up damaging response in structures even if the amplitude of motion is high. On the other hand, a ground motion with moderate amplitude but long duration can produce enough load reversals to cause substantial damage. The duration of strong ground motion is related to the time required for the release of accumulated strain energy from the rupture along the fault. If the length or area of fault rupture increases, the time required for the release of strain energy increases and thus leading to the increased duration of strong motion with increased earthquake magnitude. Hank and McGuire (1981) have provided a theoretical relation showing that the duration of an earthquake is proportional to the cube root of the seismic moment.

● ● ●

## 3.1 WAVE EQUATIONS

Wave equations are deduced using theory of elasticity. The theory of elasticity deals with the strain experienced by deformable material subjected to the application of a system of forces.

Wave equations have been developed on the following assumptions :

i)    The matter is continuous, i.e., the theory of continuum is valid, and

ii)   The elastic theory is considered within framework of continuum mechanics. The presence of cracks, joints, bedding planes and other disturbances in rocks could raise doubts on the continuity of rock mass. Where these disturbances are small in comparison with the dimensions of a given body in a rock, they would alter the mechanical properties of the rock mass, but the body may still be considered as continuum. Experience shows that the continuum mechanics even when applied to discontinuous materials, often provided correct results, and it is mathematically much simpler than the theory of discontinua.

Using force equilibrium concept at any point, and with mathematical simplifications, we get wave equations for P-SV wave as given below:

### 3.1.1  P-SV Wave Equations :

P-SV wave equations in terms of stresses and strain for 2D case are:

$$\rho \, \frac{\partial^2 U}{\partial t^2} = \frac{\partial}{\partial x} \left( \sigma_{xx} \right) + \frac{\partial}{\partial z} \left( \sigma_{xz} \right) \qquad (3.1)$$

and

$$\rho \frac{\partial^2 W}{\partial t^2} = \frac{\partial}{\partial z} (\sigma_{zz}) + \frac{\partial}{\partial x} (\sigma_{xz}) \qquad\qquad (3.2)$$

Equations (3.1) and (3.2) are elasto-dynamic equations for P-SV wave in a homogeneous medium.

Here,

$\sigma_{xx}$ = Normal stress in X-direction

$\sigma_{zz}$ = Normal stress in Z-direction

$\sigma_{xz}$ = Shear stress in X-Z plane

U = Particle displacement in X-direction

W = Particle displacement in Z-direction

$\rho$ = Density of the medium.

The relations among the stresses, strains and Lame's parameters are as follows:

$$\sigma_{xx} = (\lambda + 2\mu) \frac{\partial U}{\partial x} + \lambda \frac{\partial W}{\partial z} \qquad\qquad (3.3)$$

$$\sigma_{zz} = (\lambda + 2\mu) \frac{\partial W}{\partial z} + \lambda \frac{\partial U}{\partial x} \qquad\qquad (3.4)$$

$$\sigma_{xz} = \mu \left[ \frac{\partial U}{\partial z} + \frac{\partial W}{\partial x} \right] \qquad\qquad (3.5)$$

Here,

$\lambda$ and $\mu$ are Lame's parameters.

## 3.2 METHODS FOR THE SOLUTION OF WAVE EQUATIONS

There are two major approaches to solve wave equations. These are,

(i) Analytical and

(ii) Numerical

9

Since numerical modelling approach has certain advantages over the analytical approach, hence numerical modelling technique has been described here in detail. The advantages of numerical modelling approach over the analytical approach are as follow:

(i)   Analytical solution for complex structure is not possible.

(ii)  Numerical methods are compatible with the analytical method, i.e., when fine grids are used in numerical method, the results obtained from both the methods are almost same.

(iii) High frequency modelling can be done using numerical modelling technique.

(iv)  Numerical method can be applied for wave propagation, even when elastic parameters change comparable to the seismic wavelength which is analytically not possible.

(v)   Numerical methods account for all types of wave phenomena in a single computer run like reflection, refraction, transmission, scattering, dispersion etc.

## 3.3 SHEAR DISLOCATION AND CRACK SOURCE MODELS

When slip occurs in the already existing faults, this phenomenon is known as shear dislocation sources; whereas, when a new fault itself it generated to cause the slip, such sources are known as crack generation sources. Shear dislocation and crack source models are associated with these two types of sources respectively. Both these models can be solved by using either analytical method or numerical modelling. Both these methods have been discussed ahead.

## 3.3.1 Analytical Methods :

It has been assumed that crustal earthquake ground motion results from unstable slip accompanying a sudden drop in shear stress on a geological fault. Seismic events display a radiation pattern, implying that shearing processes are at the roots of their generation. Seismic radiation is the main source of information on the faulting processes of earthquake phenomena. The radiation can be computed by a space-time convolution of Slip-function with a Green-function. The Slip-function describes the fault displacement during an earthquake as a function of time and position on the fault plane, while Green-function represents the Earth's response to the slip. The Slip-function and Green-function, therefore, express quantitatively the source and propagation effects on seismic motion. Thus, from seismic radiation together with field observations, the rupture history of a specific event could be reconstructed, and in an ideal case seismic radiation would be used to perform tomographic study of the fault. This task, however, is very difficult because of the limited azimuthal coverage by seismic stations and limited frequency band of the available instruments. As a result, highly idealised models of rupture with a highly restricted number of source parameters are in general use.

Seismic radiation can be calculated using either dislocation or a crack approach. A dislocation is considered to be a defect in an ideally elastic or visco-elastic medium formed by a cut along a given surface and a finite relative displacement of the two faces of the cut, which means that the dislocation is represented by a discontinuity in the displacement. Dislocations for which the relative displacement is of the rigid body motion is called Volterra dislocation. Thus, in the dislocation approach the earthquake is represented in terms of the Slip-function on the fault plane, and its form is generally chosen intuitively, without rigorous analysis of the time-dependent stress acting in the area. Frequently used models of this type

11

are the propagating dislocation model of Haskell (1953) and the model of Brune (1970). The last one, although assuming an infinite rupture velocity, is rationalized in terms of the dynamic properties of the source. Numerical source generation based on shear dislocation has been done by Vidale (1985 & 1987) and Coutant (1995).

In contrast to dislocation models, in crack models an explicit account of the driving and resisting stresses in the source region is taken, and the resulting slip is derived by solving the equations of motion. Thus to describe the fracture of an earthquake source as a crack, it is necessary to know the initial distribution of stress on the fracture surface before the earthquake and the laws governing the fracture propagation and interaction of the fault faces. The distribution of the displacement on the faults becomes then one of the unknowns. When fracture is described as a dislocation, the model is called kinematic, and when it is described as a crack, the model is called dynamic. Although dynamic crack modeling is physically more proper, the kinematic dislocation models are much simpler and involve more efficient computation, preserving at the same time enough degree of freedom to represent some realistic models. The various dislocation solutions can be classified according to the model dimensions (two- and three-dimensional models), the characteristics of earth structure (Uniform and layered models), the various methods of solution and according to the range of considered rupture velocities (sub-, trans-, and super-critical) and the type of Slip-function used.

Another popular dislocation source model is the model of Brune (1970). In this model it is assumed that a tangential stress drop is applied to the interior of a dislocation surface resulting in the fault blocks movement in the opposite directions. For simplicity, the fault propagation effects are neglected and the stress drop is assumed to apply instantaneously over the fault surface. It is also

12

assumed that the fault surface reflects elastic waves during rupture. The stress drop sends a pure shear stress wave propagating perpendicularly to the fault surface. Brune (1970) also developed a relation among seismic parameters as given below :

$$\Delta\sigma = \frac{7}{16} \frac{M_0}{r_0^3}$$  (3.6)

Where,

$\Delta\sigma$ = Dynamic stress drop or Effective stress (MPa)

$M_0$ = Seismic moment (N.m)

$r_0$ = Radius of the circular fault (m)

Other relation existing between the magnitude of earthquake and the seismic moment was developed by Hanks and kanamori (1979) as

$$M = \frac{2}{3} \log M_0 - 6.0$$  (3.7)

Where,

M  = Magnitude of the earthquake and

$M_0$ = Seismic moment in N.m

Construction of a dynamic model of faulting requires a description of the dynamic stress drop, the rupture velocity and the rupture complexity over the rupture region. Analytical solution of crack propagation for any given initial and boundary conditions is extremely difficult, and the existing solutions involve several simplifying assumptions. For this reason, only a few simple geometric models have been solved analytically. But recently, Mikumo and Miyatake (1987) have generated shear crack sources using finite difference method. Practically all the other available solutions have been obtained with the use of numerical methods.

The next step in approximation of realistic seismic sources is to assume that the self-similar shear crack stops suddenly once a final radius $r_o$ is reached. The solution of this problem was obtained numerically by Madariaga (1976). Initially, until the sudden drop of the rupture at the final radius, the Slip-function is a numerical approximation. the stopping of rupture generates very strong P, S, and Rayleigh waves that propagate inward from the edge of the fault. After the arrival of a Rayleigh wave the slip velocity is reduced to zero. Madariaga (1976) called this process "healing". At that time it was assumed that function is sufficiently high to freeze the slip at that point on the fault.

Around the edges of a circular crack there is a mixed mode of rupture with a variable stress intensity. As a consequence, the apparent simplicity of the solutions should disappear as soon as a rupture criterion is introduced. The crack will rapidly deform into more or less elliptical shapes. The only possible way to study spontaneous rupture in three dimensions is by numerical modelling. It should be noted, however, there are considerable differences between analytical and numerical solutions. The analytical solutions are obtained using Griffth's theory and for a single crack development describing the fracture phenomenon.

### 3.3.2 Numerical Method :

In numerical modeling three techniques are in general use. These are,

    i)    Finite element method

    ii)   Finite difference method, and

    iii)  Spectral method

The spectral method seems to be more accurate than the other two, since it does not suffer from dispersion, which is the case with the finite-element and finite-difference methods. Though the accuracy of finite-element method is more than that

of the finite-difference method, yet the memory required and the time allocation in computation is more using F.E.M. For big systems, finite-element method requires very complex procedure hence it is not in frequent use. Finite-difference method is frequently used since this method has merits over the above mentioned disadvantages of F.E.M.

Let us consider the Acoustic wave equation as written below:

$$\frac{\partial^2 p}{\partial t^2} = V^2 \left[ \frac{\partial^2 p}{\partial x^2} + \frac{\partial^2 p}{\partial z^2} \right] \qquad (3.8)$$

In this equation, the term lying to the left of the equality sign, i.e., $\frac{\partial^2 p}{\partial t^2}$ is known as "Temporal Part", whereas the term lying to the term lying to the right of the equality sign is known as "Spatial Part".

Though, to solve the spatial part of the above equation any one of the above three methods can be used; yet to solve the temporal part of the equation only finite-difference method is invariably used.

Here, we have used finite-difference method to get the solutions of both the parts.

### 3.3.2.1 Finite Difference Method :

Finite difference is one of the three numerical techniques available for SGM simulation. The models prepared to be used in finite difference simulation may be either homogeneous or heterogeneous. Since earth's body is a multi-layered system, hence heterogeneous modelling simulates field conditions in a much better way with an added advantage of no requirement of boundary conditions at the interfaces. While preparing 2D models; stability, grid-dispersion and edge reflection are taken

15

into account properly as discussed in the next chapter. While using finite difference methods for numerical solution, generally standard staggered grid scheme is used. A separate discussion on parsimonious staggered grid scheme used in the simulation is given below:

**Parsimonious Staggered Grid Scheme :**

Differencing procedure of the elasto-dynamic equations for P-SV wave can be developed by using either conventional staggered grid method or parsimonious staggered grid method. But, since parsimonious staggered grid scheme (Luo and Schuster, 1990) has a number of plus points over the conventional grid scheme; hence the former has been used here for the development of differencing procedure. Superiority of parsimonious staggered grid scheme over the other schemes are as follows :

i) Parsimonious staggered grid scheme is stable for large range of Poisson's ratio.

ii) Parsimonious staggered grid scheme is free from the spatial derivative of elastic parameters over the second order central difference scheme (Kelly et al., 1976)

iii) Parsimonious staggered grid scheme has lesser storage requirement over the standard staggered grid scheme (Virieux, 1986) and the Lax Wendroff scheme (Vafidis et al., 1992; and Ram and Narayan, 1995).

iv) The stability criteria for this scheme is the same as the usual schemes such as standard staggered grid scheme and Lax Wendroff scheme.

When the time and spatial derivatives of elasto-dynamic equations (3.1) and (3.2) are replaced by the second order differencing operator, we get following equations :

16

$$\rho_{1,m}\left[\frac{U_{1,m}^{n+1} + U_{1,m}^{n-1} - 2U_{1,m}^{n}}{\Delta t^2}\right] = \left[\frac{(\sigma_{xx})_{1+1,m}^{n} - (\sigma_{xx})_{1,m}^{n}}{\Delta x}\right]$$

$$+ \left[\frac{(\sigma_{xz})_{1,m+1}^{n} - (\sigma_{xz})_{1,m}^{n}}{\Delta z}\right] \qquad (3.9)$$

$$\rho_{1,m}\left[\frac{W_{1,m}^{n+1} + W_{1,m}^{n-1} - 2W_{1,m}^{n}}{\Delta t^2}\right] = \left[\frac{(\sigma_{xz})_{1+1,m}^{n} - (\sigma_{xz})_{1,m}^{n}}{\Delta x}\right]$$

$$+ \left[\frac{(\sigma_{zz})_{1,m+1}^{n} - (\sigma_{zz})_{1,m}^{n}}{\Delta z}\right] \qquad (3.10)$$

The stress at the time 'n' used in equations (3.9) and (3.10) are computed using differenced stress-strain equations given below:

$$(\sigma_{xx})_{1,m}^{n} = (\lambda_{1,m} + 2\mu_{1,m})\left[\frac{U_{1,m}^{n} - U_{1-1,m}^{n}}{\Delta x}\right] + \lambda_{1,m}\left[\frac{W_{1,m}^{n} - W_{1,m-1}^{n}}{\Delta z}\right] \qquad (3.11)$$

$$(\sigma_{zz})_{1,m}^{n} = \lambda_{1,m}\left[\frac{U_{1,m}^{n} - U_{1-1,m}^{n}}{\Delta x}\right] + (\lambda_{1,m} + 2\mu_{1,m})\left[\frac{W_{1,m}^{n} - W_{1,m-1}^{n}}{\Delta z}\right] \qquad (3.12)$$

$$(\sigma_{xz})_{1,m}^{n} = \mu_{1,m}\left[\frac{U_{1,m}^{n} - U_{1,m-1}^{n}}{\Delta z} + \frac{W_{1,m}^{n} - W_{1,m-1}^{n}}{\Delta x}\right] \qquad (3.13)$$

17

The use of the stresses derivatives at time 'n' into the equations **(3.9)** and **(3.10)** is the main reason of the parsimony in the parsimonious staggered grid scheme. Here $\Delta t$ is the time step, and $\Delta x$ and $\Delta z$ are the grid intervals, in the X- and Z-directions respectively. 'l' and 'm' are the grid indices in the X- and Z-directions and 'n' is the time index.

## 3.4 SOURCE GENERATION

Having prepared models, we need to generate source to implement it at the designed co-ordinate of the model. After setting up the source at desired point in grid, we calculate the response at the desired locations. In the numerical modelling two types of sources have been used, namely,

    i)    Point/Explosive source, and

    ii)   Earthquake source

Nuclear explosions, dynamite explosions etc. are few examples of point/explosive sources, and the different types of earthquake sources are,

    i)    Strike-Slip

    ii)   Dip-Slip

    iii)  $45°$-Dip-Slip

Both the explosive and earthquake sources can be generated using a disturbance/stress drop in the form of Ricker wavelet in some specified manner. The governing equation to generate a Ricker wavelet is,

$$f(t) = C\, e^{-\alpha(t-to)^2}$$

Where, $C$ = A constant whose value is fixed depending upon the required amplitude, '$t_o$' is decay time, and $\alpha$ is a constant which controls the frequency of the source.

Partial stress drop in the form of Ricker wavelet has been shown in **Fig.3.1**.

18

Different types of earthquake sources (Strike-Slip, Dip-Slip and 45°-Dip-Slip) and explosive sources have been generated based on shear dislocation using dynamic stress drop in the form of Ricker wavelet instead of instantaneous stress drop (Brune, 1970). Shear dislocation criterion of source generation involves the consideration of dynamic stress drop. Dynamic stress drop is the difference between the original in-situ shear stress $\sigma_o$ and the dynamic frictional stress $\sigma_d$. Hence, dynamic stress drop $\Delta\sigma_f$ is given as,

$$\Delta\sigma_f = \sigma_o - \sigma_d$$

**The Asperity Model and Shear Dislocation Source Generation**

The basic idea regarding this was suggested by Madariaga (1976), and by Rudnicki and Kanamori (1981). According to this model, an earthquake is caused by the failure of isolated, highly stressed regions of the fault; the rest of the fault having little or no resistance to slip (being partially broken and pre-slipped) and contribute little or no stress drop to the earthquake process. This results in a non-uniform stress drop over the fault. The spontaneous, dynamic fracturing of one or more such isolated asperities of general shape and size on a fault has not yet been studied. The simpler problem of radiation from the fracturing of a circular asperity at the centre of a circular fault was studied by Das and Kostrov (1986).

The discussions on the generation of different types of sources are as follows:

**Strike-Slip Source :**

We have generated the strike-slip source using partial stress drop in the form of Ricker wavelet in the X-direction only. In this source generation, the model
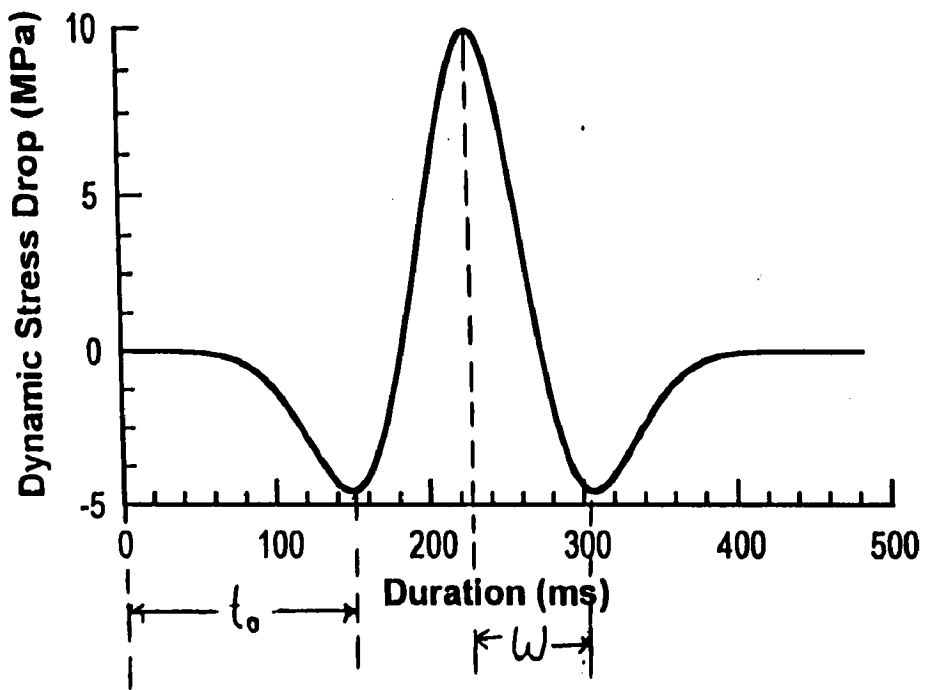
Fig. 3.1 PARTIAL STRESS DROP IN THE FORM OF RICKER
WAVELET

parameters such as $\lambda$, $\mu$ and density are taken as $10^7 \text{N/m}^2$, $10^7 \text{ N/m}^2$ and 2.5 g/cc respectively. In this case, duration of the wavelet is 0.4625 second, and stress drop has been applied at equal intervals of 0.0025 second instead of instantaneous stress drop (Brune, 1970) to control the frequency content, initiation and stopping of the rupture.

The snapshot of the stress drop has been taken just after the complete implementation of the wavelet. **Fig.3.2** depicts the stress drop patterns in the X-direction. Most of the stress drop is from a rectangular region. This figure depicts that there are so many asperities instead of a single circular asperity in contrast to madariaga (1976). The radius of rupture is equal to the product of wavelet duration and P-wave velocity.

The rupture area is found to be circular, although most of the moment has been released from a rectangular region. Similarly, the shape of apparent stress drop distribution and rupture area in Z-direction and X-Z plane have been shown in **Fig.3.3** and **Fig.3.4** respectively. From **Fig.3.3**, which shows apparent stress drop patterns in Z-direction, it is clear that stress drop is mainly from a circular region. Here, again so many asperities have been seen contradicting the single circular asperity concept by Madariaga (1976). In this case rupture area is circular, and at the same time most of the moment has been released from a circular region only. Similarly, **Fig.3.4**, depicts the apparent stress drop distribution and rupture area in X-Z plane. This figure shows that; though most of moment is released from a rectangular area, yet the rupture area is again circular. So many asperities are again observed in contrast to the Madariaga (1976). In all these cases, it has been found that the radius of circular rupture area is equal to the product of wavelet duration and P-wave velocity.
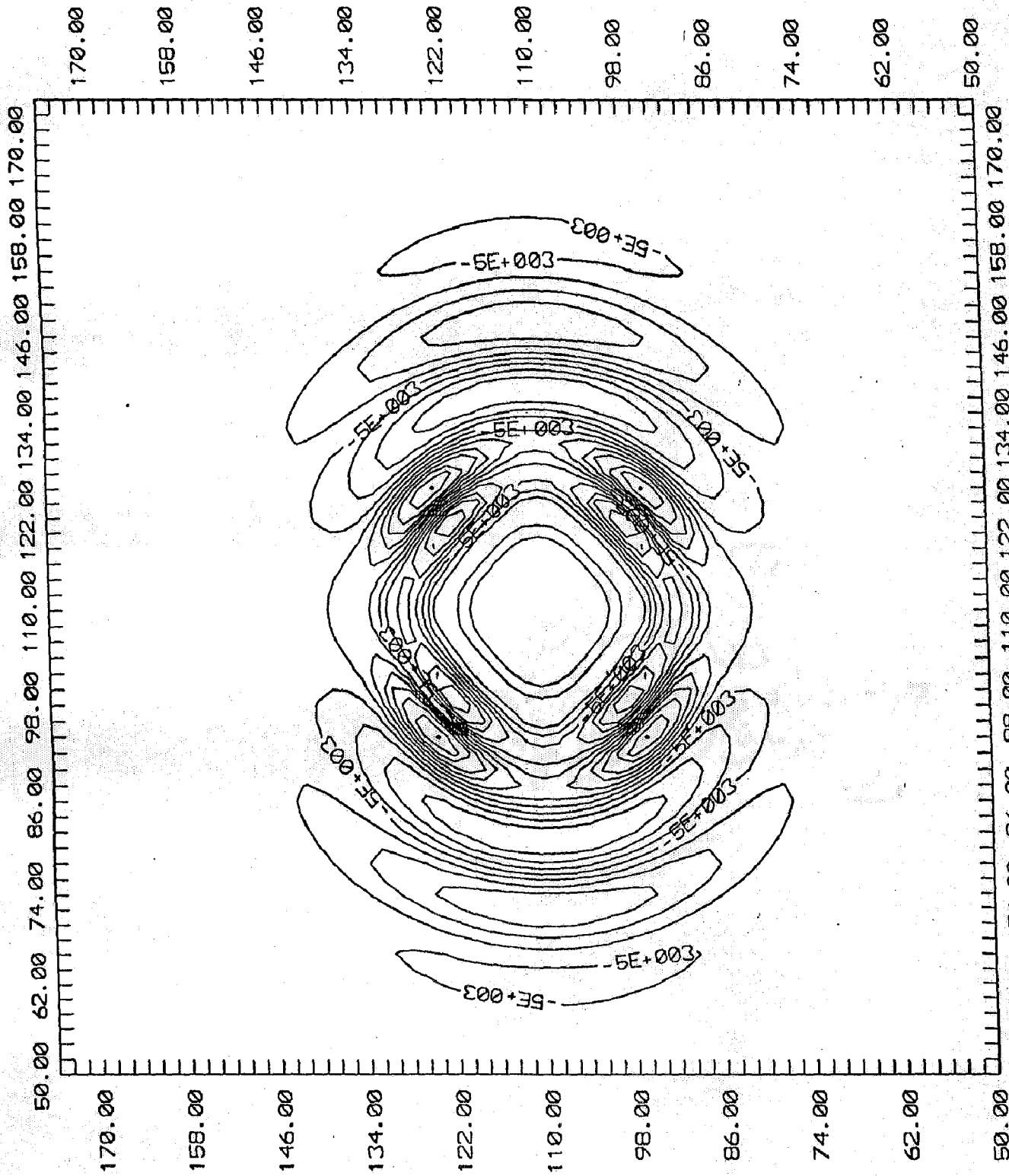
Fig. 3.2 SNAPSHOT OF APPARENT STRESS DROP IN X-DIRECTION FOR STRIKE-SLIP
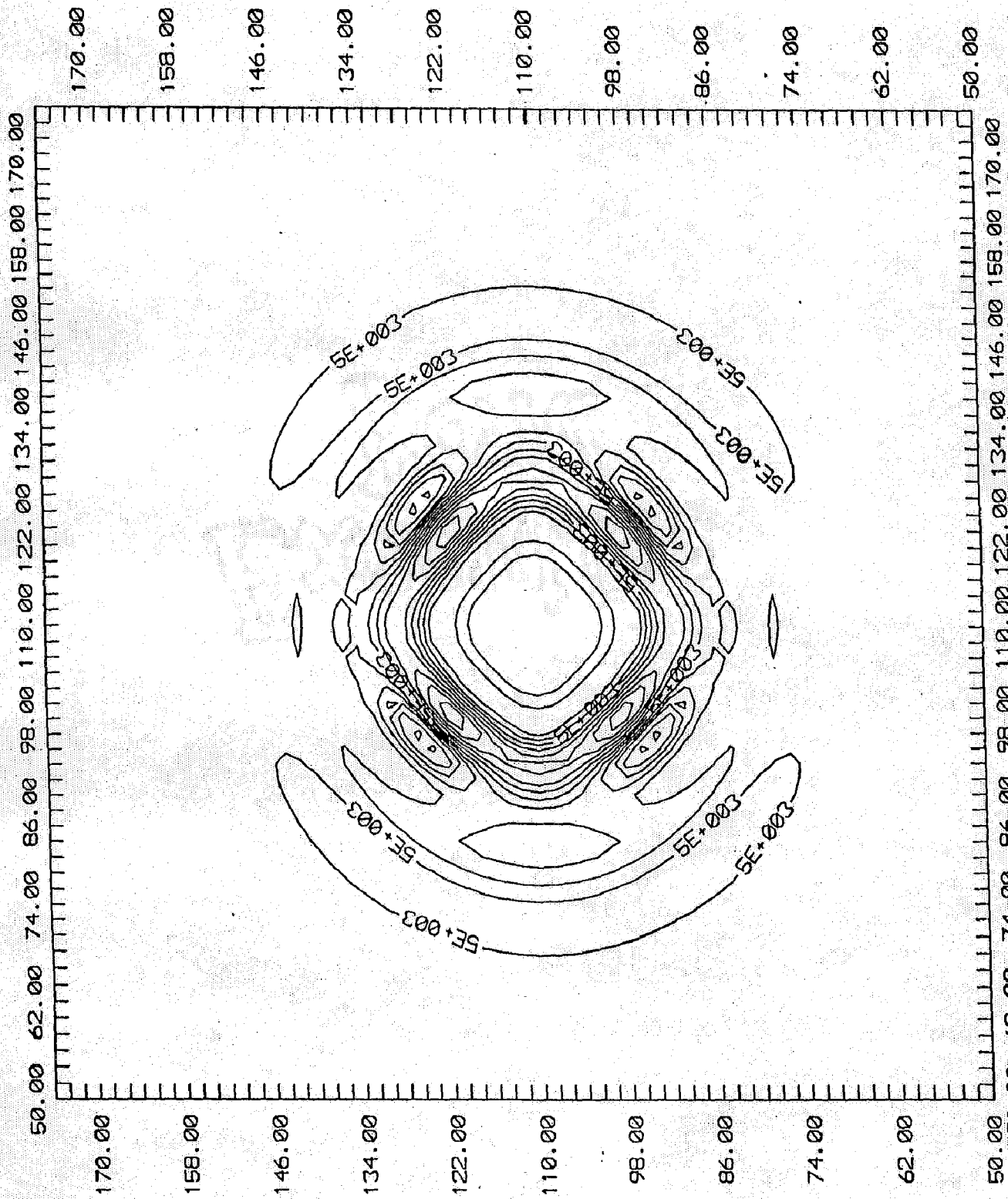SOURCE

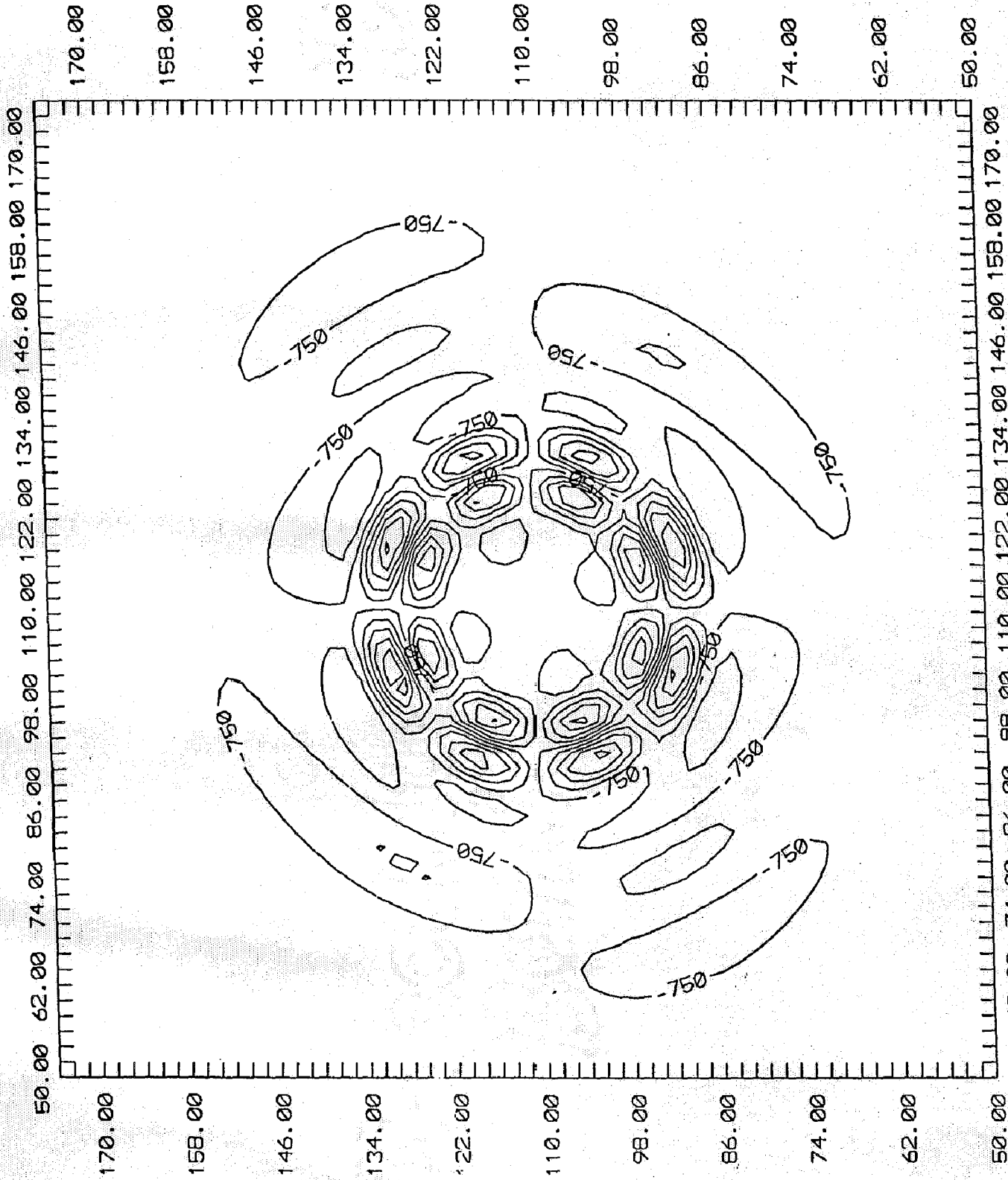Fig. 3.3 SNAPSHOT OF STRESS DROP IN Z-DIRECTION FOR STRIKE-SLIP SOURCE

23

Fig. 3.4 SNAPSHOT OF STRESS DROP IN X-Z PLANE FOR STRIKE-SLIP SOURCE

## Dip-Slip Source :

We have generated dip-slip source using partial stress drop in the form of a Ricker wavelet in the X-Z plane only. In this source generation, the model parameters such as $\lambda$, $\mu$ and density ($\rho$) have been taken as $10^7$ N/m$^2$, $10^7$ N/m$^2$ and 2.5 g/cc respectively. Duration of the ricker wavelet is again 0.4625 second, and stress drop has been applied at equal intervals of 0.0025 second in contrast to the spontaneous stress drop (Brune, 1970). The snapshot of the stress drop has been taken just after the complete implementation of the Ricker wavelet. **Figs.3.5, 3.6,** and **3.7** depict the stress drop patterns in the X- direction, Z- direction and X-Z plane respectively. **Fig.3.5**, showing the stress distribution pattern in X-direction, confirms that rupture area is circular but the area releasing the moment is rectangular. It has been found that the radius of the circular rupture area is equal to the product of duration of wavelet and P-wave velocity. So many asperities are seen in the rupture region contradicting the concept of single circular asperity by Madariaga (1976). **Fig.3.6** depicts the stress distribution pattern in Z-direction. It shows that rupture area as well as most of the moment releasing region is circular. A good number of asperities are again visible here, thus contradicting the single circular asperity concept by Madariaga (1976). **Fig.3.7** is showing apparent stress pattern and asperities in rupture area. It shows fully circular rupture, though the moment releasing region is slightly tilted rectangular region. Large number of asperities are again visible here.

## 45° - Dip-Slip Source :

Here, 45°-Dip-Slip source has been generated using partial stress drop in both X- and Z- directions. However,the polarity of the stress drops applied in X- and Z- directions is opposite to each other. The stress drop in both the directions has

Fig. 3.5 SNAPSHOT OF STRESS DROP IN X-DIRECTION FOR DIP-SLIP SOURCE
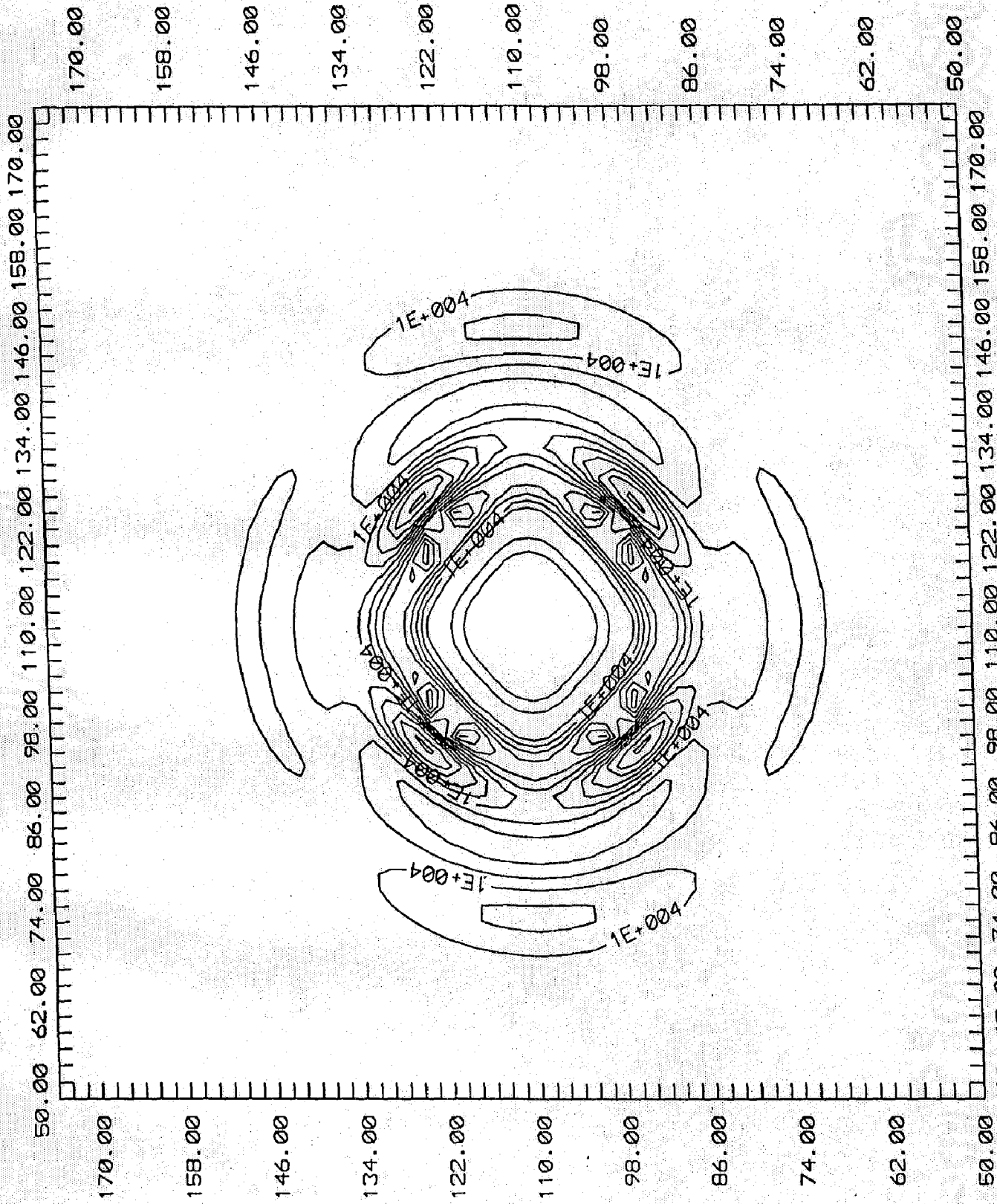
Fig. 3.6 SNAPSHOT OF STRESS DROP IN Z-DIRECTION FOR DIP-SLIP SOURCE
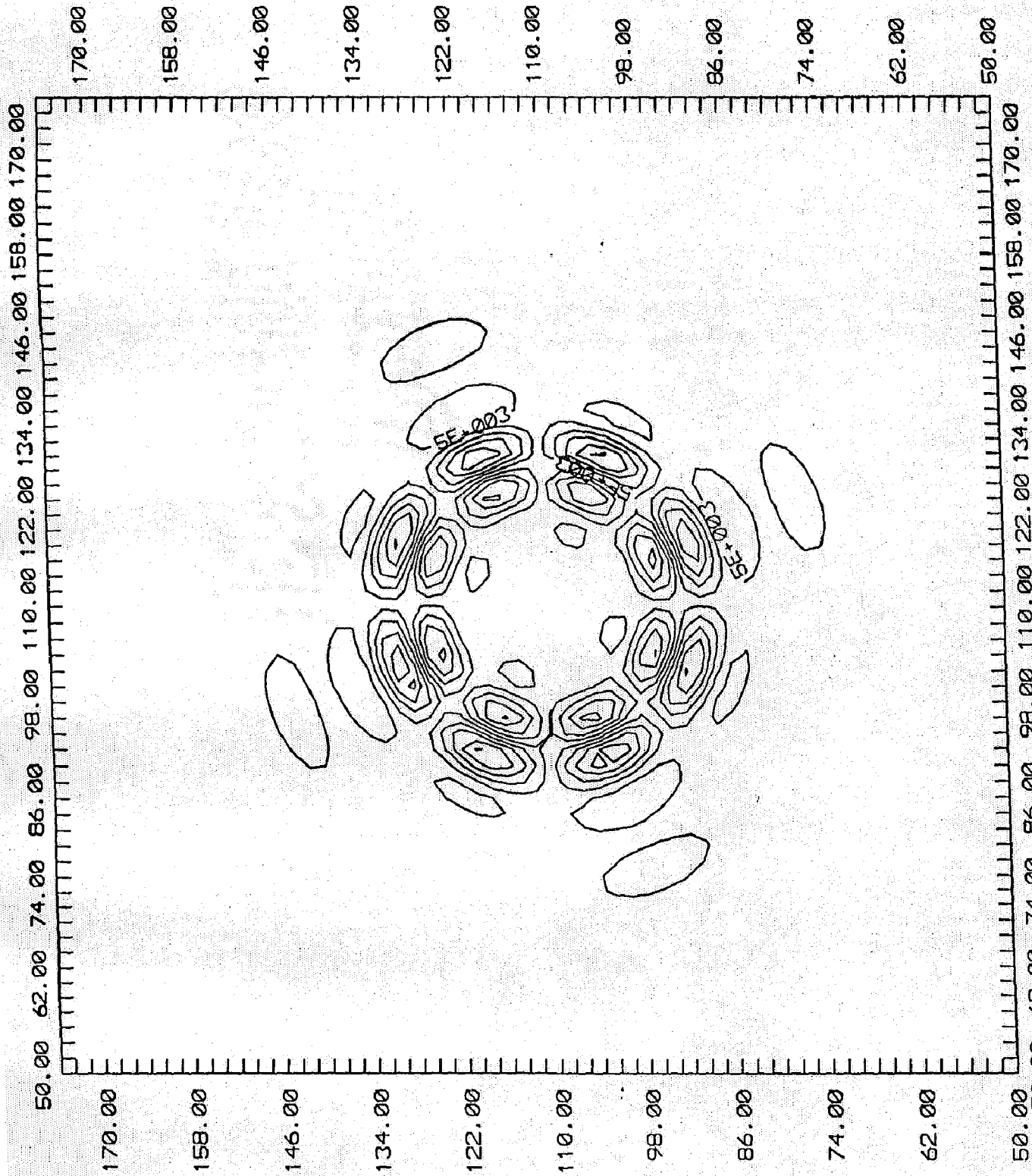
27

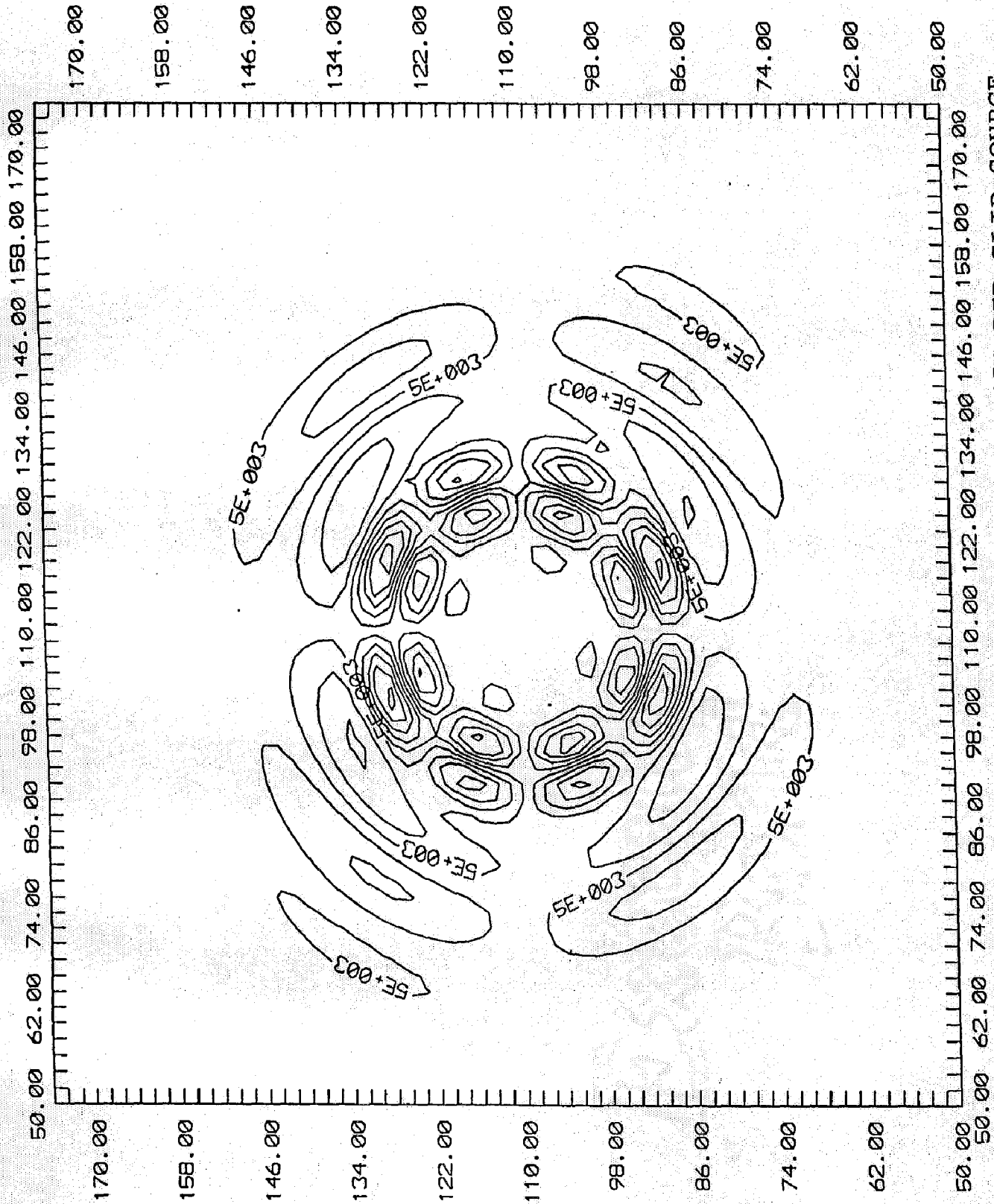Fig. 3.7 SNAPSHOT OF STRESS DROP IN X-Z PLANE FOR DIP-SLIP SOURCE

28

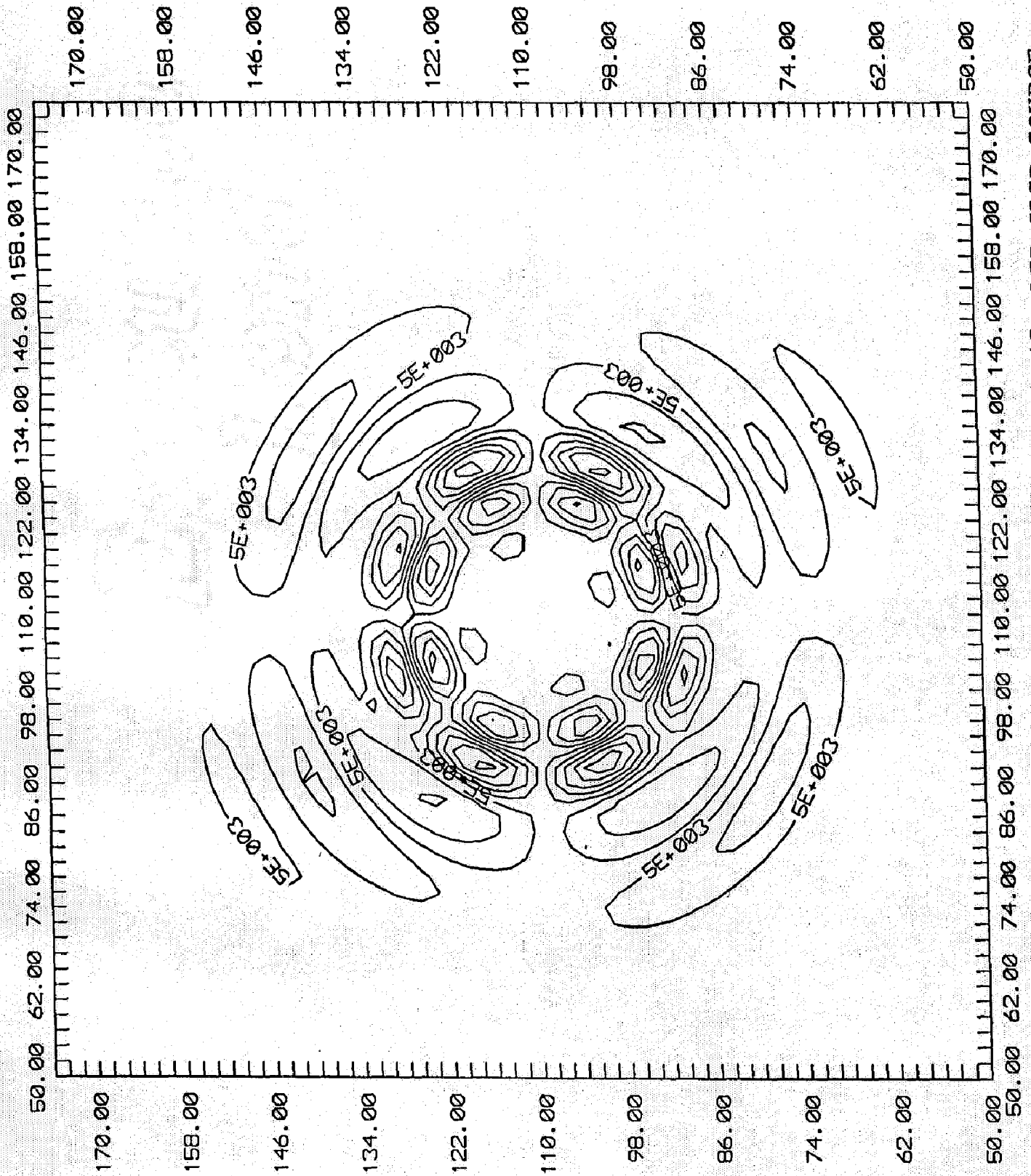Fig. 3.8 SNAPSHOT OF STRESS DROP IN X-DIRECTION FOR 45° DIP-SLIP SOURCE

29

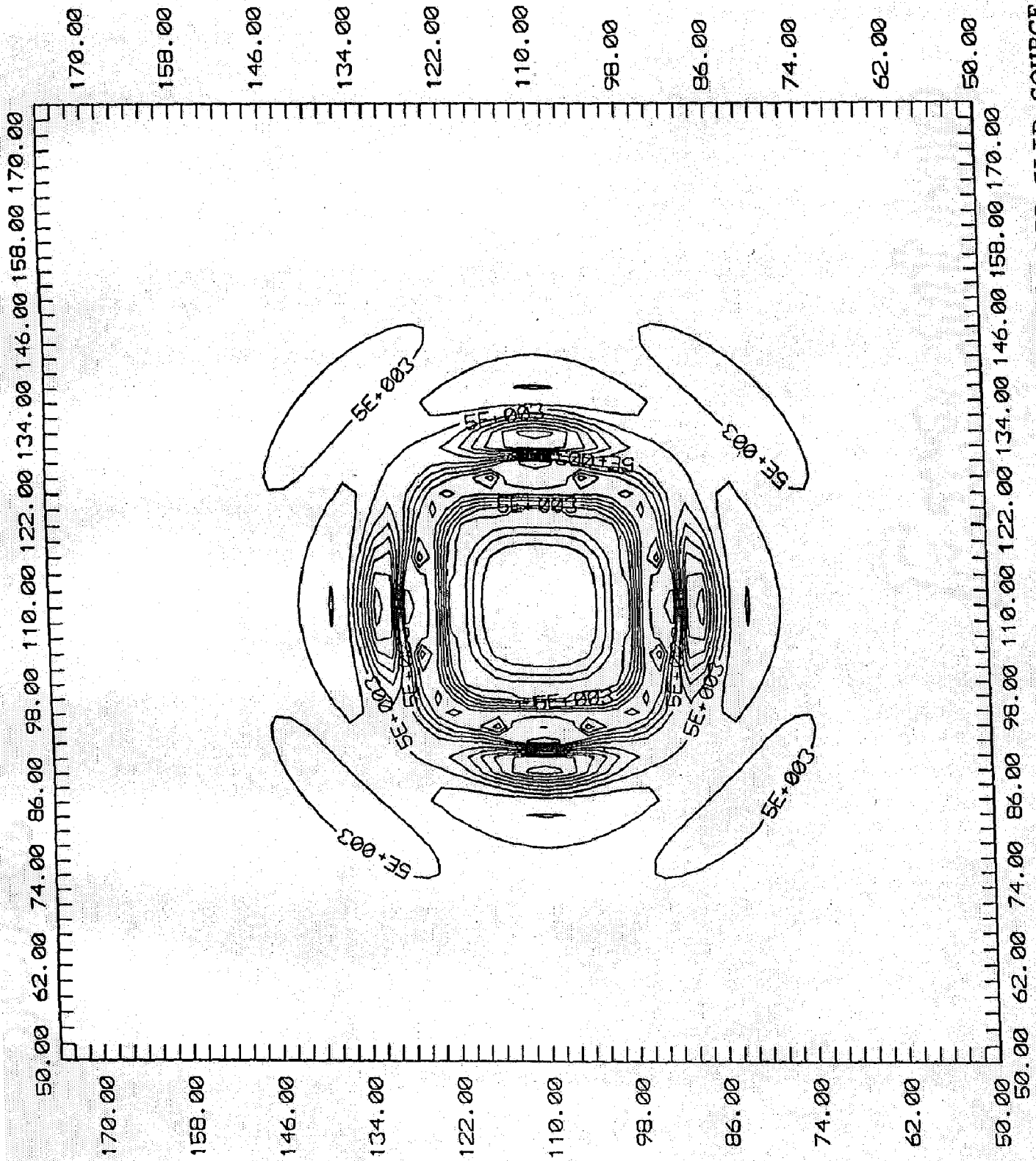Fig. 3.9 SNAPSHOT OF STRESS DROP IN Z-DIRECTION FOR 45° DIP-SLIP SOURCE

30

Fig. 3.10 SNAPSHOT OF STRESS DROP IN X-Z PLANE FOR 45° DIP-SLIP SOURCE

31

been applied in the form of Ricker wavelet. In this source generation, the model parameters are $\lambda$, $\mu$ and density $(\rho)$ with their respective values as $10^7 \text{N/m}^2$, $10^7 \text{N/m}^2$ and 2.5 g/cc. Duration of the Ricker wavelet has been kept equal to 0.4625 second, and the stress drop has been applied at equal intervals of 0.0025 second, against the spontaneous stress drop used by Brune (1970). The snapshot of the stress drop has been taken soon after the complete implementation of the wavelet. **Figs.3.8, 3.9,** and **3.10** are showing these snapshots in X- direction, Z- direction and X-Z plane respectively. **Fig.3.8** confirms that the rupture area is circular, though the region releasing most of the moment is a rectangular one. Many asperities are visible in the snapshot. **Fig.3.9** shows the stress pattern, asperities and moment realeasing region in Z-direction. It is clear here, that the rupture area is circular. Most of the moment has been released from a rectangular region. **Fig.3.10** depicts the stress pattern and moment releasing region in X-Z plane. In this case, both the rupture area and the moment releasing region are circular. Most of the moment is released from a circular area. There are so many asperities visible in contrast to the single circular asperity by Madariaga (1976).

## 3.5 COMPARATIVE ANALYSIS OF ANALYTICAL AND NUMERICAL RATIDATION PATTERNS

The source can be generated and implemented using either the analytical method or numerical method. After implementation of source and its triggering, different types of radiation patterns are found for different types of sources.

The comparative study of radiation patterns for the earthquake sources using different methods has been done. Analytically, radiation patterns for different sources were obtained by coutant et. al. (1995). These patterns have been shown in **Fig.3.11.** Parsimonious staggered grid approximation of elasto-dynamic equation for

Radial        Transverse
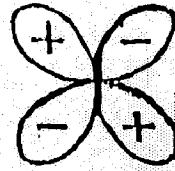


(a) STRIKE - SLIP
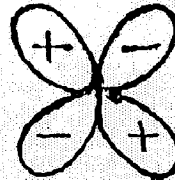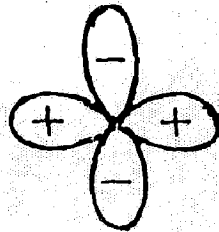
(b) 45° - DIP - SLIP
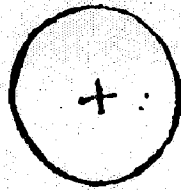
(c) EXPLOSION
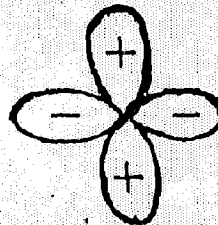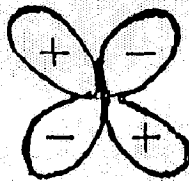
(d) DIP - SLIP

**Fig. 3.11** ANALYTICAL SOURCE RADIATION PATTERNS FOR P-SV AND SH-WAVES (AFTER COUTANT ET AL. 1995)

33
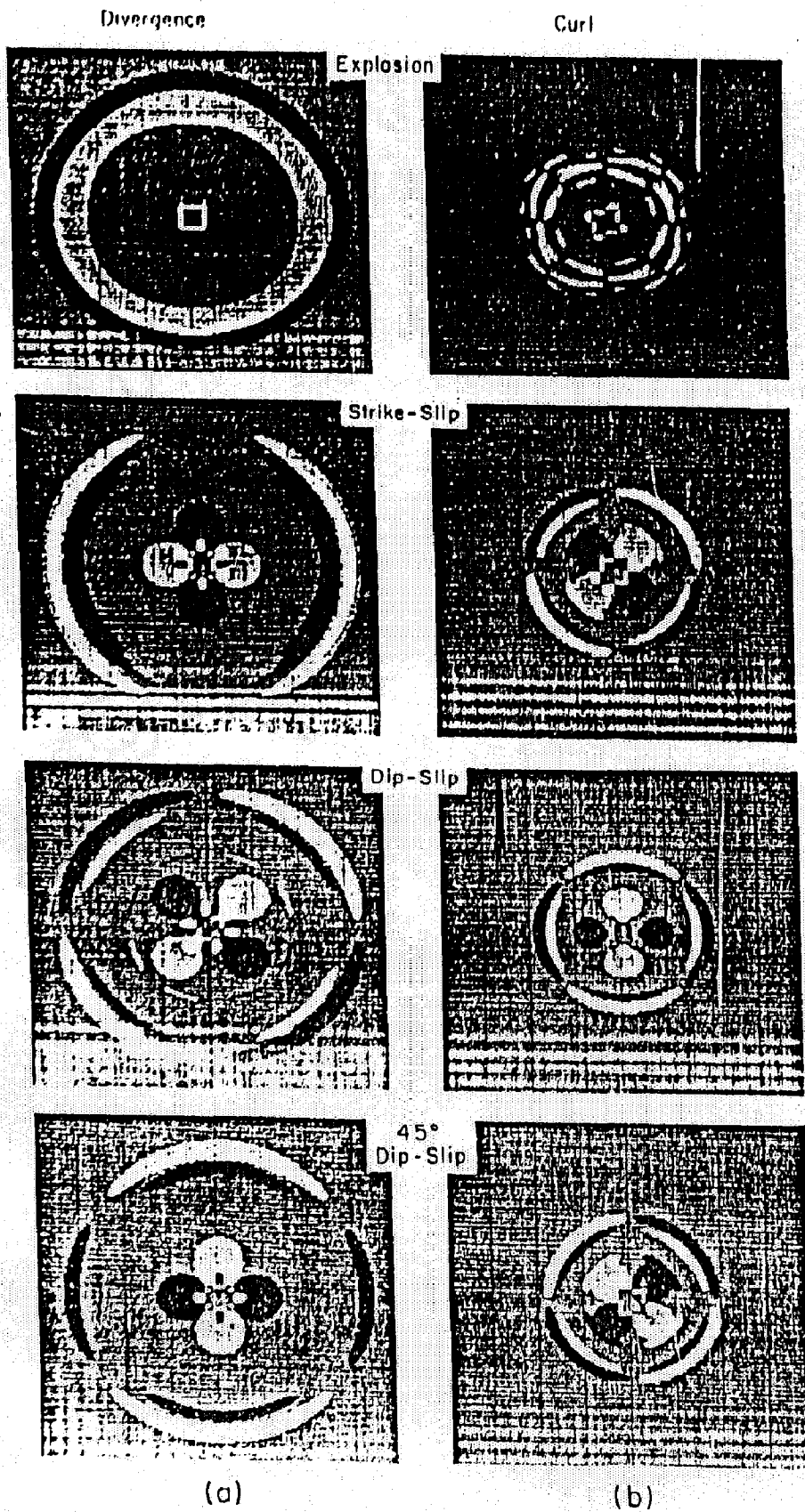
Fig. 3.12 NUMERICAL SOURCE VERTICAL RADIATION PATTERNS
FOR P-SV WAVE (AFTER VIDALE 1987)
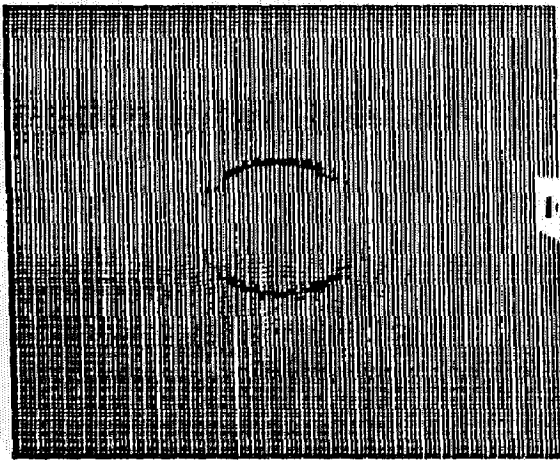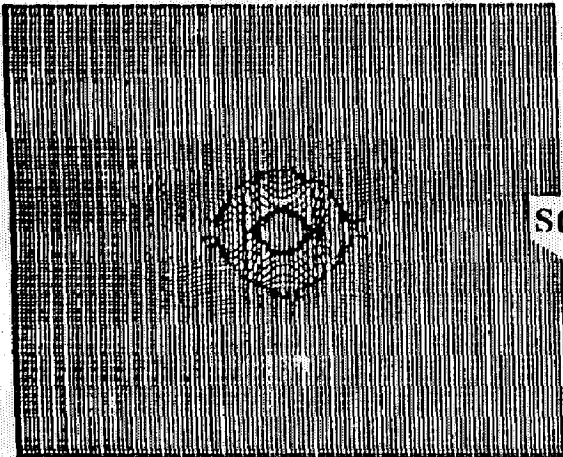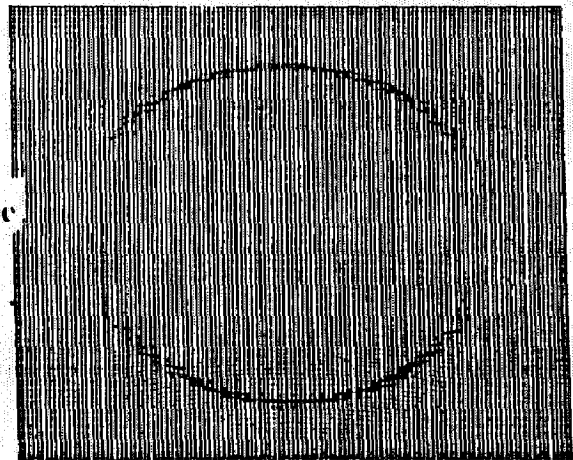
Explosive
(a)
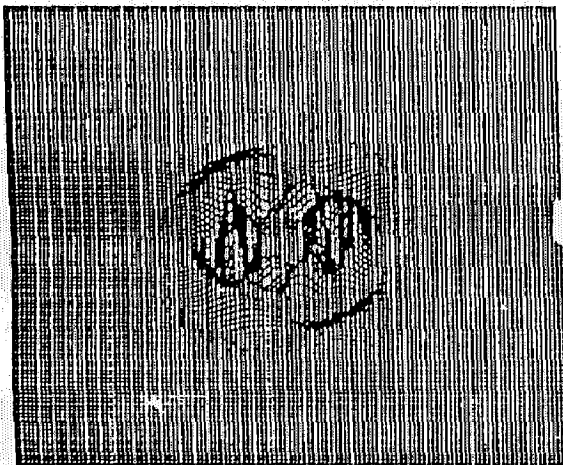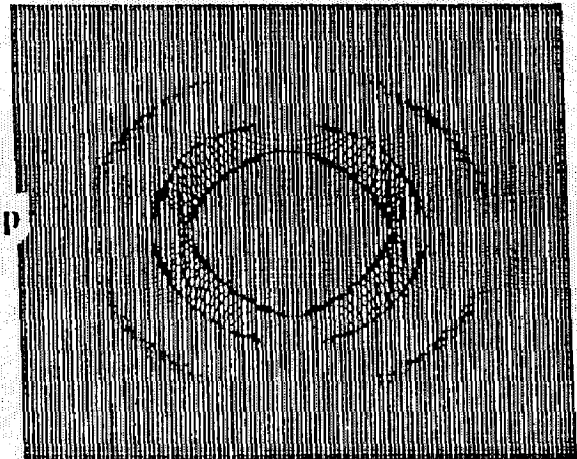
Strike Slip
(b)
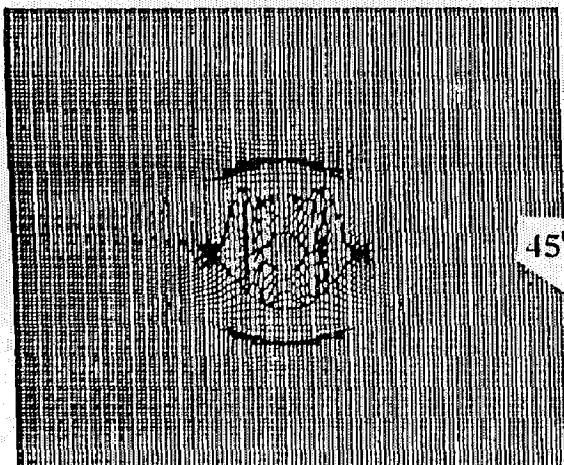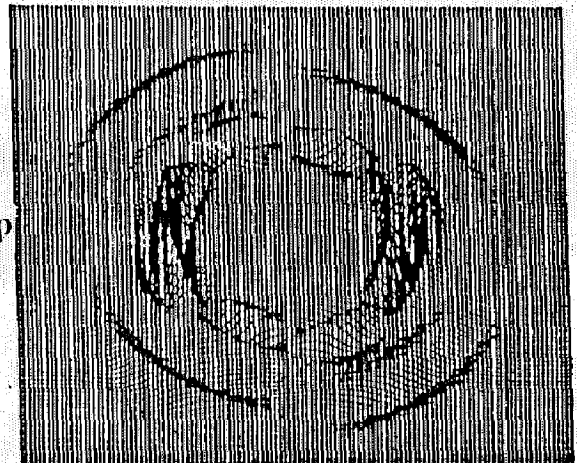
Dip Slip
(c)

45⁰-Dip Slip
(d)
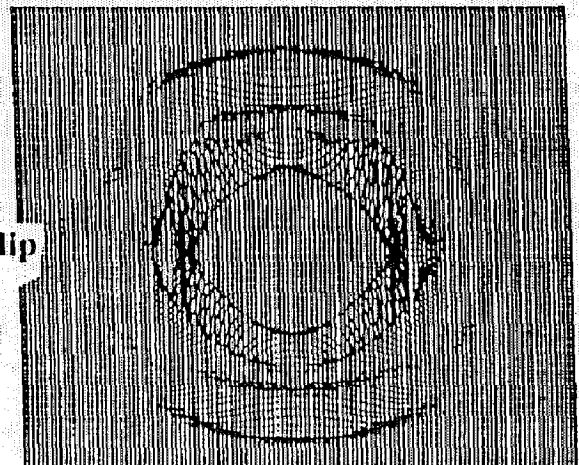
Fig. 3.13 NUMERICAL SOURCE VERTICAL RADIATION PATTERNS
FOR P-SV WAVE (AFTER J.P. NARAYAN, 1998)
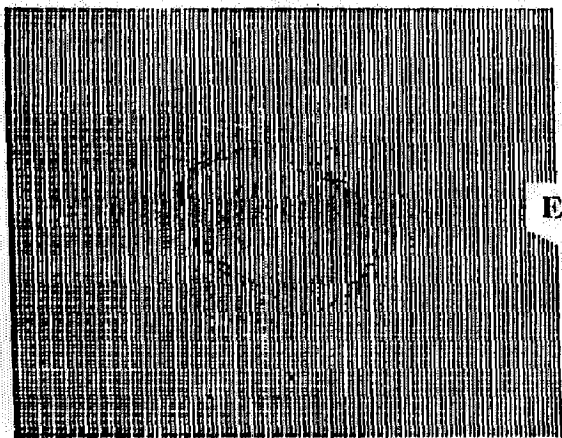
Explosive
(a)
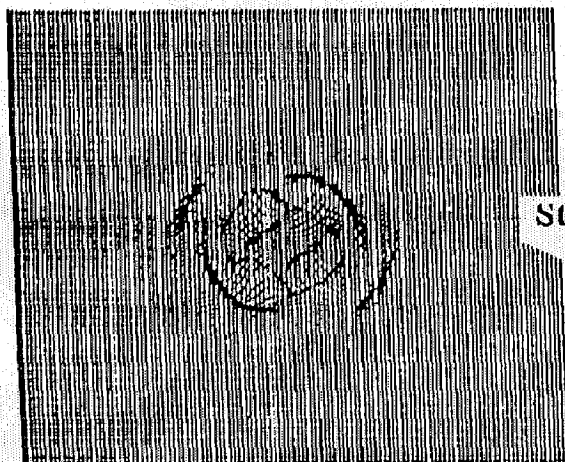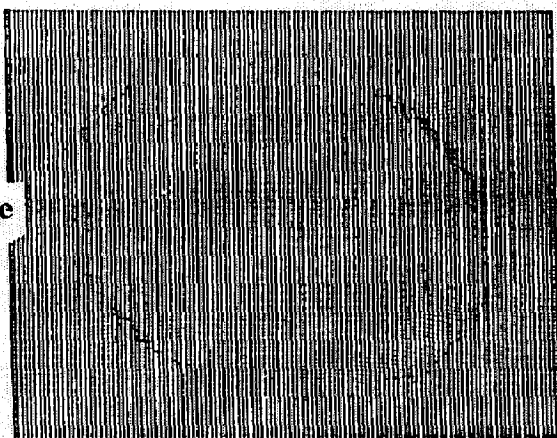
Strike Slip
(b)
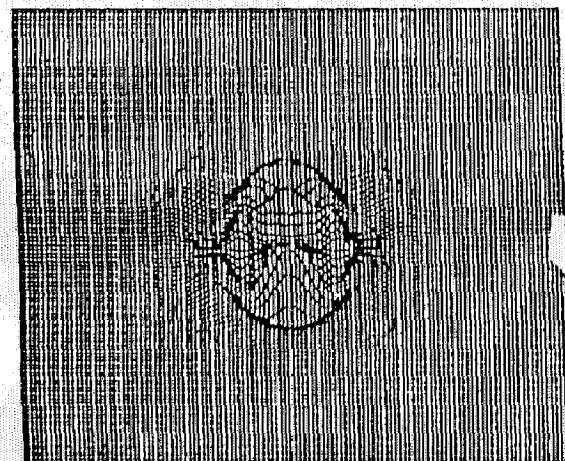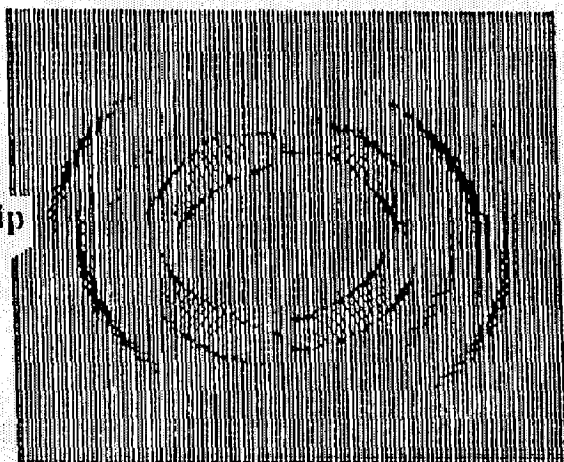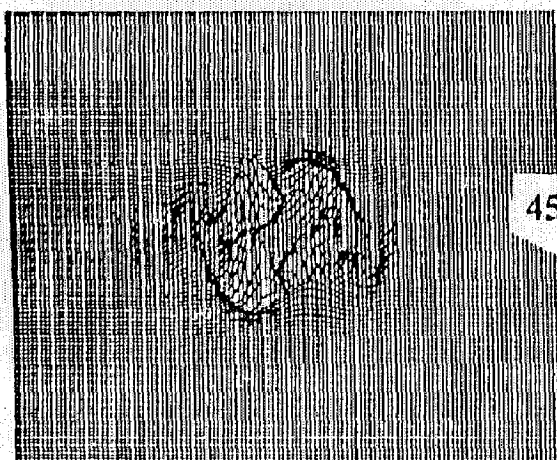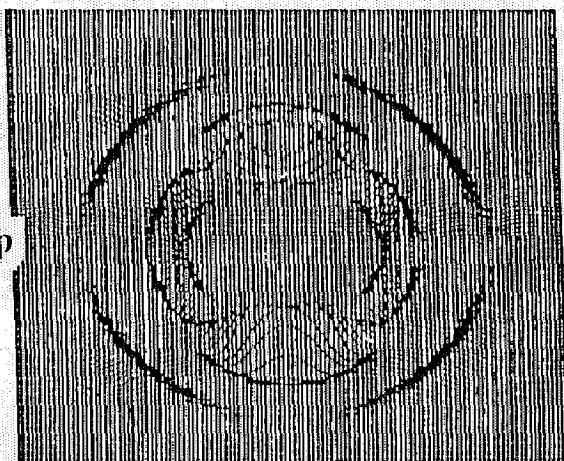
Dip Slip
(c)

45⁰-Dip Slip
(d)
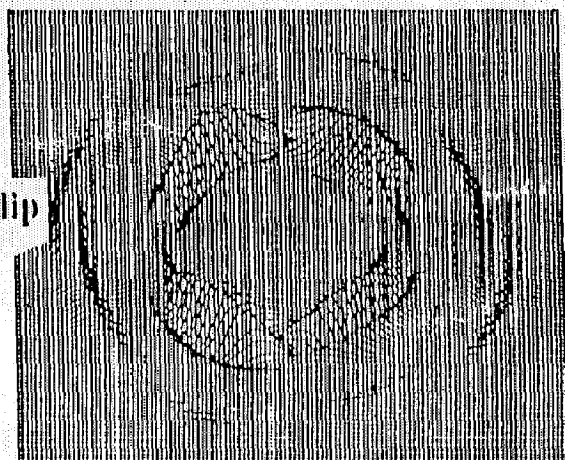
Fig. 3.14 NUMERICAL    SOURCE    HORIZONTAL    RADIATION
PATTERNS FOR P-SV WAVE (AFTER J.P. NARAYAN,
1998)

P-SV waves has been done using the staggering technique of Luo and Schuster (1990) and an algorithm has been developed by Narayan (1998). Vidale (1995 & 1987) developed radiation patterns for different types of sources using numerical method, but his method involves very intricate mathematical calculations also. The radiation patterns found by Vidale have been shown in **Fig.3.12**. The radiation pattern obtained using the recently developed numerical method by J.P. Narayan have been shown in **Figs.3.13** and **3.14**, using the following model parameters:

Rigidity, $\mu = 10$ MPa $= \lambda$

Density, $\rho = 2.5$ g/cc

Comparative study of these radiation patterns for different types of earthquake sources depicts that the numerically computed radiation patterns by Vidale (1985 & 1987) and Narayan (1998) Corroborate with the analytical and observed radiation patterns.

• • •

## 4.1 GENERAL

Scaling relation describes the manner in which characteristics of the ground motion changes with a change in earthquake source parameters namely, stress drop, rupture area, slip and slip-orientation. Most "Seismic" source theories, based on kinematic or quasi dynamic dislocation models predict that the far field displacement spectrum should remain constant at low frequencies and become inversely proportional to some power of frequency at higher frequencies (AKi, 1967; Brune, 1970; Randall, 1973; Madariaga, 1976). Thus three independent parameters specify the far field displacement spectrum: the low-frequency level, the corner frequency defined as the intersection of the low-and high-frequency asymptotes, and the slope co-efficient controlling the rate of high-frequency decay of the spectrum. It has been found that the far-field displacement spectrum is characterized by frequency-invariant amplitudes below the corner frequency and decay of amplitudes at frequencies above the corner frequency. The corner period, the reciprocal of the corner frequency, is proportional to the source duration and is related to the source dimensions. A source scaling relation describes the manner how seismic moment increases with the increase of source duration or the source dimension. For a given Seismic moment, smaller source dimensions would give rise to a shorter source duration, a higher corner frequency and larger amplitudes above the corner frequency. This in turn means an increase in stress drop.

In studies of large earthquakes of the world, it has been found that stress drop is roughly, independent of the seismic moment (Kanamori and Anderson, 1975). This

indicates that $M_o$ (seismic moment) is proportional to the cube of source dimension ($r_o$, equation 3.6, of last chapter). A constant stress drop scaling relation has been confirmed by so many independent studies and has become an accepted model for large and moderate earthquakes. Recently, a constant stress drop pattern was reported for small volcanic events in Italy (De Natale et al., 1987). Same type of constant stress drop patterns were also reported for the after shocks with magnitude about 2 near the Norwegian coast (Chael and Kromer, 1988) and for micro earthquakes with magnitudes less than about 2 observed at Anza, California (Frankel and Wennerberg, 1989). The constant-stress-drop model implies a self-similar rupture process regardless of the scale of seismic events.

But, some studies have showed the results in contrast to the above results. There are evidences of a breakdown in similarity between large and small earthquakes (Chouet et al., 1978; Archuleta, 1986; Fletcher et al., 1986; Fletcher et al., 1984; Archuleta, 1986; Fletcher et al., 1986; Dysart et al. 1988; Glassmoyer and Borcherdt, 1990). In general, a marked decrease in stress drop with decreasing seismic moment, for seismic moment below about $10^{13}$N.M (M<3), has been observed. Fletcher et al. (1986) have shown the seismic moment (1.0 N.M.) as a function of the source radius, bounded by the contours of constant stress drop ($1MPa = 10^6$bar), for Anza (California) earthquakes of smaller magnitudes. The source radii for these events are roughly constant over four orders of magnitude in seismic moment. This constancy of source radii concludes a strong dependence of stress drop on the seismic moment. One reason for this breakdown in similarity is the divergence of the scaling of the peak acceleration and ground velocity from theoretical considerations following the similar relation (McGarr, 1986). Stress drop decreasing with decreasing seismic moment has been observed for small mine tremors all over the world (Gibowicz, 1985; Bicknell and McGarr, 1990). Similarly, the

study made by Gibowicz et al. (1990) has given evidence that for small Seismic events with the seismic moment $10^{11}$-$10^{12}$ N.M, the stress drop is moment dependent.

The non-similar behaviour of small earthquakes has been interpreted as a source effect, involving either an upper limit to the radiated frequency, i.e., the presence of a characteristic fault length, or the dependence of stress on the seismic moment. The change in spectra scaling is explained by attenuation effects or by any process that limits high frequencies, whether it is due to the source, the propagation path, the local site, or the recording instrument. Boore (1986) has shown that a moment-independent filter that attenuates high frequencies, regardless of its origin, produces marked changes in the scaling expected from the usual analysis of self-similar models.

## 4.2  NUMERICAL SCALING STUDIES

In this chapter, it has been tried to observe the effect of variation of source parameter on the change in the characteristics of strong ground motion (SGM) at the surface, i.e., the purpose of this computational work is to verify scaling relations among different parameters of source such as slip, stress-drop, source dimension, dominant frequency and the time-step adopted in the partial stress-drop.

A lengthy and time consuming computational process was required to perform this job using computers. To verify scaling relations, dip-slip source has been used in this work. All those responses which were caused by P-SV wave only have been recorded. The responses were found by successive iteration done by the computers. It was assured that the model should be stable and grid dispersion should be minimum. Also, the absorption of the wave reaching the model edges was ensured. To ensure stable model and minimum grid dispersion, the values of grid size ($\Delta x$) and time step ($\Delta t$) were selected such as to satisfy the following relations:

$$\frac{V_{max} \cdot \Delta t}{\Delta x} \leq \frac{1}{2\sqrt{2}}$$

(4.1)

Equation (4.1) needs assurance that the distance travelled by the wave in time $\Delta t$ with velocity $V_{max}$ must not exceed 0.35 times the grid size $\Delta x$. Since here we have considered only homogeneous models, hence $V_{max}$ is same at each grid point in the model. Again, to ensure full absorption of wave reaching the boundaries of the model, an absorbing boundary at 35 grid point has been implemented. Having ensured that above requirements are satisfied, the models were run with the specifications given for the different cases.

## 4.2.1 EFFECT OF FREQUENCY

### Specifications:

Model Parameters:

| | |
|---|---|
| Type | : Homogeneous |
| Horizontal Extent | : 3000 m |
| Vertical Extent | : 4000 m |
| Receiver | : At Epicentre |
| Density ($\rho$) | : 2.5 g/cc |
| Lame's Parameters | : $\lambda = \mu = 10^7$ N/m$^2$ |
| Shear Wave Velocity | : $Vs = 2000$ m/s |
| P-Wave Velocity | : $Vp = 3464$ m/s |

Source :

| | |
|---|---|
| Type | : Dip-Slip |
| Focal Depth | : 3500 m at the Centre of Model. |
| Maximum Stress Drop | : $10^7$ N/m$^2$ |

To ensure stability and to avoid grid-dispersion, square grids of size 10m×10m and time step (Δt) equal to 0.0015 second were selected. The partial stress drop in the form of Ricker wavelet was implemented in the model. The response at the epicentre has been computed for a maximum time of 3.0 second. Program has been run for different frequencies of Ricker wavelet, such as 20,17,14,11,8 and 5 Hz. Having run the program with the input values as mentioned above, we got output as particle displacement (cm) and Stresses (N/m$^2$, in X- direction and X-Z plane) for different frequencies. The final results have been shown in graphical form in **Figs 4.1, 4.2,** and **4.3.**

**Conclusions**

From **Fig.4.1,** showing the graph of particle displacement (cm) Vs. time (second), we can conclude the following facts :

i)      The maximum amplitude of particle displacement increases with the increase in frequency. Though this conclusion seems wrong while viewing the graph with the highest selected frequency equal to 20 Hz, yet this misleading result is due to high dispersion which could not be avoided owing to the limitations of the computational facilities.

ii)     As frequency is increasing, the arrival time of wave is decreasing. The decrease in arrival time with increase in frequency is due to implementation of wavelet at a faster pace. But explanation of increase in amplitude with frequency needs detail analysis. However, it may be due to divergence effect or may be due to the implementation of stress drop at a faster pace. It is found that only displacement due to the shear component is increasing with increase of frequency.

42

iv)     The higher the frequency content, the greater is the chance of dispersion.

From **Fig 4.2**, showing the graph of stress ($N/m^2$, normal stress in X-direction) Vs. time (second); following facts can be concluded:

i)      The amplitude of stress is increasing with frequency.

ii)     With the increase in frequency, some higher amplitudes of stress is visible before the maximum amplitude, at much earlier time-step.   It may be due to the compressional wave.

iii)    The maximum amplitude of stress is observed at much earlier time-step with increasing frequency.

iv)     The amplitude of stress with higher frequency is seen higher at all times.

v)      With increasing frequency, amplitude of stress is visible for larger duration.

From **Fig 4.3** , showing a graph of stress ($N/m^2$, shear stress in X-Z plane) Vs. time (second), following conclusions have been drawn:

i)      The maximum amplitude of stress increases as the frequency increases.

ii)     The duration of stress increases with increasing frequency.

iii)    Some higher amplitudes of stress are visible before the attainment of maximum amplitude in case of higher frequencies.

iv)     The amplitude of stress is higher at all times with increasing value of frequency.

Fig. 4.1 PARTICLE DISPLACEMENT AT THE EPICENTRE DUE TO DIFFERENT DOMINANT FREQUENCY OF DIP-SLIP SOURCE

44

Fig. 4.2 NORMAL STRESS IN X-DIRECTION AT THE EPICENTRE DUE TO DIFFERENT DOMINANT FREQUENCY OF DIP-SLIP SOURCE

45
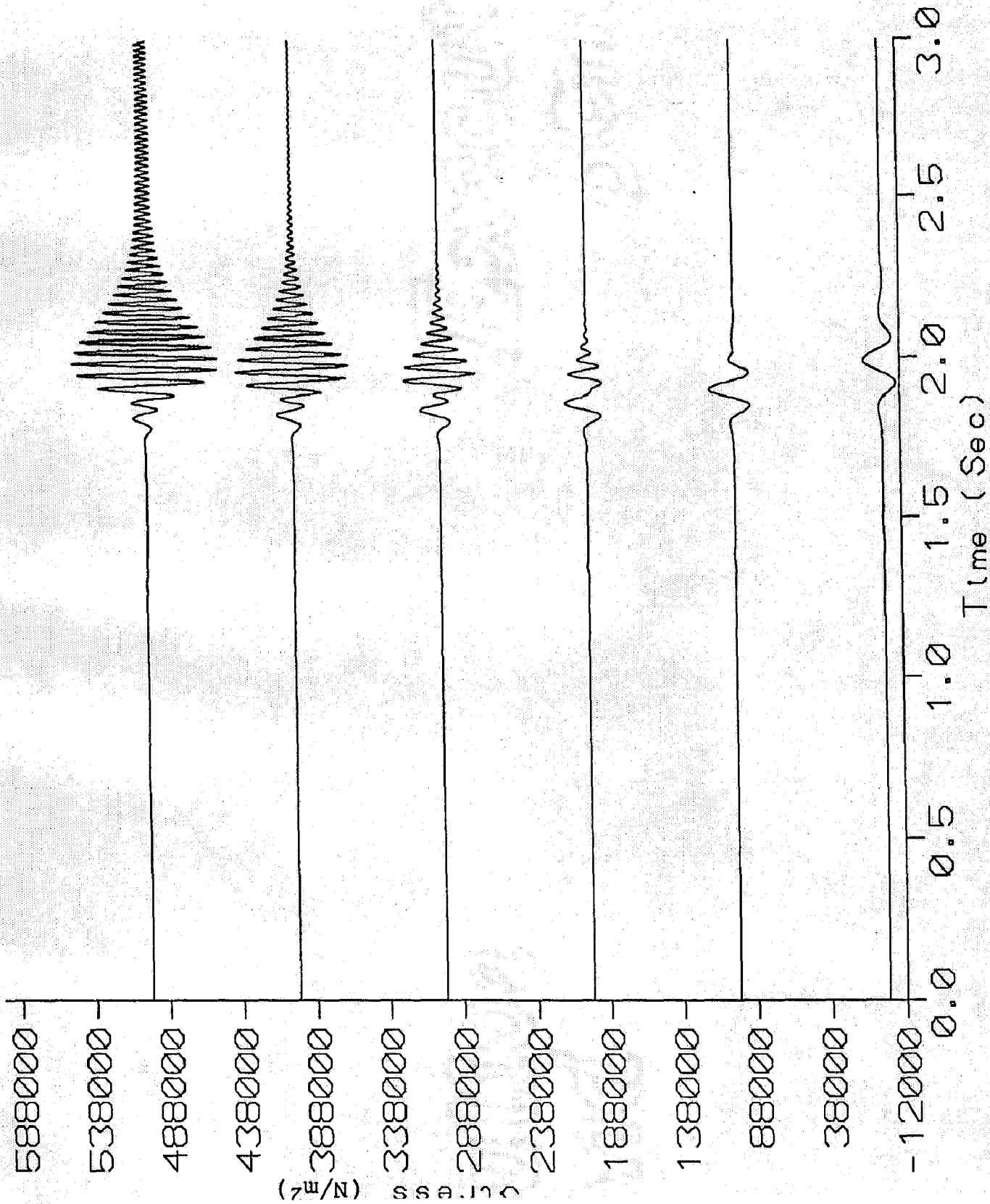
Fig. 4.3 SHEARSTRESS IN X-Z PLANE AT THE EPICENTRE DUE TO DIFFERENT DOMINANT FREQUENCY OF DIP-SLIP SOURCE

### 4.2.2 Effect of Stress Drop ($\Delta\sigma$)

**Specifications :**

i) Model:

| | |
|---|---|
| Type | : Homogeneous |
| Horizontal Extent | : 3000 m |
| Vertical Extent | : 4000 m |
| Receiver | : At Epicentre |
| Density ($\rho$) | : 2.5 g/cc |
| Lame's Parameters | : $\lambda = \mu = 10^7$ N/m$^2$ |
| Shear Wave Velocity | : Vs = 2000 m/s |
| P-Wave Velocity | : Vp = 3464 m/s |

ii) Source :

| | |
|---|---|
| Type | : Dip-Slip |
| Focal Depth | : 3500 m at the Centre of Model. |
| Frequency | : 5 Hz |

To provide stability and to avoid grid dispersion, square grids of size 10m×10m and time-step ($\Delta t$) equal to 0.0015 second were selected. The partial stress drop in the from of Ricker wavelet was implemented in the model. The response has been computed for a maximum time of 3.0 second. The responses have been computed for different values of maximum stress drop, such as 10,13,16,19,22 and 25 MPa.

The output of the computations are found as particle displacement (cm) amd stresses in two directions (normal stress in X-direction and shear stress in X-Z plane, in N/m$^2$). The final results have been shown in **Figs.4.4, 4.5,** and **4.6** in graphical form.

47

## Conclusions

From **Fig.4.4**, showing the graph of displacement (cm) Vs. time (second), following facts can be interpreted:

i)   The maximum amplitude of particle displacement increases with the increase in stress drop ($\Delta\sigma$).

ii)  The amplitude of particle displacement increases with increase in stress drop at all time steps in the range of visible particle displacement amplitude.

iii) The duration of particle displacement is independent of the magnitude of stress drop.

From **Fig.4.5**, showing the graph of stress ($N/m^2$, normal stress in X-direction) Vs. time (second), following conclusions can be drawn:

i)   The maximum amplitude of stress increases with increasing stress drop.

ii)  The total duration of stress is independent of the magnitude of applied stress drop.

iii) In the visible range of stress, increase in applied stress drop increases the value of stress at all time steps.

From **Fig.4.6**, showing graph of stress ($N/m^2$, shear stress in X-Z plane) Vs. time (second), following points can be interpreted:

i)   The maximum amplitude of stress is found in case of maximum applied stress drop.
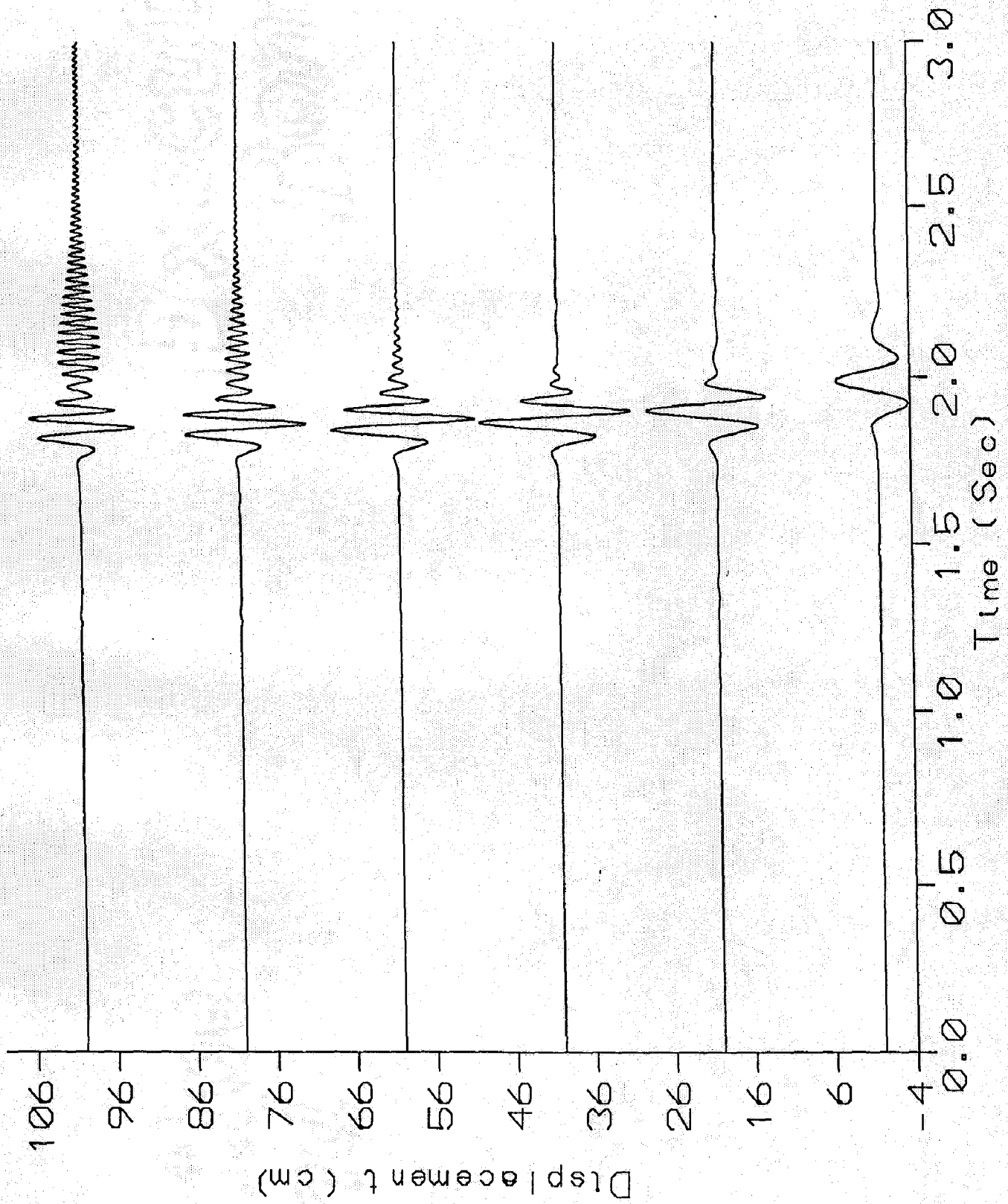
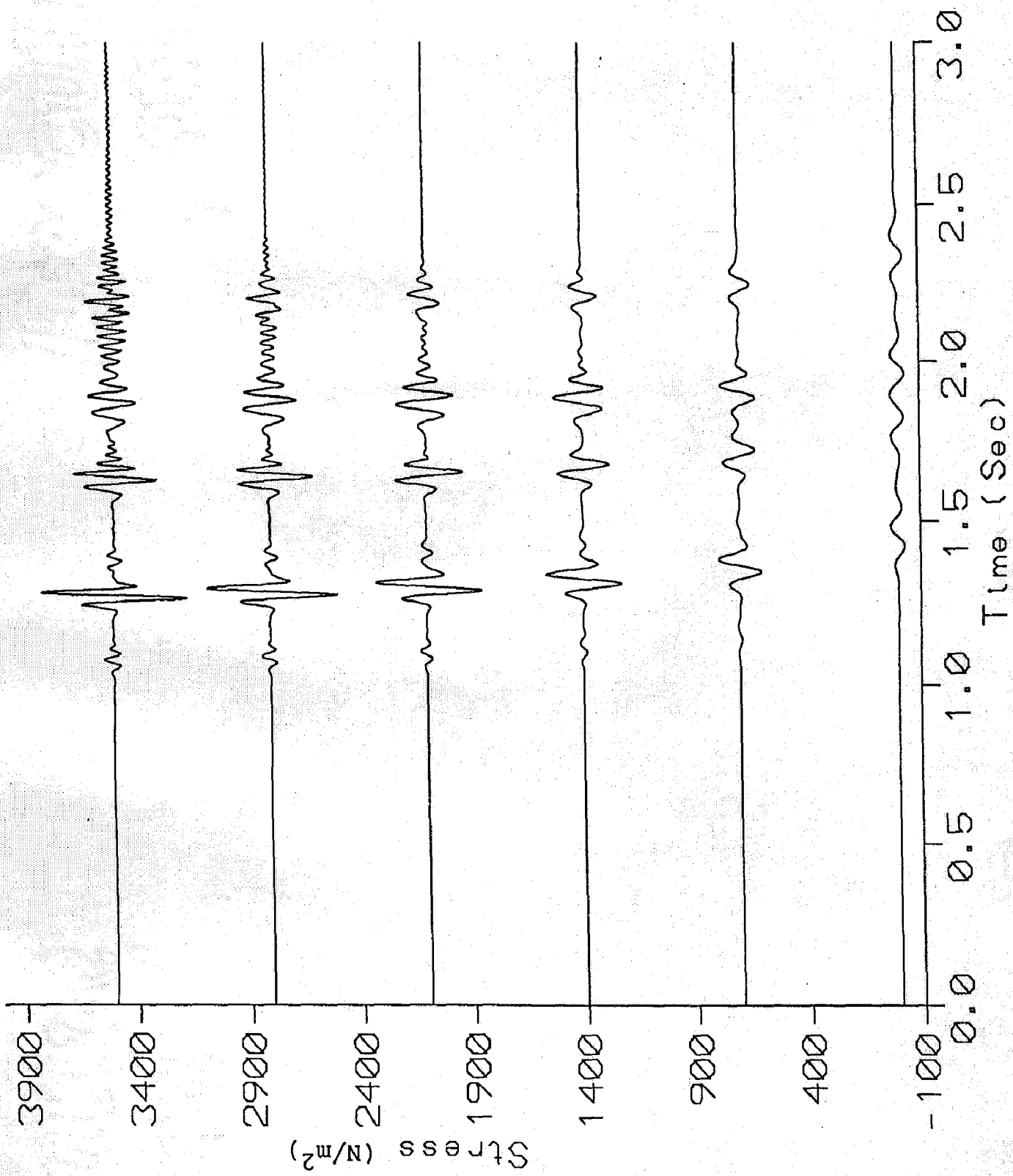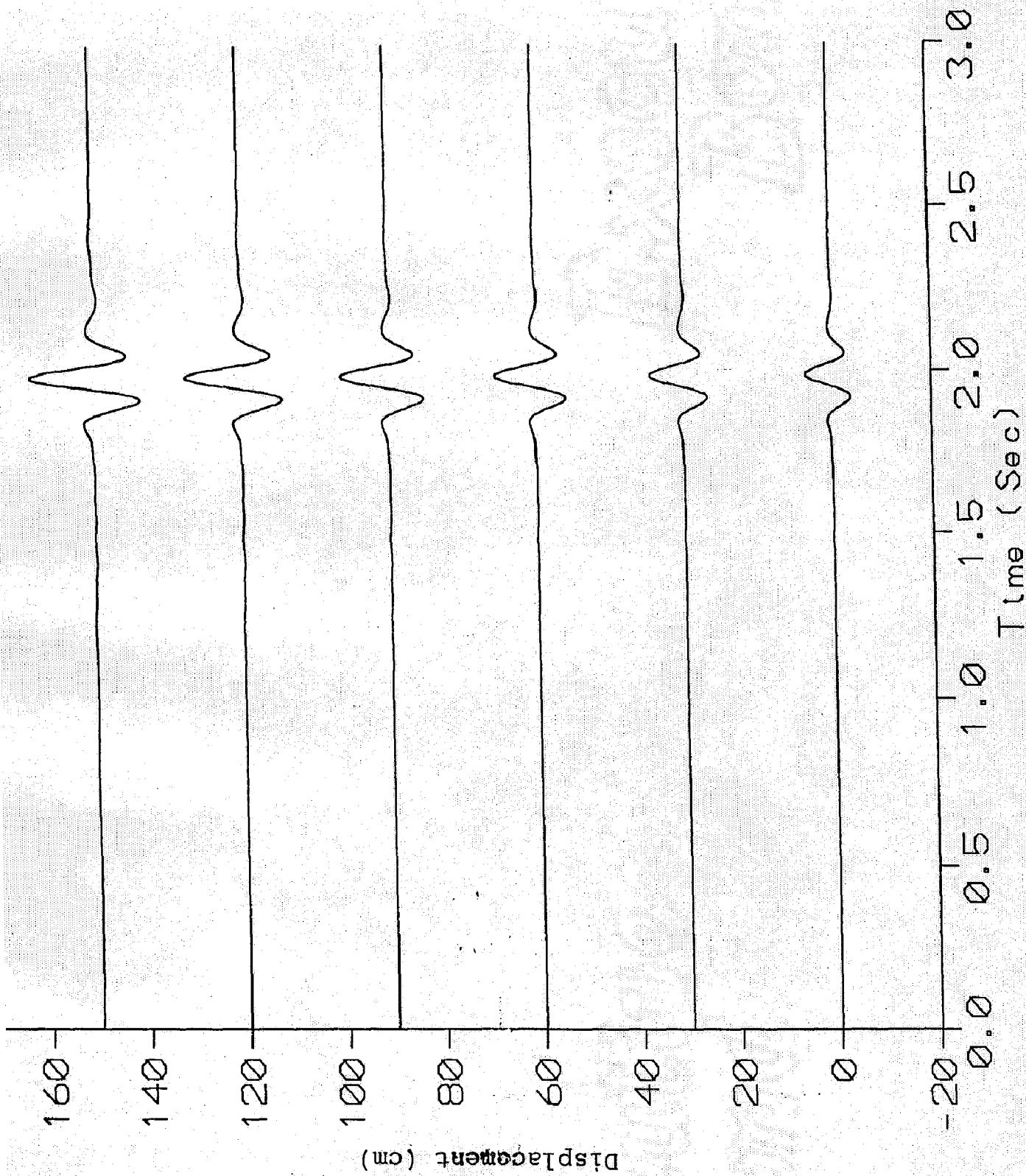Fig. 4.4 PARTICLE DISPLACEMENT AT THE EPICENTRE DUE TO DIFFERENT STRESS-DROP OF DIP-SLIP SOURCE

49
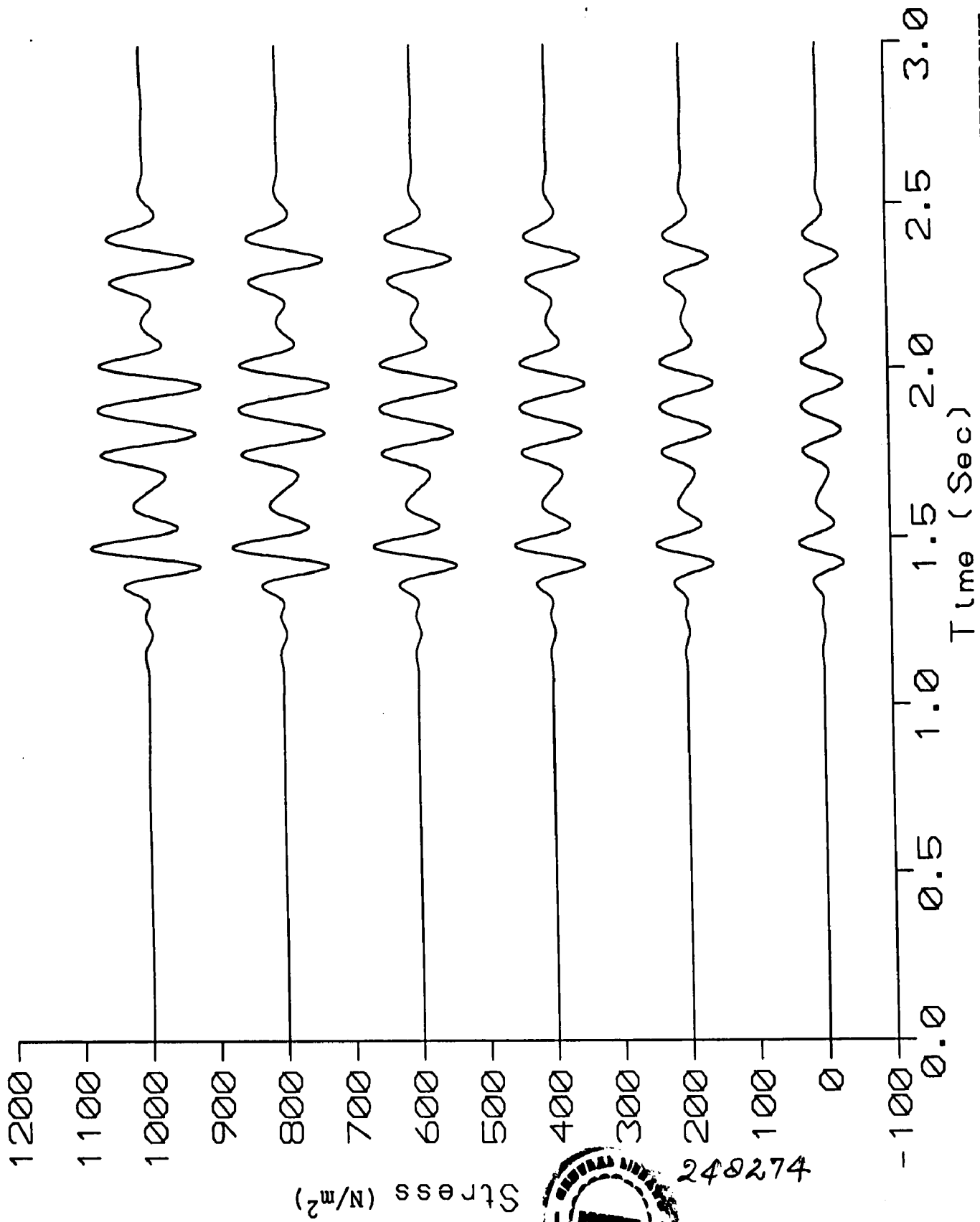
Fig. 4.5  NORMAL STRESS IN X-DIRECTION AT THE EPICENTRE DUE TO DIFFERENT STRESS-DROP OF DIP-SLIP SOURCE

50
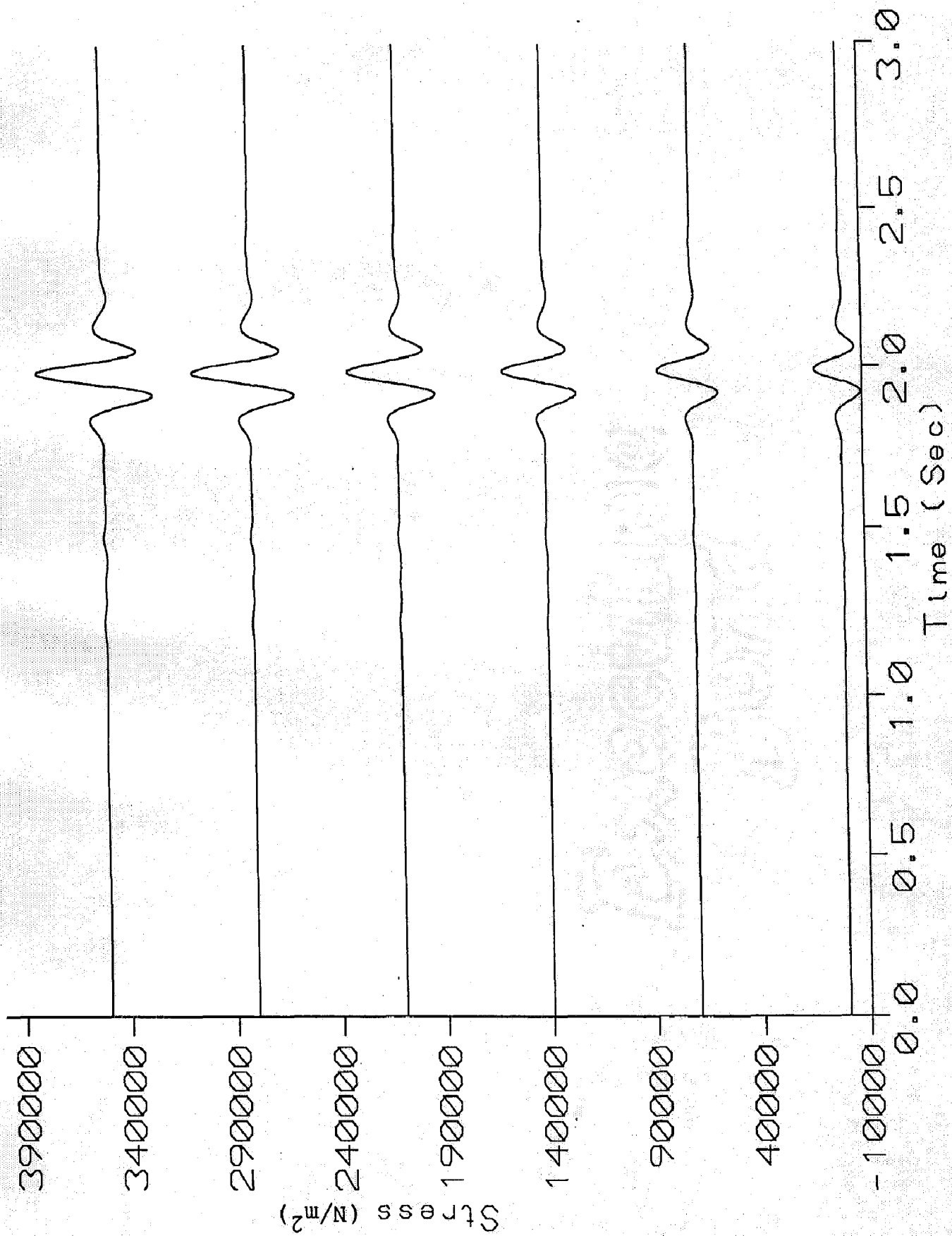
Fig. 4.6 SHEAR STRESS IN X-Z PLANE AT THE EPICENTRE DUE TO DIFFERENT STRESS-DROP OF DIP-SLIP SOURCE

ii)     The duration of the amplitude of stress is independent of the magnitude of applied stress drop.

### 4.2.3  Effect of Time-Step (Δt)

**Specifications :**

i)   Model:

|                      |                                                                              |
|----------------------|------------------------------------------------------------------------------|
| Type                 | : Homogeneous                                                                |
| Horizontal Extent    | : 3000 m                                                                     |
| Vertical Extent      | : 4000 m                                                                     |
| Lame's Parameters    | : $\lambda = 10^7 \text{N/m}^2 = \mu = 1.2 \times 10^7 \text{N/m}^2$         |
| Receiver             | : At Epicentre                                                               |
| Density ($\rho$)     | : 3.0 g/cc                                                                   |
| Shear Wave Velocity  | : Vs = 2000 m/s                                                              |
| P-Wave Velocity      | : Vp = 3366.5 m/s                                                            |

ii)   Source :

|             |                                    |
|-------------|------------------------------------|
| Type        | : Dip-Slip                         |
| Focal Depth | : 3500 m at the Centre of Model.   |
| Frequency   | : 5 Hz                             |

To ensure stability and to avoid grid-dispersion, square grids of size 10m×10m and different values of time-step (Δt) were selected, such as 0.001, 0.0012, 0.0015 and 0.0018 second. The partial stress drop was implemented in the form of a Ricker wavelet. The responses were computed for a maximum time of 3.0 second.

The output of the computation are particle displacement (cm) and stresses in two directions (N/m$^2$, normal stress in X-direction and shear stress in X-Z plane). The final results have been shown in **Figs.4.7,4.8,** and **4.9** in graphical form.
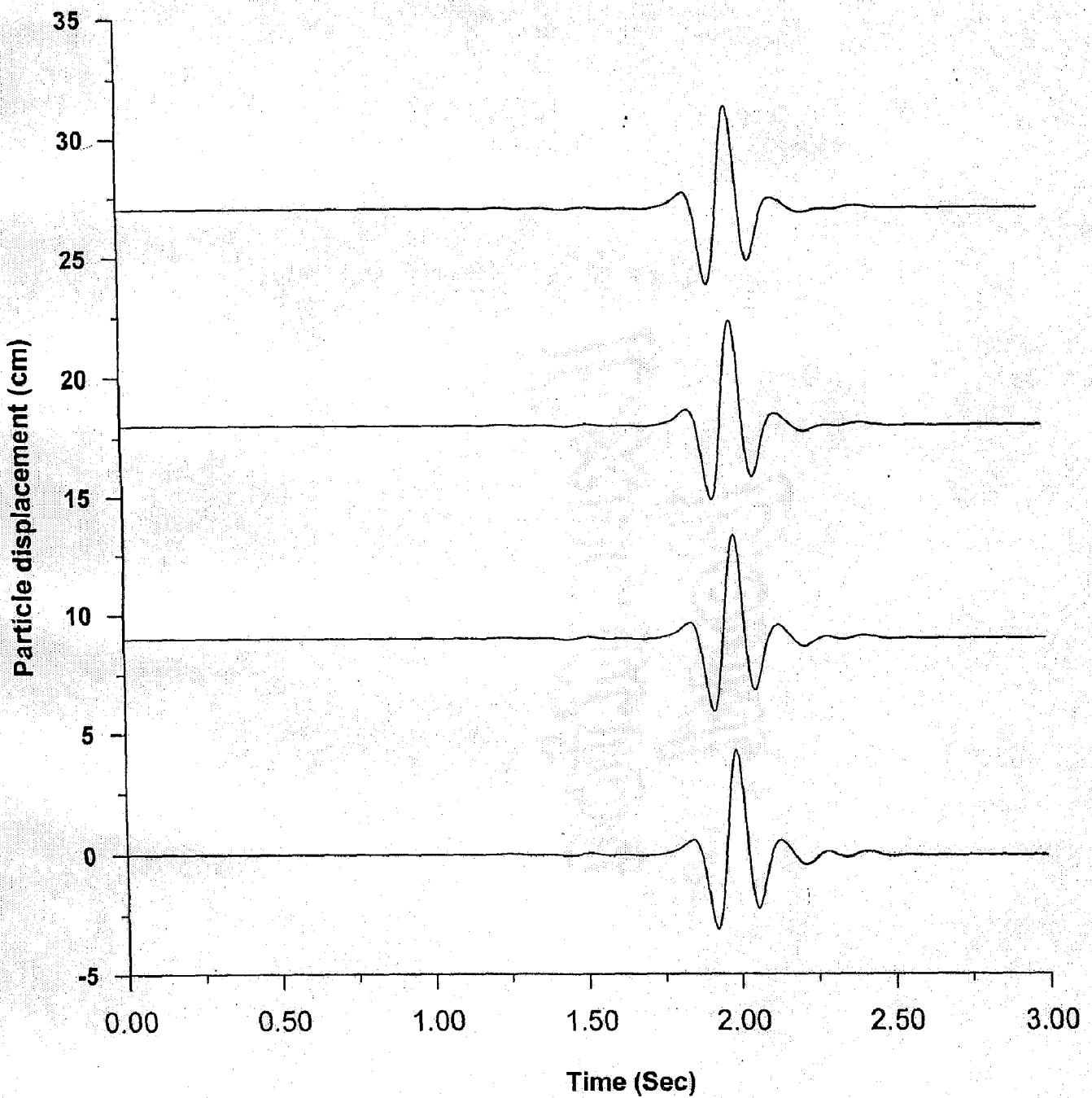
Fig. 4.7 PARTICLE DISPLACEMENT AT THE EPICENTRE DUE TO
DIFFERENT TIME STEPSOF PARTIAL STRESS DROP FOR
DIP-SLIP SOURCE

53

Fig. 4.8 NORMAL STRESS IN X-DIRECTION AT THE EPICENTRE
DUE TO DIFFERENT TIME STEPS OF PARTIAL STRESS
DROP FOR DIP-SLIP SOURCE
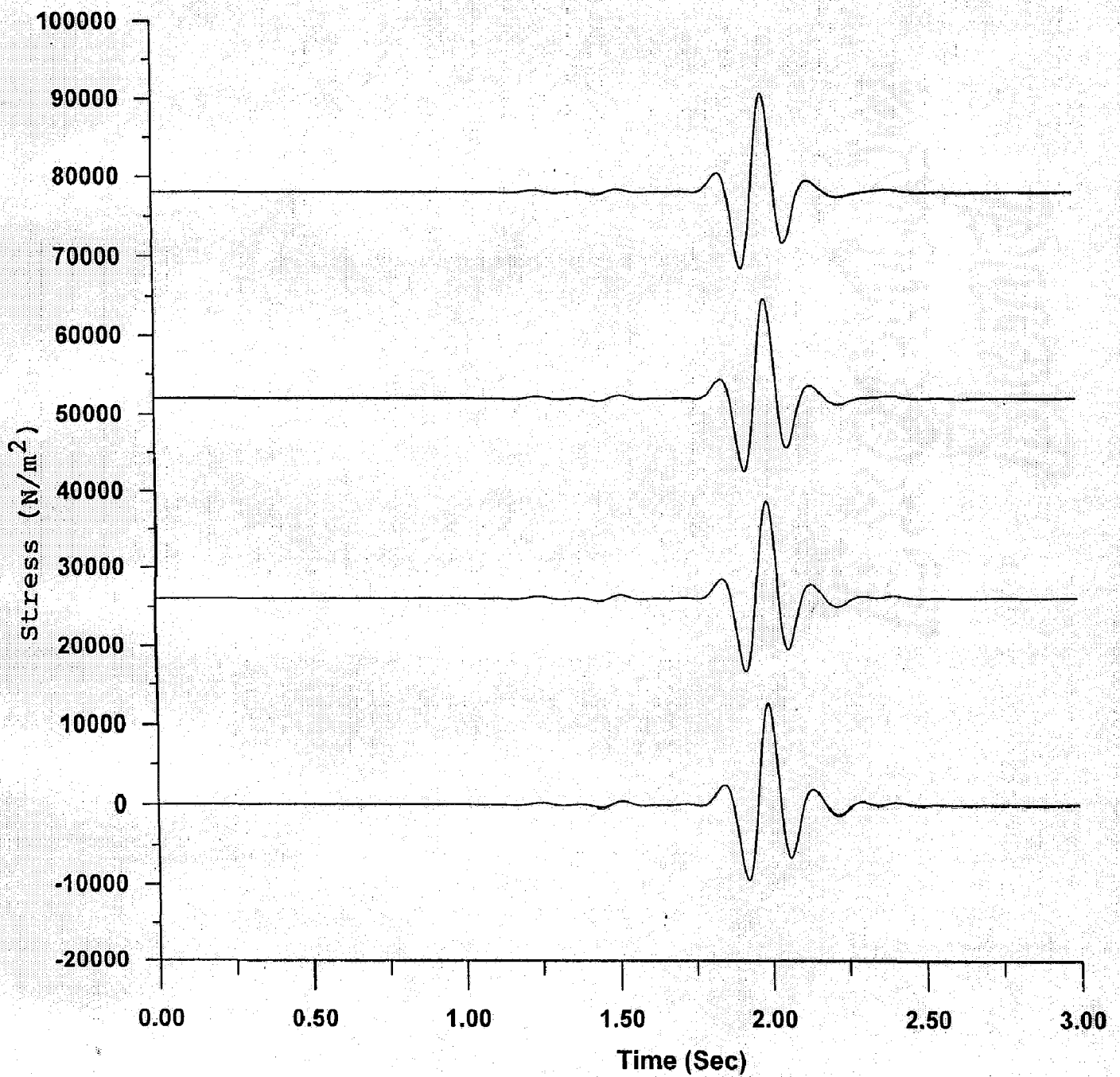
Fig. 4.9 SHEAR STRESS IN X-Z PLANE AT THE EPICENTRE DUE TO DIFFERENT TIME STEPS OF PARTIAL STRESS DROP FOR DIP-SLIP SOURCE

55

**Conclusions :**

Following interpretations have been drawn from these graphs:

i)    The amplitude and duration of particle displacement is independent of the used value of time-steps **(Fig.4.7)**

ii)   Slight decrease in the amplitude of normal stress in X-direction has been observed with decreasing value of time-step ($\Delta t$), though the duration of stress is unaffected by the time-step ($\Delta t$) **(Fig.4.8)**.

iii)  Almost zero effect of change of time step ($\Delta t$) has been found on both the amplitude and duration of shear stress in X-Z plane, though slightly higher amplitude of stress is seen with higher values of time-step before the demise of stress amplitude **(Fig.4.9)**.

## 4.2.4 Effect of Slip ($\bar{u}$) :

**Specifications :**

i)    Model :

|  |  |
|---|---|
| Type | : Homogeneous |
| Horizontal Extent | : 3000 m |
| Vertical Extent | : 4000 m |
| Receiver | : At Epicentre |
| Density ($\rho$) | : 2.5 g/cc |
| Lame's Parameters | : $\lambda = \mu = 10^7$ N/m$^2$ |
| Shear Wave Velocity | : $V_s = 2000$ m/s |

ii)   Source :

|  |  |
|---|---|
| Type | : Dip-Slip |
| Focal Depth | : 3500 m at the Centre of Model. |
| Frequency | : 20 Hz |

Grid size ($\Delta x$) and time-step ($\Delta t$) have been chosen as 10m×10m and 0.0015 second respectively. These selected values satisfy the equation of stability and ensure that grid dispersion must not occur. The slip has been computed using following relation:

$$\Delta\sigma = \frac{7}{8} \times \frac{1}{2.34} \times \pi^2 \times \frac{\bar{u}\mu f_s}{\beta_0}$$

$\Delta\sigma$ = Stress drop = $10^6$ N/m$^2$

$\bar{u}$ = Slip (m)

$\mu$ = Lame's Parameter (N/m$^2$)

$f_s$ = Dominant frequency of source = 20 Hz

$\beta_0$ = Shear wave velocity = 2000 m/s

The values of Lame's parameter ($\mu$), material density ($\rho$) and corresponding slip ($\bar{u}$) have been tabulated in Table 4.1.

## TABLE 4.1

### Values of Lame's Paramerer ($\mu$), Material Density ($\rho$) and Corresponding Slip ($\bar{u}$)

| SL.NO. | LAME'S PARAMETER $\mu$ (N/m$^2$) | MATERIAL DENSITY $\rho$ (g/cc) | SLIP $\bar{u}$ (m) |
|--------|-----------------------------------|--------------------------------|--------------------|
| 1 | $12 \times 10^6$ | 3.0 | 2.26 |
| 2 | $11.6 \times 10^6$ | 2.9 | 2.34 |
| 3 | $11.2 \times 10^6$ | 2.8 | 2.42 |
| 4 | $10.8 \times 10^6$ | 2.7 | 2.51 |
| 5 | $10.4 \times 10^6$ | 2.6 | 2.61 |
| 6 | $10.0 \times 10^6$ | 2.5 | 2.71 |
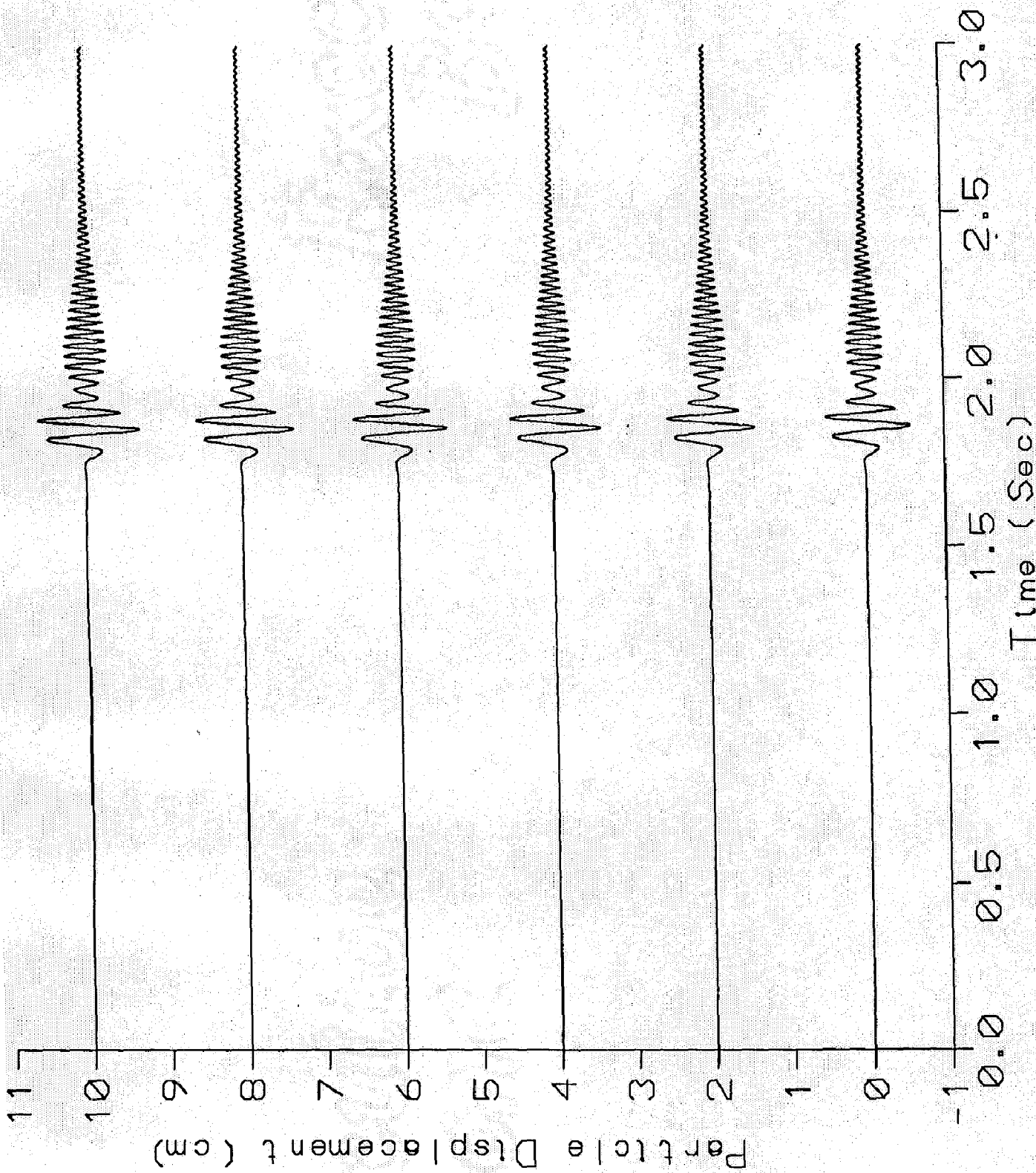
Fig. 4.10 PARTICLE DISPLACEMENT AT THE EPICENTRE DUE TO DIFFERENT SLIP OF DIP -SLIP SOURCE
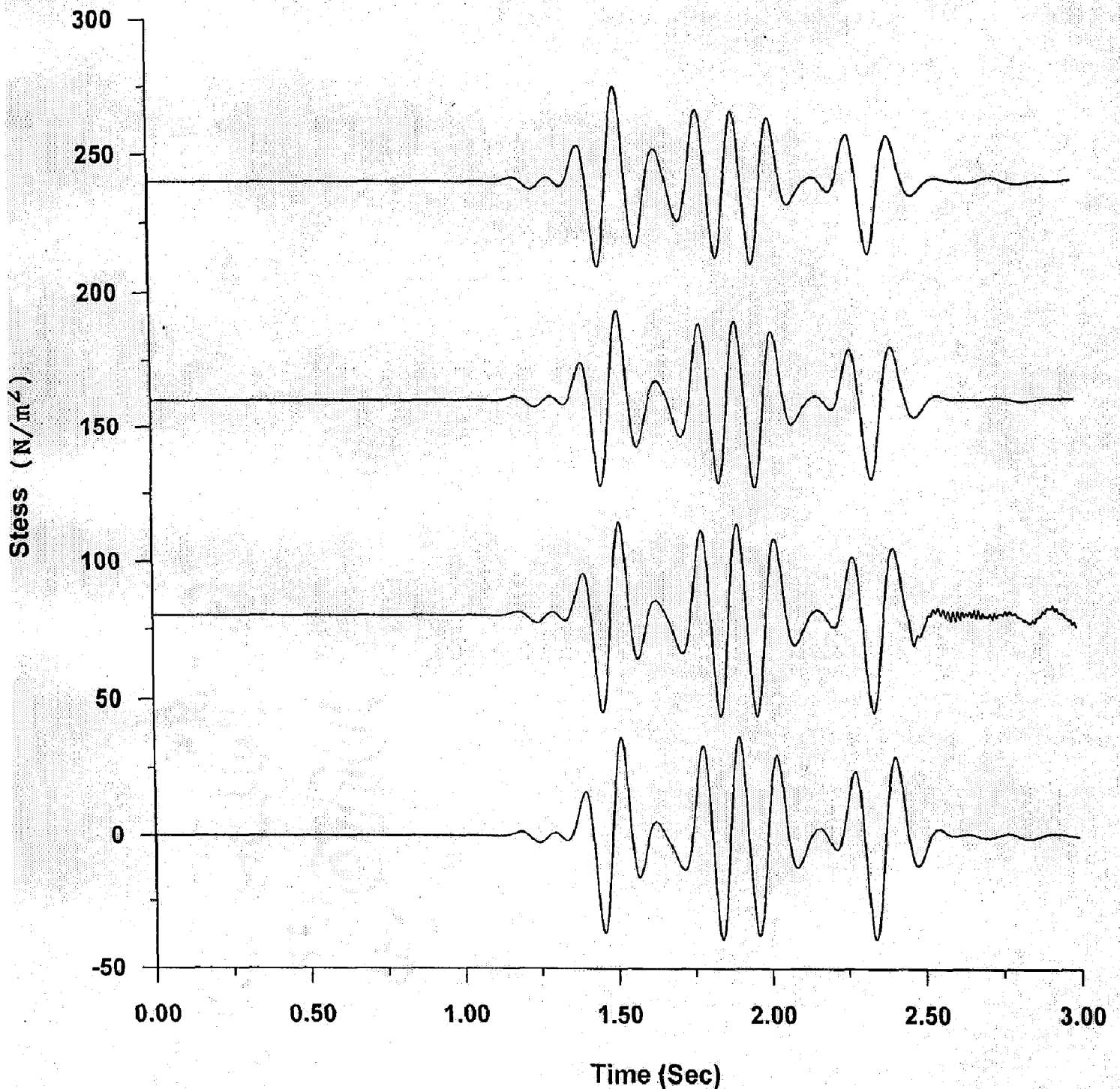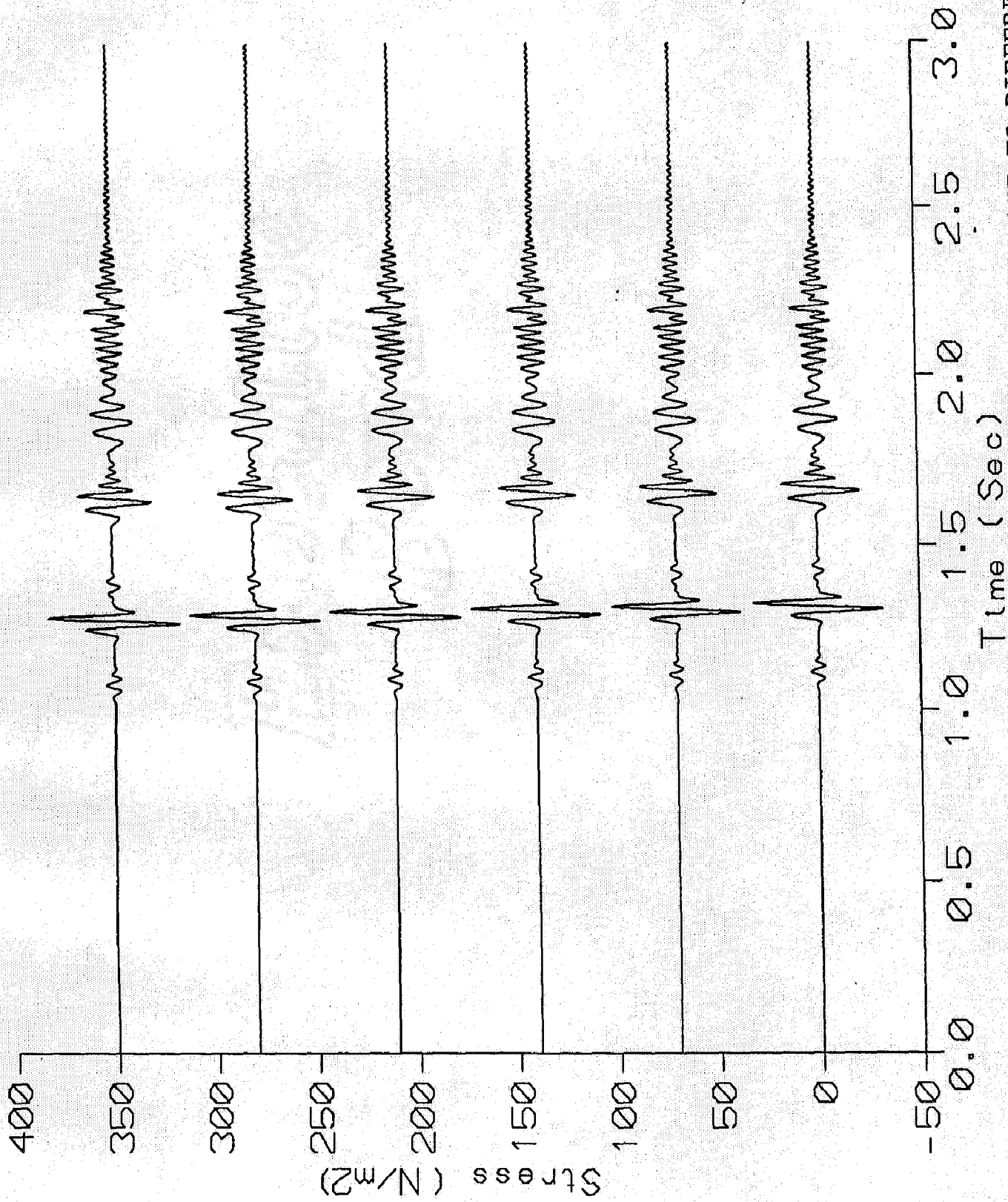
Fig. 4.11 NORMAL STRESS IN X-DIRECTION AT THE EPICENTRE DUE TO DIFFERENT SLIP OF DIP-SLIP SOURCE
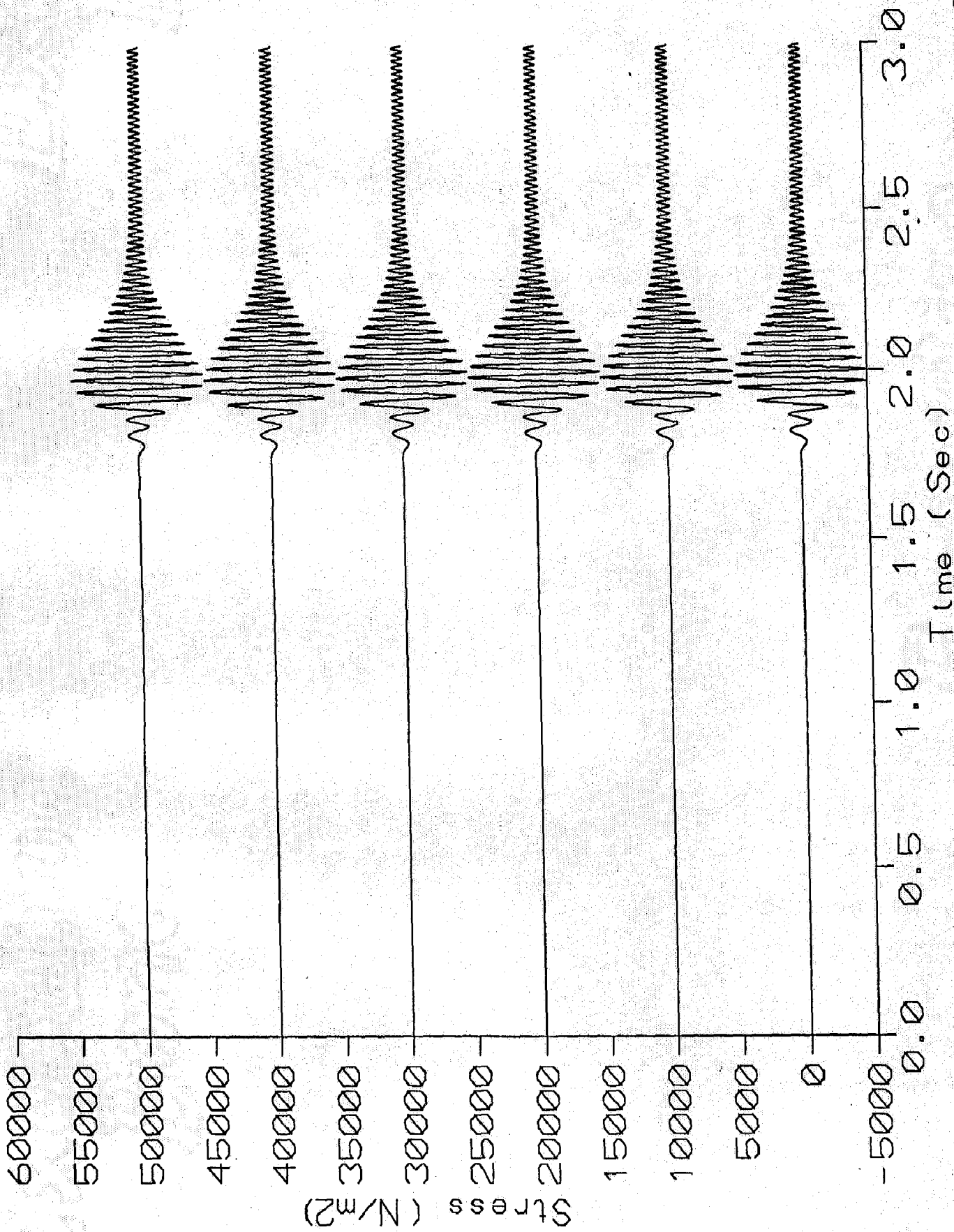
Fig. 4.12 SHEAR STRESS IN X-Z PLANE AT THE EPICENTRE DUE TO DIFFERENT SLIP OF DIP-SLIP SOURCE

Here, again the partial stress drop was implemented in the form of Ricker wavelet. Responses were computed for a maximum time of 3.0 second.

After running the program, we get the responses as particle displacement (cm) and stresses (N/m$^2$, normal stress in X-direction, and shear stress in X-Z plane), at each time-step. These results have been shown in **Figs.4.10,4.11**, and **4.12** in graphical form. Seeing these graphs, following points can be concluded :

**Conclusions :**

i) Though the graph of particle displacement (cm) Vs. time (second) shows almost nil effect of fault slip on the particle displacement, yet this graph does not seem conclusive owing to high dispersion seen in the graph. That is why, we are not so sure about the effect of slip ($\bar{u}$) on the particle displacement **(Fig.4.10)**.

ii) Similarly, the graphs of stresses (N/m$^2$, in two directions) Vs. time (second) show no effect of slip ($\bar{u}$) on these stresses, but we can not be so sure about this conclusion because we could not avoid grid dispersion precisely **(Figs.4.11 and 4.12)**.

Hence, though we see no effect of variation of slip ($\bar{u}$) on the particle displacement and stresses, yet this conclusion is not very dependable because of the high dispersion seen in the graph. This dispersion could have been avoided, had there been highly sophisticated computational facilities available. Owing to the computational memory limitation and its speed, distinct graphs without dispersion could not be found.

● ● ●

## 5.1 GENERAL

In this chapter, we shall discuss applications of numerical modelling in study of the characteristics of the strong motions, produced from earthquakes. Here, the effect of up going source energy incident on basins has been investigated. Many large cities are located on or near alluvial valleys. The curvature of a basin in which softer alluvial soil is deposited, can trap body waves and cause some incident body waves to propagate through the alluvium as surface waves (Vidale and Helmberger, 1988). These waves can produce stronger shaking and longer duration than that of the values predicted by one-dimensional analysis, which considers only vertically propagating S-waves.

One of the other puzzling features in strong motion seismograms is the noticeably long duration of high-frequency P-waves in sedimentary basins. The P-waves are seen to rotate onto the vertical component in the strong velocity gradient near the surface (Lui and Helmberger, 1985). The latter portion of these records are generally depleted in low frequency. Thus, it can be concluded that there are propagational wave guides that preferentially prolong high frequency motions. This prolonged high frequency motions are displayed by non-planer surface layering.

In basins, the S-waves that dominate the horizontal motions generally do not show the strong ringing nature associated with the P-waves. Also, the higher frequency content of the P-waves relative to the S-waves is quite apparent which is a property of many basins. Though the difference in frequency content of P- and S- waves is not easily explained, yet it may be that this difference is caused by different source histories for P- and S- waves (Hanks and McGuire, 1981).

King and Tucker (1984) measured ground motions along transverse and longitudinal profiles across the Chusal valley near the Afghanistan border of former Soviet Union. Interpretation of their responses in a series of small earthquakes (M≤4.0) suggested that one dimensional ground response analysis could predict the average response of sediments near the centre of the valley but not at edges. Significant difference between the amplification functions at the centre and edges of the valley were observed, explaining why the motion at those locations were considerably different. Similar effects have been observed for other valleys (e.g., Caracas in 1967, San Fernanda in 1970, and Leninakan Armenia in 1988) in different earthquakes.

Recently, a study made in the city of Brisbane (Australia) has revealed the significant effects of basin geometry and the mode conversion on the characteristics of the strong ground motion. In this study a 2D geological model based on a 20×20 Km area of the city of Brisbane, which is situated on the east coast of Australia, was selected. Near-surface layers of this basin consisted of unconsolidated sediments, and thus, this region, was prone to site amplifications. Four sites were chosen in this study, three of them lie on sediments and one is situated on bed rock. The geology was laterally variable, notably under the sediment sites, and significant difference in the spectral ratios between these sites were observed. After study by Fabien Coutel and Peter Mora (1988), it was found that site situated on bedrock near the basin edge has almost no site amplification; in contrast to site which lies on sediments on the basin. In case of site situated at the edge of the basin, both 1D and 2D responses for site were plotted for two incidence angles. For vertical incidence the fundamental frequency found using SBSR (Sediment-to-Bedrock Spectral Ratio) method was slightly higher than that of the values found using 1D response, but larger differences were encountered for higher harmonics. These

differences were even more noticeable for the 45° incidence angle . This difference was explained by the geometry of the basin in this area that consisted of dipping layers, where complex reflections and refractions occur. These discrepancies observed between the different methods demonstrate the limitations of 1D modelling and the influence of 2D effects. But, in case of site situated in the middle of the basin where sediments consisted of nearly horizontal plane layers, all adopted methods revealed considerable similarity especially for the resonant frequencies. In this case very good agreement between the 1D and 2D results were founds which showed 1D response and 2D response predicting the same resonant frequencies and similar amplitude level (notably for vertical incidence angle). Hence, notable differences in site amplification (for resonant frequencies and peak amplitude) were observed between the edge and the centre of the basin, showing the limitation of 1D modelling as a basis for predicting site amplifications.

Again, on the same basin in the city of Brisbane (Australia), 2D models were prepared for narrow and large basins. The first model had a shape ration of 0.35 (narrow basin) while the second model had a rather extreme shape ratio of 0.12 (very large basin). Shape ratio is defined as the ratio of the maximum thickness of sediments 'h' to the valley half width 'l' (Bard and Bouchon, 1985). It was found that in case of a narrow basin, 2D effects are important. A huge difference in amplification between the middle and near the edge of the basin was observed. For vertical incidence, the amplification factor was close to 10 for the fundamental frequency, i.e., two times the amplification predicted by the 1D response. In addition, although the 2D response gave a slightly higher fundamental resonant peak than the 1D response, higher modes disagree. For site situated in the middle of the basin, the fundamental resonant frequency and the 1D response agreed, but the peak amplitudes did not agree. These differences were explained by the shape of the

64

basin that focusses waves toward the basin centre. such "focussing effects" could be responsible for large amplification factors.

Thus, these experiments showed that 2D effects such as basin edge effects and focussing effects greatly influence the site response. Strong variations were noted in the site amplification spectrum (frequencies and amplitude) as a function of basin structure and incidence angle of the incoming waves, partially at the edge of the basin. So, it was concluded in this study that estimation of site amplification spectra using observational methods yield unreliable or incorrect results when sub-surface basin structure is present.

## 5.2 STRONG GROUND MOTION (SGM) SIMULATION IN BASIN USING 2D SHEAR DISLOCATION SOURCES

The characteristics of earthquake shaking at a given site during a particular event depends on a number of factors such as, the source mechanism, the distance and the geological characteristics of the rocks from the source to site, wave interference and local soil conditions at the site. The effects of local site conditions on the characteristics of SGM have been the focus of research by both seismologists and earthquake engineers. The analysis of source mechanism and effect of path on waves is an important area of seismology. We have seen the erratic characteristics of SGM on or near the basin as studied by many scientists using explosive sources. Here, further an extensive study has been made to know the characteristics of strong ground motion in basin environments, using shear dislocation sources based on partial stress drop in the form of Ricker wavelet, a realistic approach. The aim of 2D basin simulation using shear dislocation source is to define design earthquakes. Since practical engineering applications have mainly relied on one dimensional analysis to predict surface motions, overlooking the effects of surface topography

and lateral effect of soils in basins. In this time domain modelling, the amplitude and duration can be computed directly and frequency can be obtained by converting the time domain response in frequency domain. Thus, all the three characteristics can be computed in contrast to response spectra, which do not provide information about duration. The study made in this thesis report is confined to know the effects of following two parameters on the characteristics of strong ground motion. These two parameters under study are,

    i)    Effect of basin geometry, and

    ii)    Effect of the position of source below the basin.

As we have already come to know the considerable effects of basin geometry on the characteristics of strong ground motion, here we shall see one other parameter, i.e., the position of the source and its effects on the ground motion characteristics.

## 5.2.1 Specifications of Models :

In this study, we have used four different geometries of the basins. These four basins have been named as : Basin1, Basin2, Basin3 and Basin4. **Figs.5.1,5.2,5.3** and **5.4** show the geometry of all these four basins. Each basin has been simulated with two different positions of source. The first position of source is just below the centre of the basin, whereas the second position of the source is at an offset of 4200 m from the centre of the basin. Both these sources have been placed at a depth of 8000 m from the free surface. Since each basin has been modelled with two different positions of source, hence with four basins we have altogether eight models to study. Different dimensions of these models have been shown in **Figs.5.1, 5.2, 5.3** and **5.4.** The properties of the different layers of model which are same

66

for all the eight models, have been given in the **Table 5.1**. Altogether ten (10) receivers have been placed in each model at an equal interval of 400 m from the left most boundary of the model. Thus, **Figs.5.1, 5.2, 5.3** and **5.4** and **Table 5.1** describe all the eight models in full sense.

The four different geometries of basins have been describes as "Basin1, Basin2, Basin3, Basin4". Basin1 has smaller areal extent and the maximum depth at centre is relatively less, hence it has been termed as, "narrow and shallow basin". Similarly, Basin2 has same areal extent but its maximum depth at centre is more than that of basin1, hence it has been termed as, "narrow and deep basin". Basin3 has relatively greater areal extent than basin1 and basin2, and the maximum depth at the centre is equal to that of basin1; hence it has been termed as, "wide and shallow basin". Considering the same reason as mentioned above, basin4 has been termed as, "wide and deep basin".

The computer program has been modified according to the basin geometries. The model parameters listed in **Table 5.1** have been assigned to each grid point. Then dip-slip source, based on partial stress drop has been implemented into the computational grid. The computational parameters such as, grid size, time-step, model size in terms of grid, total no. of time steps and dominant frequency are 20×20 m square grid, 0.0015 second, 400(H)×450(V) grids, 7334 and 5Hz respectively.

We get the particle displacement registered by the different receivers after running the computer program. The graphs of particle displacement (cm) Vs. time (second), as recorded by different receivers, have been drawn.

The keen study of these graphs and their mutual comparison establishes following facts :

# BASIN 1

RECEIVERS

LAYER 1

LAYER 2

LAYER 3

LAYER 4

8000 M

LAYER 5

LAYER 6

DIP-SLIP SOURCE

4200 M

2800 m

5200 m

400 m  400 m

1600 M

160 M

800 M

400 m
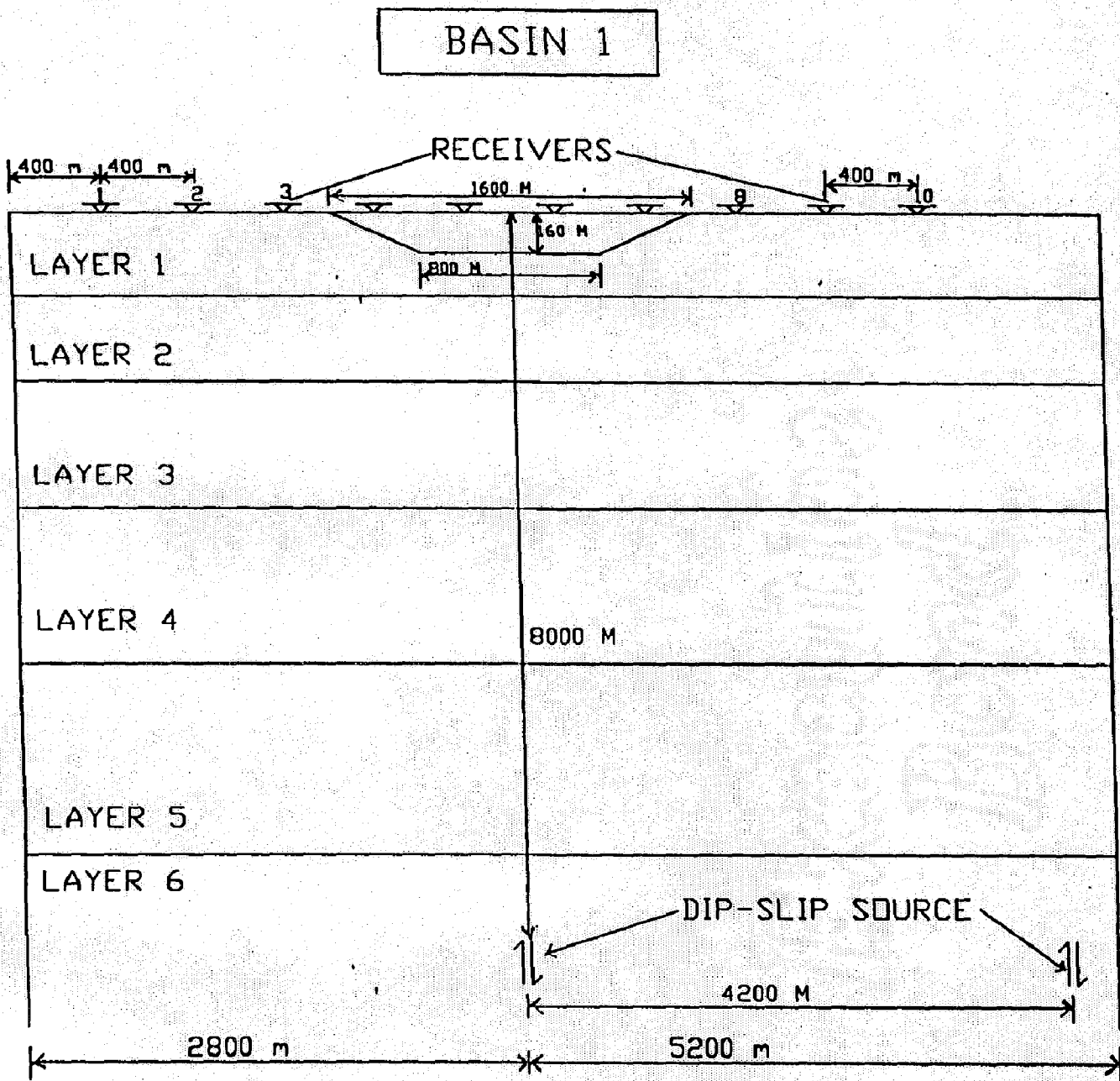
Fig. 5.1 MODEL GEOMETRY OF BASIN 1
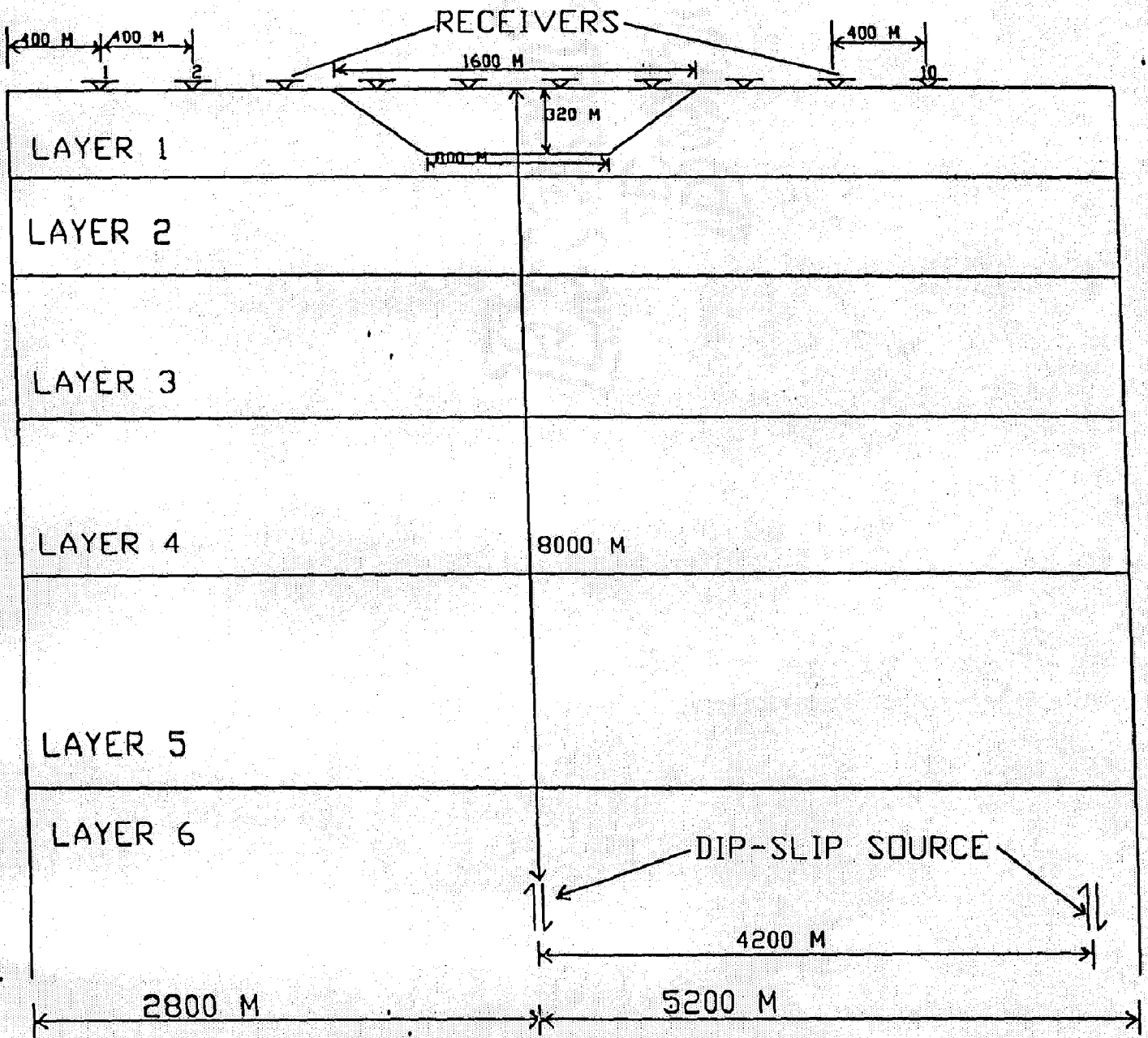
Fig. 5.2 MODEL GEOMETRY OF BASIN 2
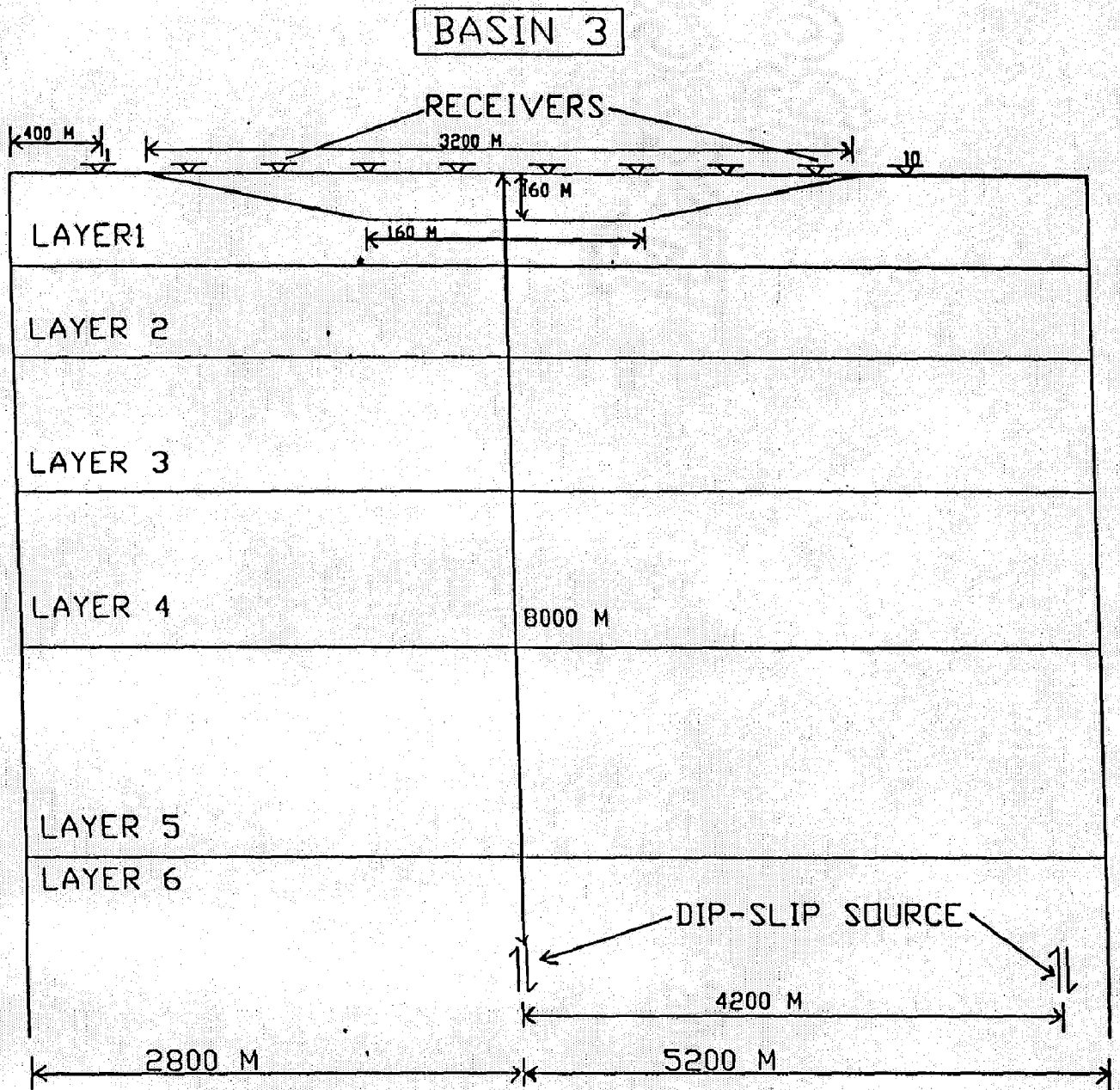
Fig. 5.3 MODEL GEOMETRY OF BASIN 3
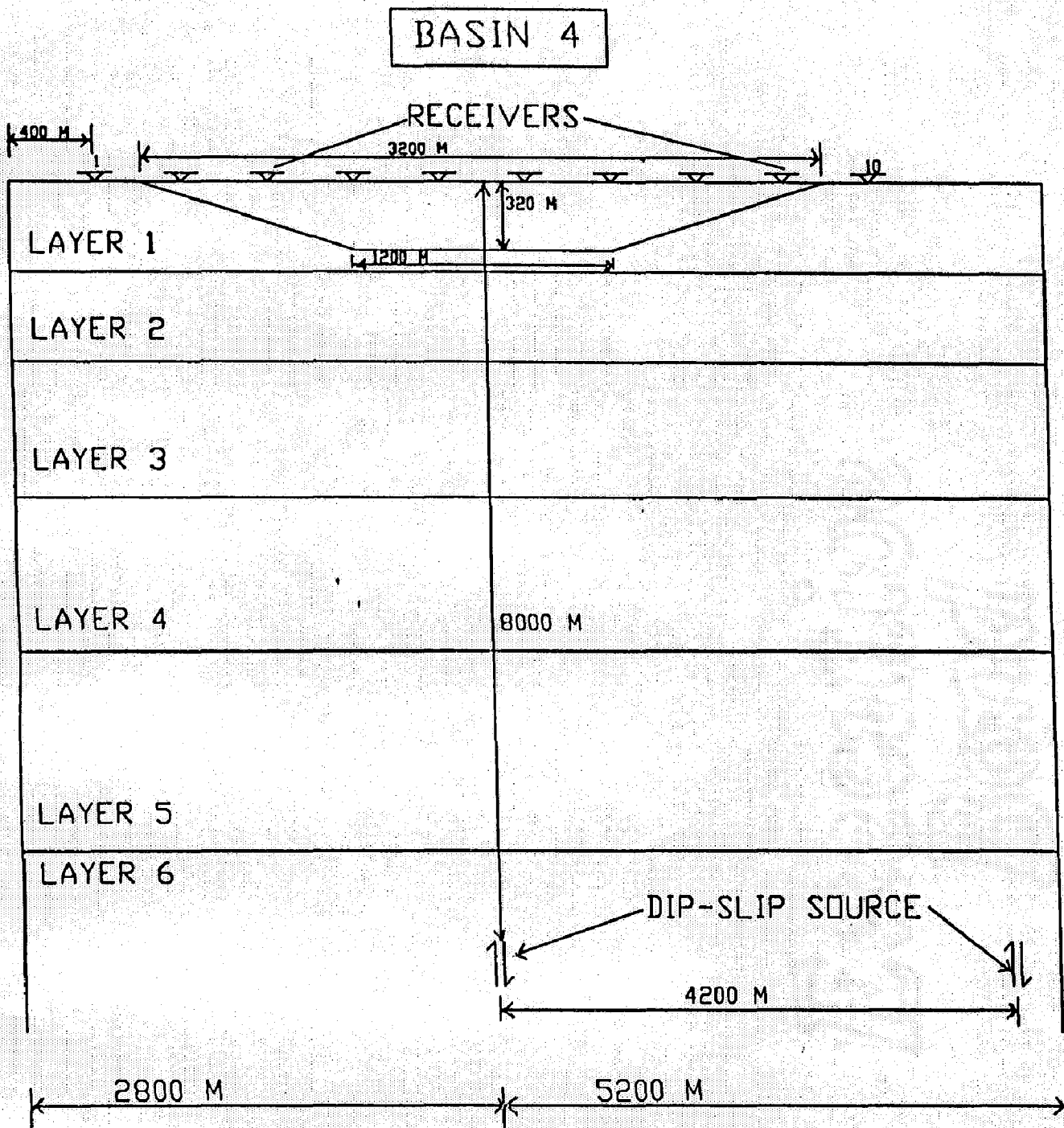
Fig. 5. 4 MODEL GEOMETRY OF BASIN 4

**TABLE 5.1   Layer Parameters of the Geological Model Excluding Basin**

| S.NO. | LAYER No. | THICKNESS (m) | MATERIAL DENSITY(ρ) (g/cc) | P-WAVE VELOCITY (Vp) (m/s) | SHEAR WAVE VELOCITY (Vs) (m/s) | LAME'S PARAMETERS | |
|---|---|---|---|---|---|---|---|
| | | | | | | $\lambda$ (N/m$^2$) | $\mu$ (N/m$^2$) |
| 1. | Layer 1 | 400 | 2.00 | 1700 | 1000 | $1.78 \times 10^6$ | $2.0 \times 10^6$ |
| 2. | Layer 2 | 400 | 2.20 | 2100 | 1200 | $3.366 \times 10^6$ | $3.168 \times 10^6$ |
| 3. | Layer 3 | 1260 | 2.30 | 2400 | 1400 | $4.232 \times 10^6$ | $4.508 \times 10^6$ |
| 4. | Layer 4 | 1340 | 2.40 | 3300 | 1900 | $8.808 \times 10^6$ | $8.664 \times 10^6$ |
| 5. | Layer 5 | 2600 | 2.50 | 4300 | 2500 | $14.98 \times 10^6$ | $15.63 \times 10^6$ |
| 6. | Layer 6 | --- | 2.60 | 4500 | 2598.07 | $17.55 \times 10^6$ | $17.55 \times 10^6$ |

72

i) When source is just below the centre of basins; though there is variation in the durations and amplitudes of particle displacement for different basins, yet the nature of the graphs is same for all the four basins.

ii) Similarly, when source is placed at an offset from the centre of the basins; despite the difference in durations and amplitudes recorded for different basins, the nature of graphs for all these four basins is same.

iii) There is wide variation in amplitudes recorded between the two cases of source at centre and source at an offset. At the same time, the graphs found with these two positions of source have entirely different characteristics. The comparative study of the graphs with these two positions of source will give the effects of position of source on the particle displacement and signal duration.

iv) To know the effects of geometry of basins; four cases of basins have been compared in two different positions of source, i.e., when source at centre and source is at an offset.

## 5.2.1.1 Nature of Graphs for all the Four Basins when Source is at the Centre :

i) The maximum of all the amplitudes of particle displacement (recorded by any of the receivers) was recorded by the two receivers which were placed nearest to the centre of the basin and where the depth of the basin is maximum. The amplitudes recorded by these two receivers are almost same in nature, magnitude and duration.

ii) Though the distance of receiver No. 1 and receiver No. 10 is same from the source, yet the amplitudes recorded by these two receivers are different. In all the four cases of basins, the maximum amplitude recorded by the receiver No. 1 is more than that recorded by receiver No. 10. This may be due to the absorbing boundary nearest to the receiver No. 1.

iii) As we move away from the centre of basins towards any one of the edges of the basins, the maximum amplitude decreases.

iv) Relatively higher amplitudes of particle displacement after the demise of maximum amplitudes are visible in case of the records by two receivers near the centre. Though all other receivers also have some amplitudes at later stage, yet they are not so dominant as shown by the receivers near the centre.

v) Primary wave is not visible at or near the epicentre due to very small amplitude. But, as offset is increasing the amplitude of primary wave is increasing. This effect is due to the radiation pattern of the Dip-Slip source. Similarly, mode converted SV-Wave from the base of the basin is not visible in the epicentral region but it can be seen with increasing offset just after the primary wave arrival.

vi) There is not much effect on the receiver placed at the edge of the basin due to increase in thickness of the basin.

vii) Large duration of signal is due to the mode conversion at the interfaces of different layers and the generation of multiples within a layer.

Fig. 5.5 PARTICLE DISPLACEMENT AT DIFFERENT RECEIVERS FOR BASIN 1 WHEN SOURCE IS AT CENTRE OF THE SPREAD
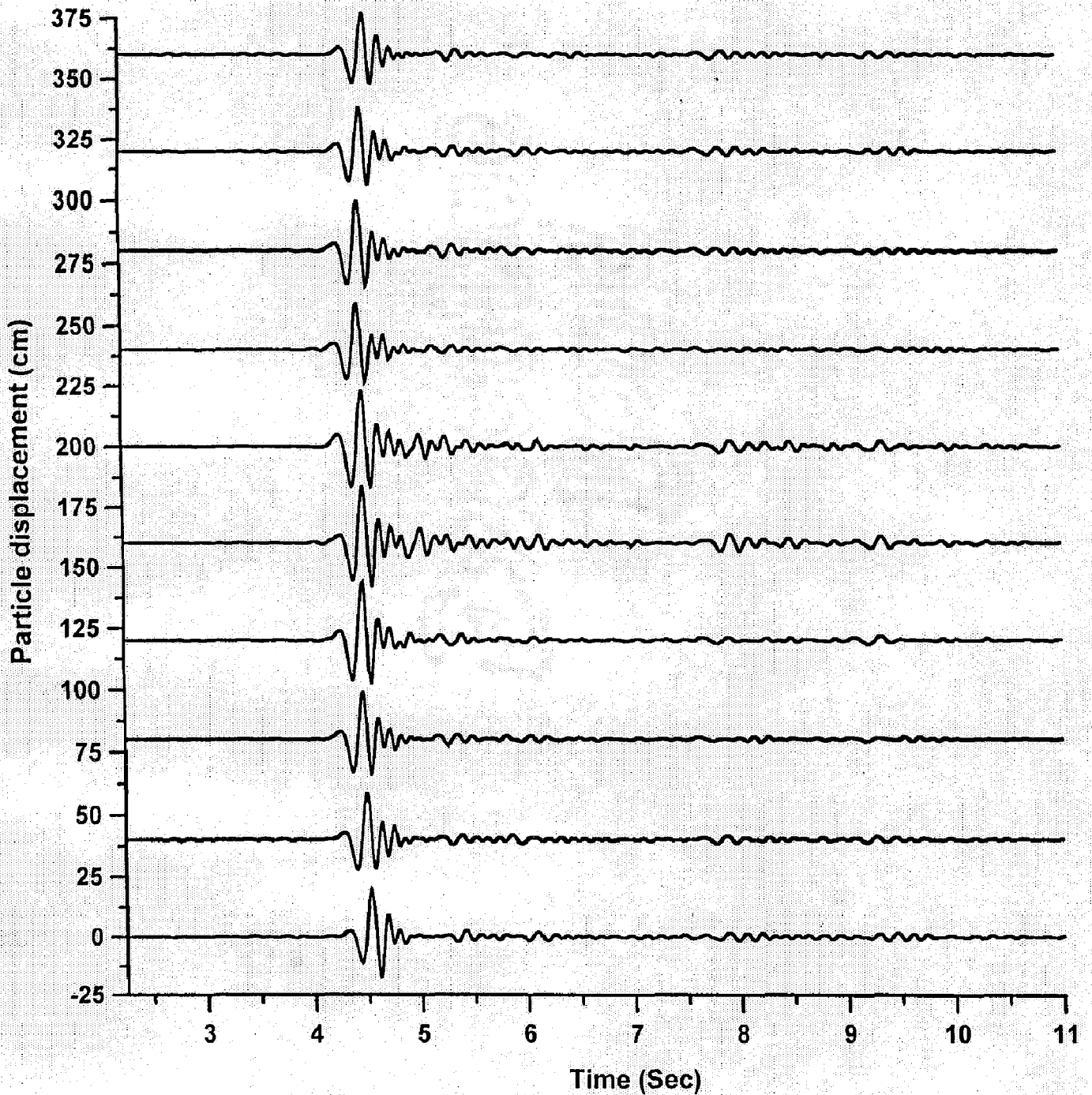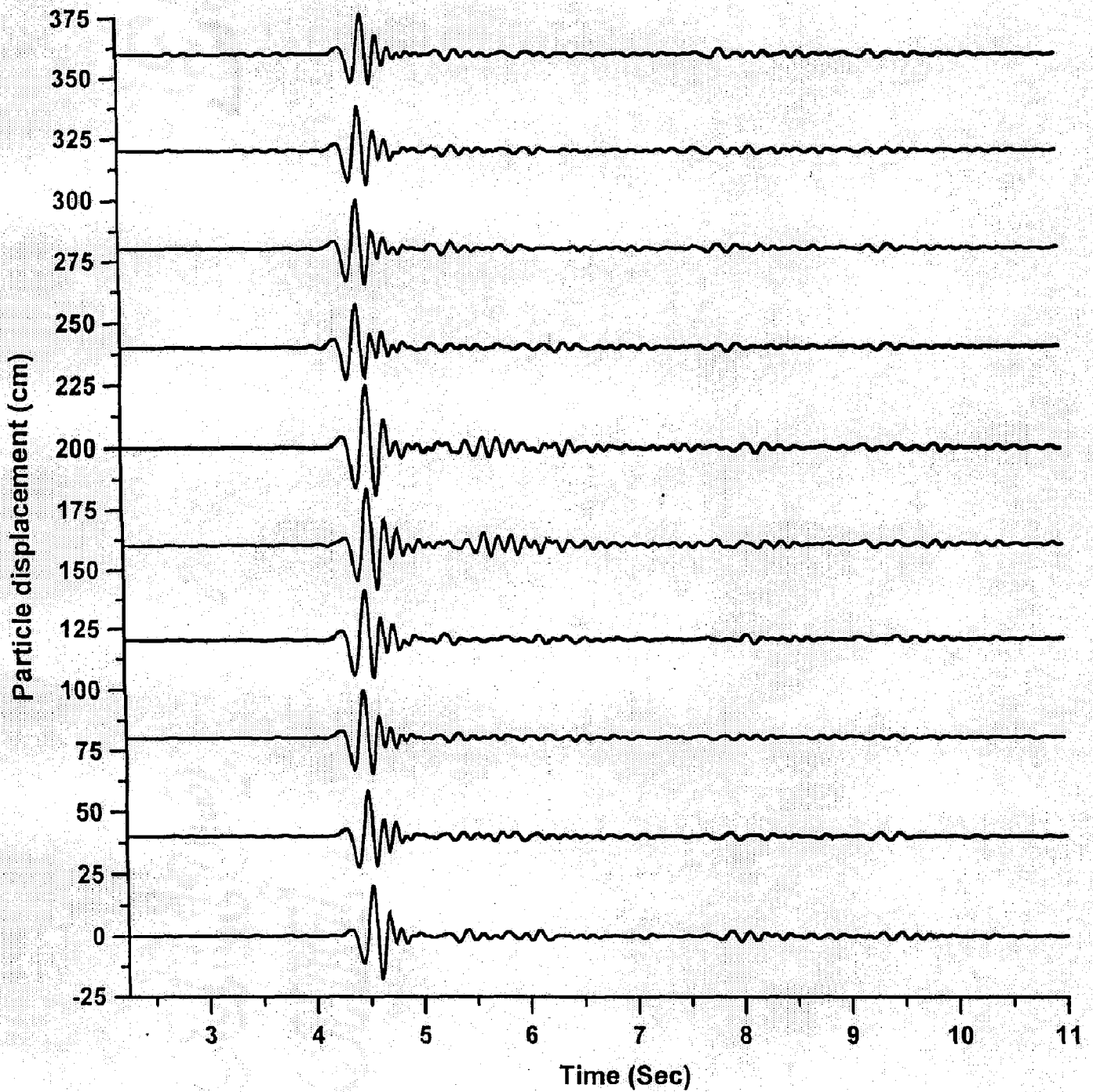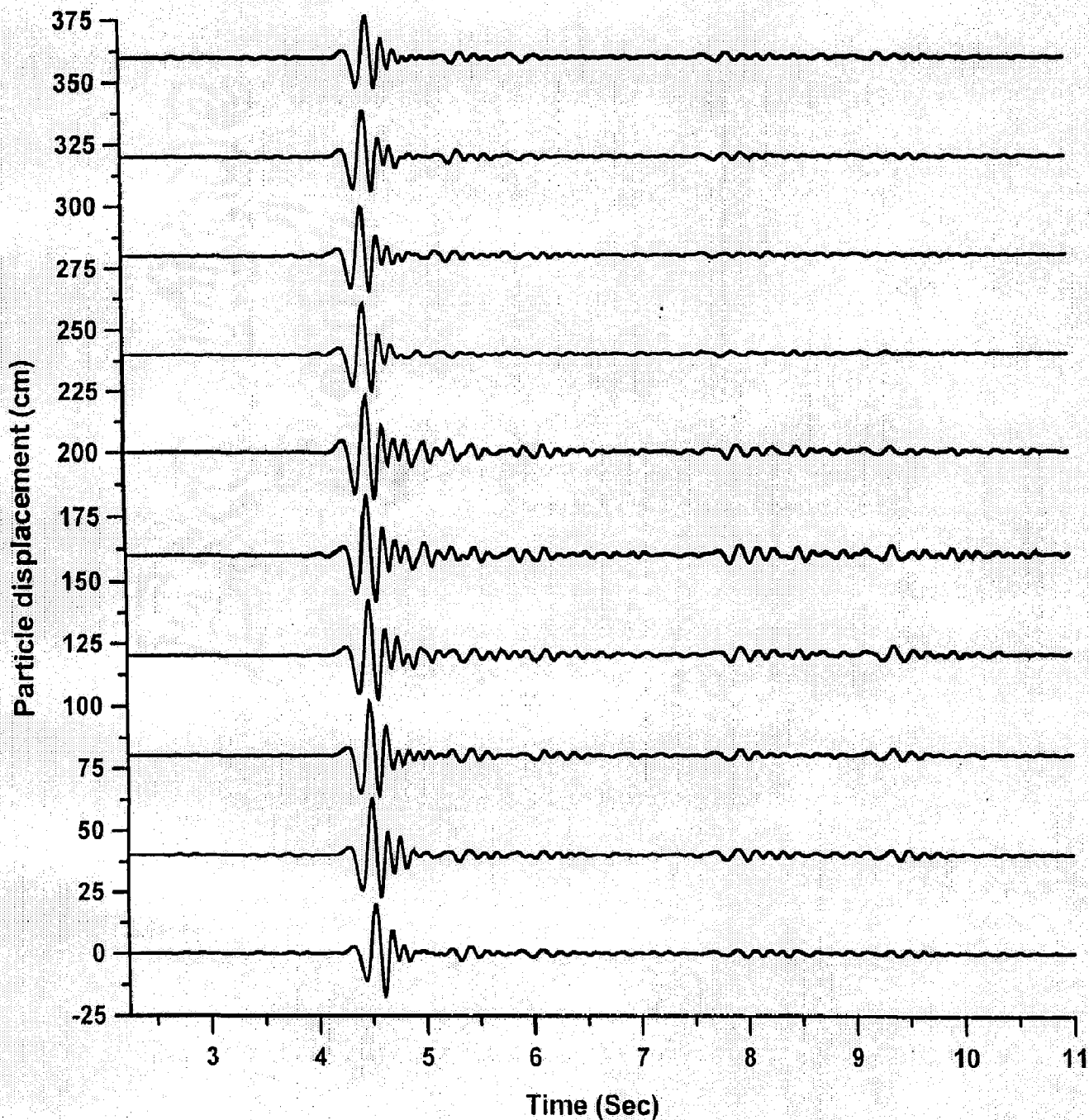
75

Fig. 5.6 PARTICLE DISPLACEMENT AT DIFFERENT RECEIVERS FOR BASIN 2 WHEN SOURCE IS AT CENTRE OF THE SPREAD

Fig. 5.7 PARTICLE DISPLACEMENT AT DIFFERENT RECEIVERS FOR BASIN 3 WHEN SOURCE IS AT CENTRE OF THE SPREAD

77
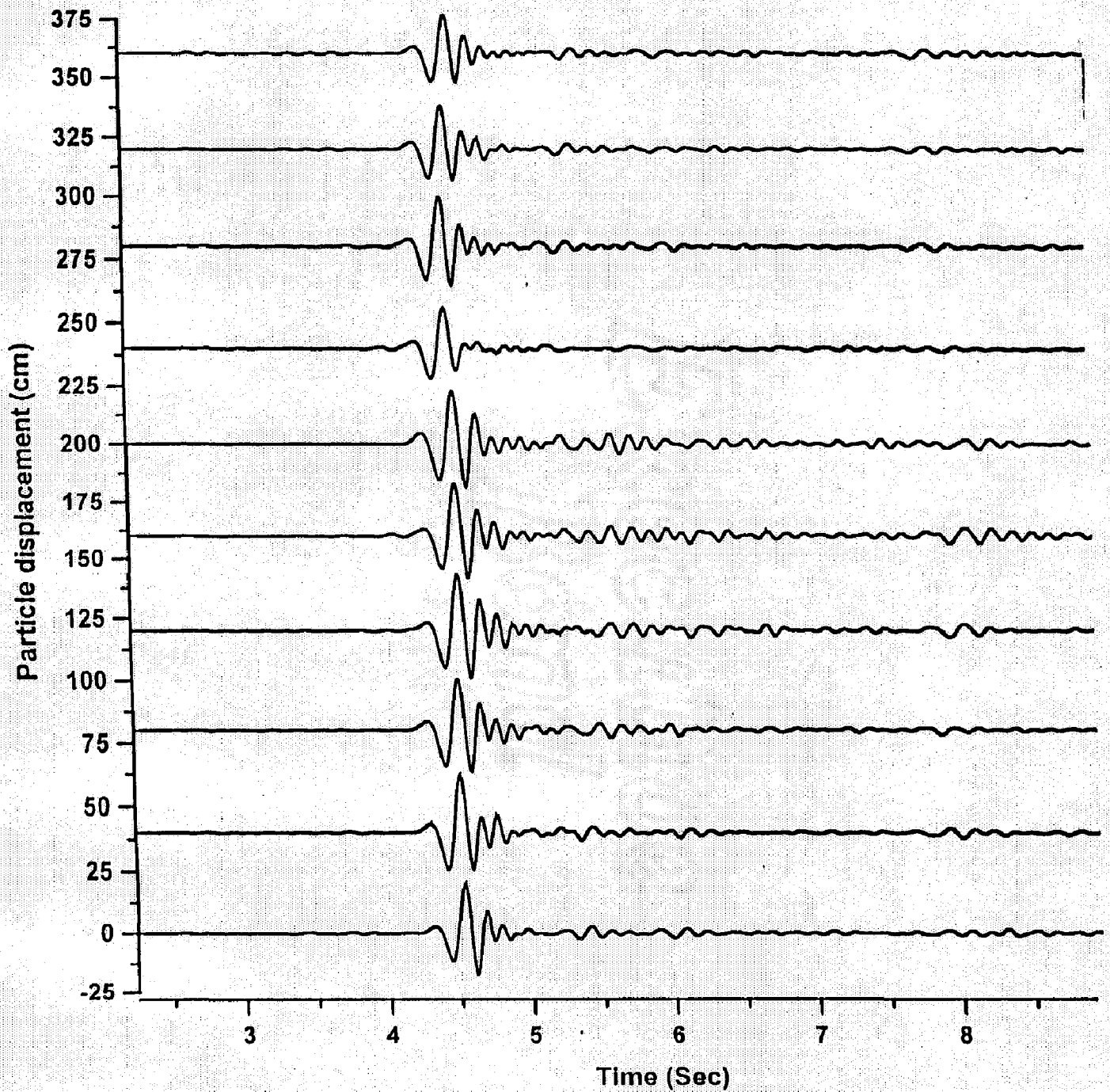
Fig. 5.8 PARTICLE DISPLACEMENT AT DIFFERENT RECEIVERS FOR BASIN 4 WHEN SOURCE IS AT CENTRE OF THE SPREAD

## 5.2.1.2 Nature of Graphs for all the Four Basins when Source is at an Offset from the Centre of the Basins :

i) The maximum of all the amplitudes recorded by any one of the receivers, has been registered by the receiver No. 10 which is nearest to the source.

ii) As we move from receiver No. 10 towards receiver No. 1, we observe that (a) the time required to attain maximum amplitude is increasing and (b) the magnitude of the maximum amplitude is decreasing due to usual divergence radiation pattern effects.

iii) All the ten receivers show some amplitude of particle displacements after the attainment of maximum amplitude, but we see that the amplitude of these later stage recordings is more dominant in case of receiver No. 10 and goes on decreasing as we move towards receiver No. 1.

iv) Any two receivers which are at equal distance from the centre of the basin; have recorded different magnitudes of the amplitude (particle displacement), with higher amplitude shown by that receiver which is nearer to the source.

v) When the source is at an offset, P-phase is visible at all the receivers and its amplitude is increasing with offset in contrast to the SV-phase due to the usual radiation pattern.

vi) The mode converted SV-wave from the first interface can be seen at all the receivers just after the P-phase. Also due to the presence of basin, the mode converted SV-wave from the base of the basin can be

Fig. 5.9 PARTICLE DISPLACEMENT AT DIFFERENT RECEIVERS
FOR BASIN 1 WHEN SOURCE IS AT AN OFFSET OF
4200m FROM THE CENTRE OF SPREAD

Fig. 5.10 PARTICLE DISPLACEMENT AT DIFFERENT RECEIVERS
FOR BASIN 2 WHEN SOURCE IS AT AN OFFSET OF
4200m FROM THE CENTRE OF SPREAD
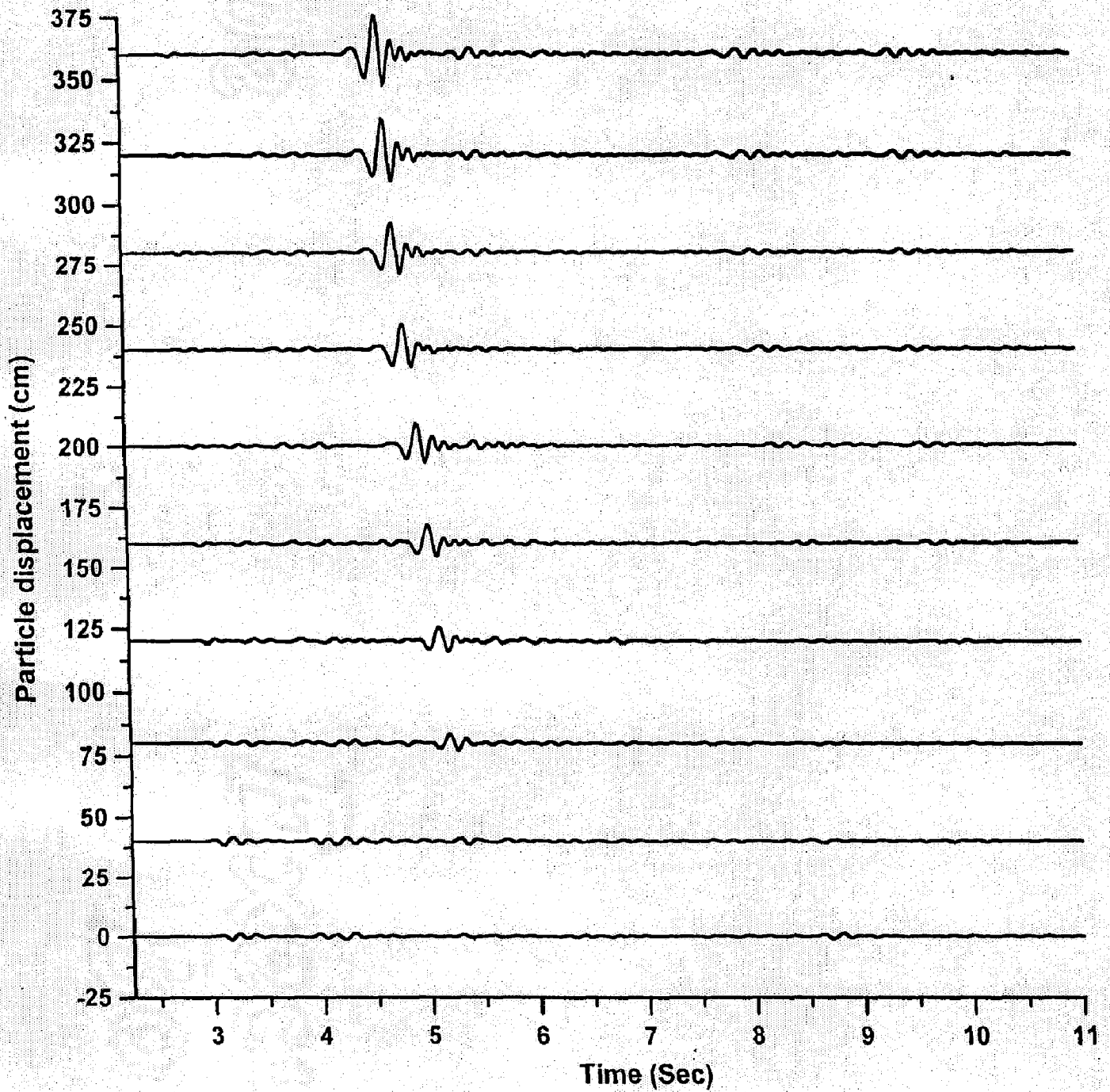
Fig. 5.11 PARTICLE DISPLACEMENT AT DIFFERENT RECEIVERS
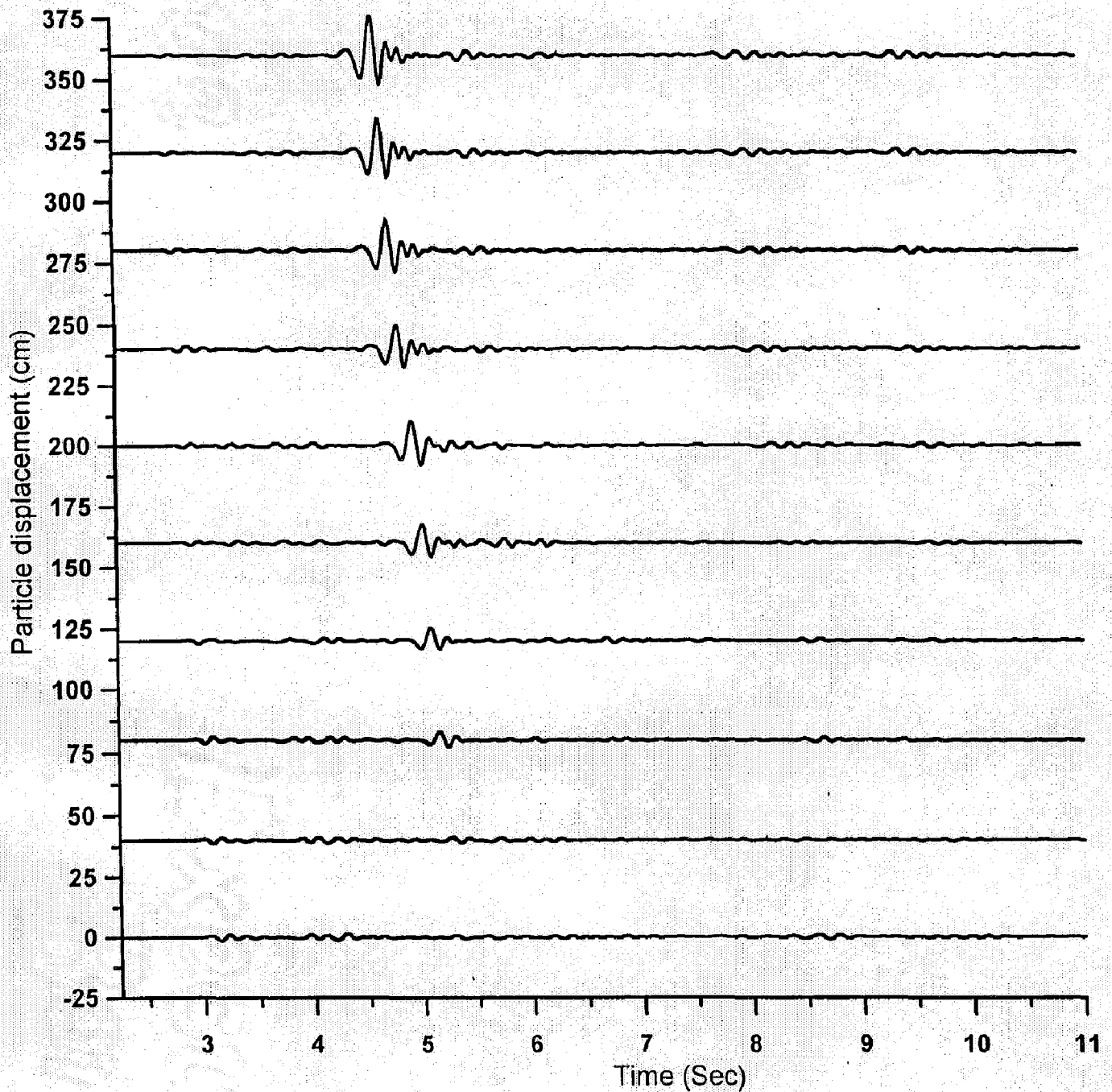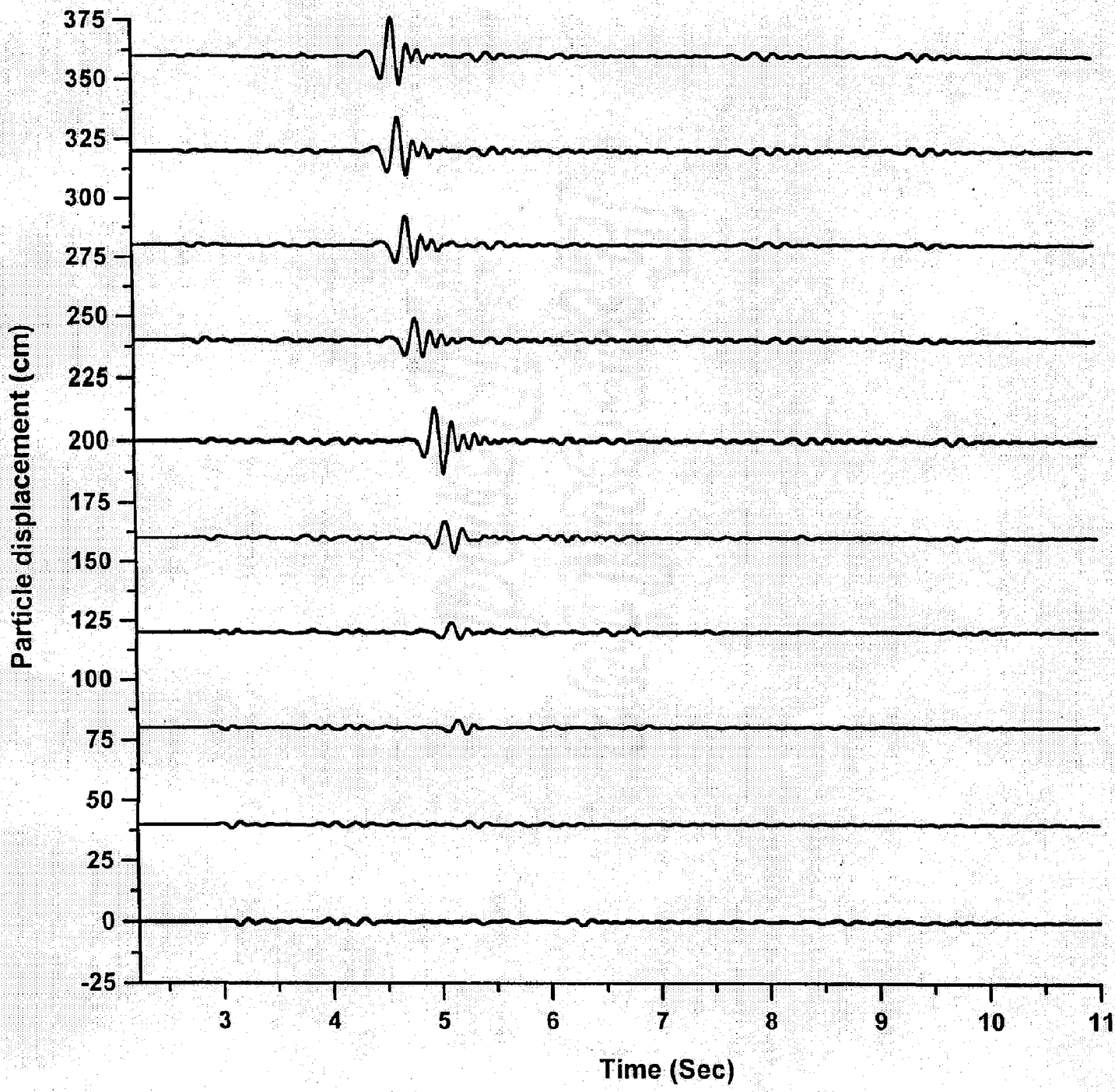FOR BASIN 3 WHEN SOURCE IS AT AN OFFSET OF
4200m FROM THE CENTRE OF SPREAD
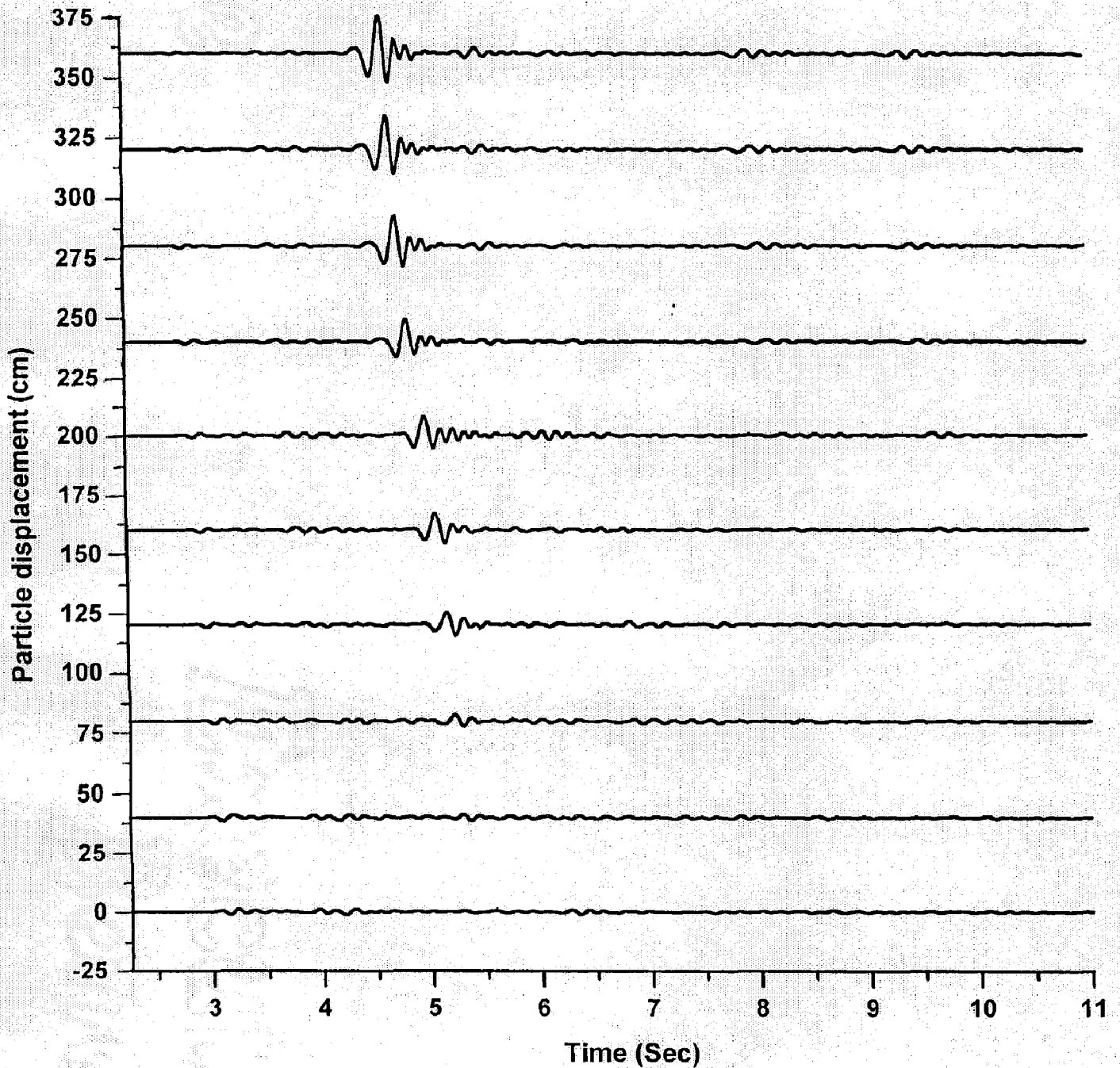
Fig. 5.12 PARTICLE DISPLACEMENT AT DIFFERENT RECEIVERS FOR BASIN 4 WHEN SOURCE IS AT AN OFFSET OF 4200m FROM THE CENTRE OF SPREAD

seen between P-phase and the mode converted SV-wave from the first interface.

vii) Other visible effects are same as mentioned in previous case.

### 5.2.1.3 Comparison between the Nature of Graphs when Source is at Centre and when Source is at an Offset (for all the Four Basins)

i) It is distinctly observed that when source is just below the centre of the basin, it gives much higher amplitude at all locations on or near the basin as compared to the other source position, at an offset from the centre of the basin. Hence, the position of the source just below the centre of the basin is much more devastating than that position of the source when it is placed at an offset from the centre of the basin.

ii) The maximum of all the amplitudes (as recorded by any one of the receivers) is found at two different locations in these two cases. The maximum of these amplitudes is at the central receiver when source is at centre; whereas it is near that edge of the basin which is nearer to the source, in case of source at an offset. Hence when source is at centre, places near the centre of the basin are much prone to earthquakes; whereas when source is at an offset, places near that edge of the basin are more prone which is nearer to the source.

iii) When source is at an offset, the particle displacement as recorded by receiver No. 1 is very small and hence that edge of the basin is almost safe which is at a far distance from the source; but when source is at the centre, the particle displacement recorded by both

84

receivers No. 1 and No. 10 are very high and hence both edges of the basin are prone to earthquake damage.

iv) Higher amplitudes of particle displacement after the attainment of maximum amplitude are visible in case of source at centre, whereas this later stage amplitudes are not so dominant as in case of source at an offset.

v) The amplitude of mode converted SV-Wave (as recorded by receiver No. 1) is visible more than that of the original SV-Wave. Many a time, it creates confusion and the mode converted SV-Wave is treated as original SV-Wave. Any calculation made using the wrong interpretation of mode converted SV-Wave as original SV-Wave gives quite an erroneous result.

## 5.2.1.4 Comparative Study of the Effect of Basin Geometry

i) The maximum amplitude recorded by the receivers near the centre, is more in case of narrow basins (Basin1 and Basin2) as compared with the maximum amplitude recorded by the receivers in case of wide basins (Basin3 and Basin4).

ii) Higher magnitude of amplitude after the attainment of maximum amplitude are more dominant in case of shallow basins (as recorded by all receivers) as compared with the later stage amplitudes for the deep basins.

iii) The amplitudes recorded by the receivers near the edges of all the four basins are almost same.

iv) As thickness of the basin in increasing, the amplitude is increasing due to increase of focussing effect from the sloping sides.

v) The arrival time of multiples is more when thickness of basin is more but amplitude is less due to the divergence effect.

vi) The focussing effect has been clearly observed only in the case of basin2, i.e., when basin is narrow and deep. In this case amplitude is amplified in the central region which is nearer to the right edge from which wave is coming.

viii) The focussing effect in the case of narrow basin is more than the wide basin due to the curvature effect.

• • •

## 6.1  DISCUSSION

Study of local site effects on the characteristics of the strong motion is of great significance, since it helps in earthquake disaster preparedness and ultimately to reduce the loss of lives and properties. Though a good lot of knowledge has already been brought to limelight, yet much more active research is needed in this field to add more to the existing known facts. In the past most of the simulations were based on point source, which is not physically correct, since in point source P-wave dominates and it can not explain the observed radiation patterns. The numerical method, based on finite difference method has simplified the procedure of double-couple source generation and its implementation into the computational grid. Use of shear dislocation models instead of crack source has enabled the source generation using dynamic stress drop in the form of Ricker wavelet against the instantaneous stress drop (Brune, 1970). The use of dynamic stress drop in the form of Ricker wavelet is a better simulation procedure of earthquake source. Since it can explain the initiation, propagation and stopping of the rupture process. In numerical method, magnitude and frequency control of the sources are possible. Frequency control of the sources is of prime importance, since higher frequency source leads to greater dispersion of the waves. Other advantage of numerical method is that the effect of frequency content on the particle displacement can be studied very easily. Though numerical method was adopted for shear dislocation source generation by Vidale (1985 & 1987) too, yet his approach involved high level mathematical dealings and great intricacies. The numerical method approach adopted

here is quite simple and can be applied for complex structures where analytical method fails. At the same time, the results obtained using the numerical method adopted here corroborate with the analytical and observed results. The numerical algorithm used in the simulation was developed by Narayan (1998) based on the parsimonious staggered grid approximation of the ealsto-dynamic equations to reduce the requirement of computational memory. The computed radiation patterns of the various shear dislocation sources are in agreement with the analytical (Coutant et al. 1995) as well as numerical radiation patterns computed by Vidale and Helmberger (1987). The computed strong ground motion for different models depicts that the parsimonious staggered grid scheme is stable for larger Poisson's ratio.

Scaling relations have been studied to see the manner in which strong ground motion characteristics change with change taking place in earthquake source parameters namely, stress drop, rupture area, slip and slip-orientation.

Since the characteristics of strong ground motion on or near the basin have been a great concern of research, hence effect of basins geometry and effect of the position of source have been studied here in detail.

## 6.2 CONCLUSIONS

The efect of change in stress drop ($\Delta\sigma$), dominant frequency ($f_s$), time-step ($\Delta t$), and slip ($\bar{u}$); on the particle displacement, and stresses (Normal stress in X-direction and shear stress in X-Z plane) at epicentre, have been studied elaborately and it has been found that:

1.  The maximum amplitude of particle displacement and stress components increases with increasing stress drop.

3. When source is at an offset, the maximum amplitude is registered by the receiver which is nearest to it irrespective of the basin geometry.

4. When source is at an offset, P-phase is visible at all receivers and its amplitude is increasing with offset in contrast to the SV-phase due to the usual radiation pattern.

5. Position of source at the centre of spread is much more dangerous, since it causes higher particle displacement at all locations with respect to that caused by source at an offset.

6. When source is at an offset, the farther edge of the basin is much safer.

7. The amplitude of mode converted SV-wave (source at an offset) is even more than that of the original SV-wave. Sometimes, mode converted SV-wave may be treated as original SV-wave. So, modelling may be usefull in removing aforesaid confusion.

8. As thickness of the basin increases, the duration and amplitude both increase due to increasing focussing effect from the sloping sides.

9. The arrival time of multiples is more when thickness of basin is more but amplitude is less due to divergence effect.

10. The focussing effect is more in case of narrow basin with respect to wide basin due to curvature effect.

● ● ●

# REFERENCES

▶ Aki, K.(1967). Scaling law of seismic spectrum, J. Geophys. Res., Vol. 72, pp. 1217-1231.

▶ Aki, K. (1987). Magnitude-frequency relation for small earthquakes: A clue to the origin of $f_{max}$ of large earthquakes, J.Geophys. Res., Vol. 92, pp. 1349-1355.

▶ Archuleta, R.J. (1986). Downhole recordings of seismic radiation. In "Earthquake Source Mechanics" (S.Das, J.Boatwright, and C.H. Scholz, eds.), Maurice Ewing, Vol. 6, pp. 319-329, Am. Geophys. Union, Washington, D.C.

▶ Archuleta, R.J., Cranswick, E., Mueller, C., and Spudich, P. (1982). Source parameters of the 1980 Mammoth Lakes, California earthquake sequence, J.Geophys. Res., Vol. 87, pp. 4595-4607.

▶ Bard, P.-Y., and Bouchon, M. (1985). The two dimensional resonance of sediment filled valleys, BSSA, Vol. 75, pp. 519-541.

▶ Bicknell, J., and McGarr, A. (1990). Underground recordings of mine tremors-implications for earthquake source scaling. In "Rockbursts and Seismicity in Mines" (C. Fairhurst, ed.), pp. 109-114, Balkema, Rotterdam.

▶ Bolt, B.A. (1987). Seismic strong motion synthetics, Academic Press, Orlando, Fla.

▶ Boore, D.M. (1986). The effect of finite bandwidth on seismic scaling relations. In "Earthquake Source Mechanics" (S. Das, J. Boatwright, and C.H. Scholz, eds.), Maurice Ewing, Vol. 6, pp. 275-283, Am. Geophys. Union, Washington, D.C.

▶ Brune, J.N. (1970). Tectonic stress and spectra of seismic shear waves from earthquakes, J. Geophys. Res., Vol. 75, pp. 4997-5009.

▶ Chael, E.P., and Kromer, P. (1988). High frequency spectral scaling of mainshock/aftershock sequence near the Norwegian coast, BSSA, Vol. 78, pp.561-570.

▶ Chouet, B., Aki, K., and Tsujiura, M. (1978). Regional variations of the scaling law of earthquake source spectra, BSSA, Vol.68, pp. 49-79.

▶ Coutant, O., Virieux, J., and Zollo, A. (1995). Numerical source implementation in a 2D finite difference scheme for wave propagation, BSSA, Vol. 85, pp. 1507-1512.

▶ Coutel, F., and Mora, P. (1998). Simulation based comparison of four site-response estimation techniques, BSSA, Vol. 88, No. 1, pp.30-42.

▶ Das, S., and Kostrov, B.V. (1986). Fracture of a single asperity on a finite fault: A model for weak earthquakes? In "Earthquake Source Mechanics" (s.Das, J. Boatwirght, and C.H. Scholz, eds.), Am. Geophys. Union, Monograph No. 37, Washington, D.C.

▶ De Natale, G., Iannaccone, G., Martini, M., and Zollo, A. (1987). Seismic sources and attenuation properties at the Campi Flegrei volcanic area. In "Advance in Volcanic Seismology" (E.A. OKal, ed.), Pure Applied Geophys., Vol.125, pp. 883-917.

▶ Dysart, P.S., Snoke, J.A., and Sacks, I.S. (1988). Source parameters and scaling relations for small earthquakes in the Matsushiro region, southwest Honshu, Japan, BSSA, Vol. 78, pp. 571-589.

▶ Fletcher, J.B., Haar, L.C., Vernon, F.L., Brune, J.N., Hanks, T.C., and Berger, J. (1986). The effects of attenuation on the scaling of source parameters for earthquakes at Anza, California. In "Earthquake Source Mechanics" (S. Das, J.Boatwright, and C.H. Scholz, eds.), Maurice Ewing, Vol. 6, pp. 331-338, Am. Geophys. Union, Washington, D.C.

▶ Frankel, A., and Wennerberg, L. (1989). Microeathquake spectra from the Anza, California, seismic network: Site response and source scaling, BSSA, Vol. 79, pp. 581-609.

▶ Gibowicz, S.J. (1985). Seismic moment and Seismic energy of mining termors in the Lubin copper basin in Poland, Acta Geophys. Pol., Vol. 33, pp. 243-257.

▶ Gibowicz, S.J., Harjes, H.-P., and Schafer, M. (1990). Source parameters of seismic events at Heinrich Robert mine, Ruhr basin, Federal Republic of Germany : Evidence for nondouble couple events, BSSA, Vol.80, pp. 88-109.

▶ Glassmoyer, G., and Borcherdt, R.D.(1990). Source parameters and effects of bandwidth and local geology on high-frequency ground motions observed for aftershocks of the northeastern Ohio earthquake of 31 January 1986, BSSA, Vol.80, pp. 889-912.

▶ Haar, L.C., Fletcher, J.B., and Mueller, C.S. (1984). The 1982 Enola, Arkansas, swarm and scaling of ground motion in the Eastern United States, BSSA, Vol.74, pp. 2463-2482.

▶ Hanks, T.C., and McGuire, R.K. (1981). The character of high-frequency strong motion, BSSA, Vol. 71, pp. 2071-2095.

▶ Haskell, N.A. (1953). The dispersion of surface waves in multilayered media, BSSA, Vol. 43, pp. 17-34.

▶ Kanamori, H., and Anderson, D.L. (1975). Theoretical basis of some empirical relations in seismology, BSSA, Vol. 65, pp. 1073-1096.

▶ Kelly, K.R., Ward, R.W., Trietel, S., and Alford, R.M. (1976). Synthetic seismograms : A finite difference approach, Geophysics, Vol. 41, pp. 2-27.

▶ King, J.L., and Tucker, B.E.(1984). Dependence of Sediment filled valley response on the input amplitude and the valley properties, BSSA, Vol. 74, No. 1, pp. 153-165.

▶ Krinitzsky, E.L, and Chang, F.K. (1987). Parameters for specifying intensity-related earthquake ground motions, Miscellaneous paper S-73-1, Report 25. U.S. Army Corps of Engineers Waterways Experiment Station, Vicksburg, Mississippi, 43 pp.

▶ Lui, H.L., and Helmberger, D.V. (1985). The 23:19 aftershock of the 15 October 1979 Imperial Valley earthquake : more evidence for an asperity, BSSA, Vol. 75, pp. 689-708.

▶ Luo, Y., and Schuster, G. (1990). Parsimonious staggered grid finite differencing of the wave equation, Geophys. Res. Lett., Vol. 17, pp. 155-158.

▶ Madariaga, R. (1976). Dynamics of an expanding circular fault, BSSA, Vol. 66, pp. 639-666.

▶ McGarr, A. (1986). Some observations indicating complications in the nautre of earthquake scaling. In "Earthquake Source Mechanics" (S.Das, J.Boatwright, and C.H. Scholz, eds.), Maurice Ewing, Vol. 6, pp. 217-225, Am. Geophys. Union, Washington, D.C.

▶ Mikumo, T., and Miyatake, T. (1987). Numerical modelling of realistic fault rupture process. In "Seismic Strong Motion Synthetics" ( Bolt, B.A., ed.), pp. 91-151, Academic Press, Orlando, Fla.

▶ Narayan, J.P.(1998). Numerical strong ground motion and study of local site effects, Proceedings eleventh symposium on earthquake engineering, Department of Earthquake Engineering, University of Roorkee, Roorkee, Dec. 17-19 (for P-SV wave).

▶ Newmark, N.M., and Hall, W.J.(1982). Earthquake spectra and design, EERI Monograph, Earthquake Engineering Research Institute, Berkeley, California, 103 pp.

▶ Ram, A., and Narayan, J.P. (1995). Simulation of the Hydrocarbon structures using the P-SV wave solution, Pure and Applied Geophysics, Vol. 144, pp. 59-77.

▶ Randall, M.J. (1973). The spectral theory of seismic sources, BSSA, Vol. 63, pp. 1133-1144.

▶ Rudnicki, J.W., and Kanamori, H. (1981). Effects of fault interaction on moment, stress drop and strain energy release, J. Geophys. Res., Vol. 86, pp. 1785-93.

▶ Trifunac, M.D., and Brandy, A.G. (1975a). One the correlation of seismic intensity with peaks of recorded strong ground motion, BSSA, Vol. 65, pp. 139-162.

▶ Vafidis, A., Abromovici, F., and kanasewich, E.R. (1992). Elastic wave propagation using fully vectorised high order finite difference algorithms, Geophys., Vol. 57, pp. 218-232.

▶ Vidale, J.E., Helmberger, D.V., and Clayton, R.W.(1985). Finite difference seismonograms for SH-waves, BSSA, Vol. 75, pp. 1765-1782.

▶ Vidale, J.E., Helmberger, D.V. (1987). Path effect in strong motion seismology. In "Seismic Strong Motion Synthetics" (Bolt, B.A., ed.), pp. 267-319, Academic Press, Orlando, Fla.

▶ Vidlae, J.E., and Helmberger, D.V. (1988). Elastic finite difference of 1971 San Fernando earthquake, BSSA, Vol. 78, No. 1, pp. 122-141.

▶ Virieux, J. (1986). P-SV wave propagation in heterogeneous media, velocity stress finite difference method, Geophysics, Vol. 51, pp. 889-901.

• • •

▶ Vidale, J.E., Helmberger, D.V., and Clayton, R.W. (1985). Finite difference seismonograms for SH-waves, BSSA, Vol. 75, pp. 1765-1782.